General Disclaimer

One or more of the Following Statements may affect this Document

- This document has been reproduced from the best copy furnished by the organizational source. It is being released in the interest of making available as much information as possible.

- This document may contain data, which exceeds the sheet parameters. It was furnished in this condition by the organizational source and is the best copy available.

- This document may contain tone-on-tone or color graphs, charts and/or pictures, which have been reproduced in black and white.

- This document is paginated as submitted by the original source.

- Portions of this document are not fully legible due to the historical nature of some of the material. However, it is the best reproduction available from the original submission.

Produced by the NASA Center for Aerospace Information (CASI)

Numerical Simulation of Turbulence in the Presence of Shear

by

S. Shaanan,
J. H. Ferziger,
and
W. C. Reynolds

Prepared from work done under Grant
NASA-NgR-05-020-622

(NASA-CR-143349) NUMERICAL SIMULATION OF TURBULENCE IN THE PRESENCE OF SHEAR (Stanford Univ.) 140 p HC $5.75 CSCL 20D
N75-30476
Unclas
G3/34 34234
FACILITY BRANCH

Report No. TF-6

Thermosciences Division
Department of Mechanical Engineering
Stanford University
Stanford, California

August 1975

NUMERICAL SIMULATION OF TURBULENCE IN THE PRESENCE OF SHEAR

by

S. Shaanan, J. H. Ferziger and W. C. Reynolds

Prepared from work done under Grant

NASA-NgR-05-020-622

Report No. TF-6

Thermosciences Division
Department of Mechanical Engineering
Stanford University
Stanford, California

August 1975

ABSTRACT

Numerical computations of three-dimensional time-dependent turbulent flows are now feasible for three main reasons. The state of the art of numerical methods for solving the nonlinear Navier-Stokes equations, of turbulent flow modeling for numerical simulations, and of fast computer hardware have all made three-dimensional simulation a reality.

The present work deals with the numerical calculations of the large eddy structure of turbulent flows, by use of the averaged Navier-Stokes equations, where averages are taken over spatial regions small compared to the size of the computational grid. The subgrid components of motion are modeled by a local eddy-viscosity model. A new finite-difference scheme is proposed to represent the nonlinear averaged advective term $\partial/\partial x_j\ (\overline{\bar{u}_i \bar{u}_j})$ which has fourth-order accuracy. This scheme exhibits several advantages over existing schemes with regard to the following:

1. The scheme is compact--it extends only one point away in each direction from the point to which it is applied.
2. It gives better resolution for high wave-number waves in the solution of Poisson equation.
3. It reduces programming complexity and computation time.

Three examples are worked out in detail.

1. Decay of isotropic turbulence. This problem serves as a test for the proposed numerical method. Comparison of numerical results to experimental data (Comte-Bellot and Corrsin, 1971) shows satisfactory agreement. This brings us to the conclusion that the numerical method properly distributes the turbulent energy among different scales, with proper decay rate.
2. Homogeneous turbulent shear flow. Numerical results confirm experimental data given by Champagne, et al. (1970) and Harris (1974) which show departure from isotropy and growth of length scales in the direction of shear as the result of the presence of mean shear.

3. Homogeneous turbulent shear flow with system rotation. Numerical results show clearly the effect of rotation on the stability of turbulence, as was shown experimentally by Johnston (1974).

The numerical simulation of the model equations of turbulence given in this work proves to be a convenient way for extracting useful information on the physics of a variety of turbulent flows. The numerical results extend existing experimental data considerably.

ACKNOWLEDGMENTS

The authors gratefully acknowledge the useful comments of Drs. H. Lomax, U. Mehta and D. Kwak. We appreciate Ms. Nancy Silvis for her conscientious typing.

This work was sponsored by NASA/Ames Research Center under Grant NASA-NgR-05-020-622. One of the authors (S. Shaanan) wishes to acknowledge the Government of Israel for their fellowship support.

TABLE OF CONTENTS

		Page
ABSTRACT		iii
ACKNOWLEDGMENTS		v
TABLE OF CONTENTS		vi
LIST OF FIGURES		viii
NOMENCLATURE		x
Chapter 1.	INTRODUCTION	1
A.	General Background	1
B.	Objective of Study	3
Chapter 2.	MATHEMATICAL FORMULATION	5
Chapter 3.	FINITE-DIFFERENCE FORMULATION	10
A.	General Considerations	10
B.	The Space-Differencing Scheme	13
C.	The Finite-Difference Poisson Equation	18
D.	The Time-Differencing Scheme	21
Chapter 4.	DECAY OF ISOTROPIC TURBULENCE	26
A.	General Description	26
B.	The Experimental Results	27
C.	The Initial Velocity Field	29
D.	Results and Discussion	30
Chapter 5.	HOMOGENEOUS TURBULENT SHEAR FLOW	39
A.	General Description	39
B.	Mathematical Formulation	40
	a. Boundary conditions	43
	b. Initial conditions	43
	c. Computational time steps	43
C.	Results and Discussion	44
	a. Comparison with experiments	44
	b. Additional numerical results	45
	c. Pressure-strain correlation T_{ij}	47

Page

Chapter 6. HOMOGENEOUS TURBULENT SHEAR FLOW WITH SYSTEM ROTATION 60

A. General Description 60

B. Mathematical Formulation 61

C. Results 63

D. Interpretation of Results 64

Chapter 7. SUMMARY 75

A. Conclusions 75

B. Recommendations 75

Appendix A. THE FILTERING OPERATOR AND ITS PROPERTIES 77

Appendix B. GENERATION OF INITIAL VELOCITY FIELD FOR ISOTROPIC TURBULENCE SIMULATION 79

Appendix C. THE DISCRETE FOURIER TRANSFORM AND ITS COMPUTATIONAL FORM 84

Appendix D. THE COMPLETE EXPANSION OF THE FILTERED ADVECTIVE TERM FOR THE STAGGERED-MESH CONFIGURATION 86

Appendix E. THE PROGRAM TFC 95

REFERENCES 125

LIST OF FIGURES

Figure		Page
3-1	Staggered-mesh configuration in two-dimensions	24
3-2	Comparison of second- and fourth-order Poisson operators to the exact Fourier transform	25
4-1	Rate of energy decay of isotropic turbulence	32
4-2	Three-dimensional energy spectra of isotropic turbulence	33
4-3	Dependence of rate of energy decay on numerical constant	34
4-4	Dependence of energy spectrum on numerical constant	35
4-5	Rate of energy decay for various model constants	36
4-6	Energy spectra for various model constants	37
4-7	Skewness for different numerical constants	38
5-1	Schematic sketch of the homogeneous turbulent shear flow	49
5-2	Mean velocity in a convective frame	50
5-3	Turbulence levels in homogeneous shear flow, comparison with experiment	51
5-4	Shear stress in homogeneous shear flow, comparison with experiment	52
5-5	Development of turbulent kinetic energy in homogeneous shear flow	53
5-6	Development of turbulence levels in homogeneous shear flow	54
5-7	Development of shear stresses in homogeneous shear flow	55
5-8	Development of length scales in homogeneous shear flow	56
5-9	Spatial correlations in homogeneous shear flow	57
5-10	Development of pressure-strain correlations in homogeneous shear flow	58
5-11	Return to isotropy from homogeneous shear	59
6-1	Turbulent kinetic energy for different gradient Richardson numbers	68
6-2	Shear stresses for different gradient Richardson numbers	69
6-3	Turbulence level of u for different gradient Richardson numbers	70

Page

6-4 Turbulence level of v for different gradient Richardson numbers 71

6-5 Turbulence level of w for different gradient Richardson numbers 72

6-6 Mixing-length ratio versus gradient Richardson number. Data from Johnston (1974) 73

6-7 $<\bar{u}\bar{v}>^{1/2}$ versus gradient Richardson number at various time steps 74

B-1 Coordinate system for decomposition of $\underline{u}$ 83

NOMENCLATURE

English letters

a	= a constant defined by Eq. (6-44)
a_1, a_2, a_3, a_4	= constants defined by Eqs. (B-13) and (B-14)
A	= Rotta's constant defined by Eq. (5-28)
b_{ij}	= anisotropy tensor defined by Eq. (5-30)
c	= turbulence model constant
c_1, c_2	= constants defined by Eq. (6-26)
D	= isotropic dissipation
D_{sgs}	= subgrid scale dissipation
E	= three-dimensional energy spectrum
f	= a function
$\hat{f}$	= Fourier transform of f
g	= filtering function defined in Appendix A
$\hat{g}$	= Fourier transform of g
h	= mesh size
H	= length of computational box
i, j, k	= indices describing spatial locations on a mesh
I, J, K	= computational indices
$\underline{k}, k_i$	= wave-number vector
$\underline{k}', k_i'$	= modified wave-number vector defined by Eq. (4-13)
k	= magnitude of k_i ($k^2 = k_i k_i$)
K	= eddy-viscosity coefficient defined by Eq. (2-13)
ℓ	= mixing length
L	= number of time steps

m	= spatial frequency ($m = k/2\pi$)
M	= diameter of bars of the isotropic turbulence generator
N	= number of mesh points
N_c	= Courant number
n	= index
p	= turbulent instantaneous pressure
P	= instantaneous pressure
P^*	= modified instantaneous pressure
$\hat{p}$	= Fourier transform of p
q	= RHS of Poisson equation (2-18)
$\hat{q}$	= Fourier transform of q
$q^2/2$	= turbulent kinetic energy
r	= rotation defined by Eq. (6-39)
$\underline{r}, r_i$	= separation vector
r_{ij}	= rotation tensor of turbulence
$\mathcal{R}_{ij}$	= rotation tensor of instantaneous field
R_{ij}	= correlation tensor
$\mathbb{R}_{ij}$	= tensor defined by Eq. (6-36)
Re	= Reynolds number
Ri	= gradient Richardson number
s	= strain rate defined by Eq. (6-39)
s_i	= RHS of momentum equation (2-17)
s_{ij}	= rate-of-strain tensor of turbulence
$\mathcal{S}_{ij}$	= rate-of-strain tensor of instantaneous field
S	= skewness
t	= time

$\underline{t}, t_i$	= reference vector defined in Appendix B
T_{ij}	= pressure-strain correlation tensor
$\underline{u}, u_i$	= instantaneous turbulent velocity vector
$\underline{U}, U_i$	= instantaneous velocity vector
u, v, w	= instantaneous turbulent velocity components
U, V, W	= instantaneous velocity components
U_o	= mean velocity
U_c	= centerline velocity
$\underline{x}, x_i$	= position vector
x, y, z	= Cartesian coordinates
$\tilde{x}$	= stretched x coordinate

Greek symbols

α	= numerical constant defined by Eq. (3-19)
β	= a constant defined by Eq. (6-2)
γ	= a constant defined by Eq. (3-2)
Γ	= mean velocity gradient
δ_{ij}	= Kronecker delta
Δ	= filter width
ε_{ijk}	= unit alternating tensor
ξ	= angle defined in Fig. B-1
η	= random number
θ	= angle defined in Fig. B-1
λ	= Taylor microscale
ν	= kinematic viscosity
ρ	= density
ρ_{ij}	= tensor defined by Eq. (6-30)

σ_{ij}	= stress tensor defined by Eq. (2-9)
τ_{ij}	= shear tensor defined by Eq. (2-10)
ϕ	= angle defined in Fig. B-1
Φ_{ij}	= spectrum tensor
$\underline{\Omega}, \Omega_i$	= angular velocity vector
$\underline{\omega}, \omega_i$	= vorticity vector

Other symbols

D_o, D_+, D_-, $4D_o$, $4D_+$, $4D_-$	= finite-difference operators for first derivative
D_j	= finite-difference operator in j^{th} direction
$(\underline{\ })$	= vector
$(\bar{\ })$	= average according to definition given by Eq. (2-4)
$(')$	= subgrid scale component
$< >_{ij}$	= averages over planes defined by ij coordinates
$< >$	= averages over the entire volume
$*$	= conjugate
$\star$	= convolution
$\mathcal{F}$, FT	= Fourier transform
DFT	= discrete Fourier transform
FFT	= fast Fourier transform
RHS	= right-hand side
RMS	= root mean square
CHC	= Champagne, Harris, and Corrsin

CHAPTER 1

INTRODUCTION

A. General Background

In recent years, because computers have become faster and larger, a new approach in handling turbulent flow simulations has emerged. This is a three-dimensional, time-dependent numerical simulation of the large-scale structures of turbulent flows. In this approach, a variation of an old idea is used; one applies a spatial averaging operator to the equations of motion. The averages are taken over regions small compared to the size of the computational domain, and the subgrid components of motion are modeled with a local eddy-viscosity coefficient.

One of the first successful attempts in using this approach was Deardorff's in a numerical study of three-dimensional turbulent channel flow at high Reynolds numbers (Deardorff, 1970). The main purpose of his work was to extend earlier work by meteorologists (Smagorinsky, et al., 1965; Leith 1965), who used these methods in calculating the general circulation of the atmosphere in two dimensions, to fully three-dimensional turbulence for a laboratory problem. Other works of interest that followed this approach are Deardorff (1972) and Schumann (1973).

The numerical discretization techniques that have been used in the mentioned works and in other investigations fall basically into two categories, namely, spectral methods and real-space methods. Spectral methods, which deal with the transformed equations in Fourier space, are the most accurate methods. However, when applied to the Navier-Stokes equations, they exhibit a major drawback. The nonlinear advective terms appear as convolution sums, and have to be treated in quite a complicated way in order to avoid aliasing errors. Another difficulty is that the method is capable of handling only geometrically simple problems with periodic boundary conditions. Detailed descriptions of the spectral methods can be found in the work of Orszag and co-workers (Orszag, 1969, 1971 a,b; Fox and Orszag, 1973; Orszag and Patterson, 1972).

Real-space methods use finite differences for discretization in various forms. The most popular methods are second-order schemes, which have particular conservation and stability properties, as will be discussed later. The main contributions to these methods can be found in the works of Fromm (1963), Harlow and Welch (1965), Lilly (1965), Arakawa (1966), Williams (1969), Deardorff (1970), and others. Although finite difference methods are inferior to spectral methods with respect to accuracy, they have the advantage of not being restricted to simply shaped regions and periodic boundary conditions, and this generality makes them suitable to flows of engineering interest, i.e., flows which contain wall-bounded as well as boundary-free regions.

Only a few three-dimensional time-dependent flow simulations have been reported so far. The main reason is the restricted capability of computers in the past, in terms of speed and capacity. Even today, with the use of the largest available computer (CDC 7600), a 32^3 mesh-point problem is the upper limit for a core-contained program, provided the simplest periodic boundary conditions are used, and an average simulation consumes about half an hour of running time. The use of peripheral equipment, such as tapes, discs, or other mass memory and storage, complicates the operation significantly in terms of programming and turn-around time.

The reported works include those of Deardorff (1970) and Schumann (1973), simulating the channel flow, using 24x14x20 and 64x32x16 mesh points, respectively, by finite-difference methods; of Orszag and Patterson (1972), simulating three-dimensional homogeneous isotropic turbulence, using 32^3 mesh points by spectral methods; and of Kwak, et al. (1975), simulating an isotropic turbulence and a pure strained turbulent flow, using 32^3 and 16^3 mesh points, respectively. Clark (ongoing Ph.D. research, Stanford University) is working on turbulence modeling, using a 64^3 mesh-point program. It is hoped that a 64^3 mesh-point problem will be standard for the ILLIAC IV computer, which will be operational in the near future.

B. Objective of Study

The main objective of this study is to apply new ideas, pointed out by Leonard (1974), to basic turbulent shear flows. According to this approach, the averaging operator is defined as the convolution integral of a normalized filtering function $g(\underline{x})$ and the quantities to be averaged. This definition relates, in a clear way, the actual instantaneous field and the averaged field. Turbulent shear flows, which exist in most natural and technological flows, exhibit peculiar characteristics dominated by the interaction of the turbulence and the mean shear. When rotation is imposed on the flow, additional effects are introduced. It is the purpose of this study to try to understand the basic characteristics of such flows by means of a numerical simulation. The numerical method adopted in this work is the finite-difference approach in real space, chosen with a view of extending it in the future to problems of practical interest, which involve nonsimple geometry.

In the course of study, a new fourth-order accurate finite-difference scheme is proposed to represent the averaged advective term $\partial/\partial x_j\ (\bar{u}_i\bar{u}_j)$. This scheme exhibits several advantages over existing schemes. It is compact, thus reducing programming complexity and computation time, and gives better resolution for high wave-number waves in the solution of the Poisson equation. In addition, it can be applied to boundaries other than periodic in a convenient way. The subgrid scale model is represented by the eddy-viscosity hypothesis with a coefficient variable in space and time of the form suggested by Smagorinsky (1963). The number of mesh points used is 16^3, which gives limited resolution but proved to be of a good size with regard to the efficient use of the CDC 7600 computer. Three examples are worked out in detail:

1. Decay of isotropic turbulence. This problem serves as a test for the proposed numerical scheme. Comparison of numerical results to experimental data (Comte-Bellot and Corrsin, 1971) shows satisfactory agreement. This brings us to the conclusion that the numerical method properly distributes the turbulent energy among different wave numbers, with the proper energy decay rate.

2. Homogeneous turbulent shear flow. Numerical results confirm experimental data given by Champagne, et al. (1970) and Harris (1974) which show departure from isotropy and growth of length scales in the direction of shear as the result of the presence of mean shear.
3. Homogeneous turbulent shear flow with system rotation. Numerical results show clearly the effect of rotation on the stability of turbulence, as was shown experimentally by Johnston (1974).

The numerical simulation of the model equations of turbulence given in this work proves to be a convenient way for extracting useful information on the physics of a variety of basic turbulent flows, and extends considerably the existing experimental data for these flows.

CHAPTER 2

MATHEMATICAL FORMULATION

The basic equations for the following analysis are the Navier-Stokes equations for an incompressible fluid:

$$\frac{\partial u_i(\underline{x},t)}{\partial t} = -\frac{\partial}{\partial x_j}(u_i u_j) - \frac{1}{\rho}\frac{\partial p}{\partial x_i} + \nu \frac{\partial^2 u_i}{\partial x_j \partial x_j} \quad i=1,2,3 \qquad (2\text{-}1)$$

$$\frac{\partial u_i}{\partial x_i} = 0 \qquad (2\text{-}2)$$

where u_i , p , ρ , ν are the velocity, pressure, density, and kinematic viscosity, respectively. The summation convention is implied.

In principle, any incompressible flow is completely determined by the solution of these equations, provided boundary and initial conditions are specified. Actually, analytical solutions exist only for a few special cases, and one must resort to approximate solutions, by assuming steady-state behavior, by assuming two-dimensionality, or by dropping terms which are estimated to be small by an 'order of magnitude' analysis, etc., or one must resort to numerical methods. One of the major difficulties arising in numerical calculations of turbulent flows is the wide range of length scales presented in the flow. Any numerical method is limited by its own nature, namely, it can represent only a finite range of length scales. The maximum wave-number that can be resolved on a grid of points a distance h apart is $k_{max} = \pi/h$, and "honest" numerical calculation of turbulence for high or even moderate Reynolds numbers, requires a number of mesh points which is far behind the capability of today's computers.

As an example, consider the problem of grid-generated isotropic turbulence (Comte-Bellot, and Corrsin, 1971). The reported Reynolds number based on Taylor microscale λ and RMS turbulent velocity level is in the range of $Re_\lambda \sim 60$ to 70. The Kolmogorov wave-number, at which molecular dissipation occurs, is $k_K = 34\ cm^{-1}$. The wave-number which corresponds to the location of the energy peak in the three-dimensional

energy spectrum is $k_E = 0.5\ cm^{-1}$. The number of mesh points required to describe all scales by Fourier methods is therefore at least

$$N = \frac{1}{\sqrt{3}} [2(k_K/k_E)]^3 \sim 1.45\times10^6 \tag{2-3}$$

If finite-difference methods are used, at least eight points are needed to describe a wave in the same order of accuracy as by the Fourier methods (Orszag, 1969), and the number of points increases to $N \sim 10^8$.

Our approach to overcome this difficulty is to average Eqs. (2-1) and (2-2). By doing so we give up the chance of resolving all scales of motion. Only the large eddy structure of turbulence is calculated, while the subgrid components of motion are modeled.

One convenient way of averaging is space averaging over small regions compared to the size of the computational region. If $f(\underline{x})$ is any function of position, then the averaged function $\overline{f}(\underline{x})$ is defined as the convolution integral of $f(\underline{x})$ with a filtering function $g(\underline{x})$ (Leonard, 1974):

$$\overline{f}(\underline{x}) = g * f = \int_{\text{all space}} g(\underline{x}-\underline{x}')f(\underline{x}')d\underline{x}' \tag{2-4}$$

If g is square integrable, this operator has the property

$$\frac{\partial\overline{f}}{\partial x_i} = \overline{\frac{\partial f}{\partial x_i}} \tag{2-5}$$

(for a proof see Appendix A).

Applying definition (2-4) to Eqs. (2-1) and (2-2) and using property (2-5) gives

$$\frac{\partial\overline{u}_i}{\partial t} = -\frac{\partial}{\partial x_j}(\overline{u_i u_j}) - \frac{1}{\rho}\frac{\partial\overline{p}}{\partial x_i} + \nu\frac{\partial^2\overline{u}_i}{\partial x_j\partial x_j} \tag{2-6}$$

$$\frac{\partial\overline{u}_i}{\partial x_i} = 0 \tag{2-7}$$

The difference between the local velocity u_i and its averaged value $\bar{u}_i$ is due mostly to the high wave-number part of the flow which cannot be included directly in the computations. If we set $u_i' = u_i - \bar{u}_i$ and substitute into the term $(\overline{u_i u_j})$, we obtain

$$\overline{u_i u_j} = \overline{\bar{u}_i \bar{u}_j} + \overline{u_i' \bar{u}_j} + \overline{\bar{u}_i u_j'} + \overline{u_i' u_j'} \tag{2-8}$$

The last three terms in Eq. (2-8) represent the subgrid scales and must be modeled in terms of the resolvable part of the velocity field, in order to close the equations. A convenient way of modeling these terms is by means of a local eddy-viscosity model. We define a stress tensor

$$\sigma_{ij} = \overline{u_i' \bar{u}_j} + \overline{\bar{u}_i u_j'} + \overline{u_i' u_j'} \tag{2-9}$$

We further subtract the trace from σ_{ij} to define the stress tensor of the subgrid scales as

$$\tau_{ij} = -(\sigma_{ij} - \frac{1}{3}\sigma_{kk}\delta_{ij}) \tag{2-10}$$

Substitution of Eq. (2-10) into Eq. (2-6) gives

$$\frac{\partial \bar{u}_i}{\partial t} = -\frac{\partial}{\partial x_j}(\overline{\bar{u}_i \bar{u}_j}) - \frac{\partial}{\partial x_i}(\bar{p}/\rho + 1/3\,\sigma_{kk}) + \frac{\partial}{\partial x_j}\tau_{ij} + \nu\frac{\partial^2 \bar{u}_i}{\partial x_j \partial x_j} \tag{2-11}$$

The term $(\bar{p}/\rho + 1/3\sigma_{kk})$ is a generalized pressure and will be designated simply as $\bar{p}$ from now on.

τ_{ij} is modeled by an eddy-viscosity hypothesis,

$$\tau_{ij} = 2K\bar{s}_{ij} \tag{2-12}$$

where

$$\bar{s}_{ij} = \frac{1}{2}\left(\frac{\partial \bar{u}_i}{\partial x_j} + \frac{\partial \bar{u}_j}{\partial x_i}\right) \tag{2-13}$$

K is a proportionality constant with the dimensions $(\text{length})^2/\text{time}$.

Following Smagorinsky (1963), K is defined to be proportional to the magnitude of the local rate-of-strain tensor of the large structure. To make K dimensionally consistent, a length scale should be introduced into the definition, and if we take it to be the mesh spacing h, then

$$K = (ch)^2(2\bar{s}_{ij}\,\bar{s}_{ij})^{1/2} \tag{2-14}$$

Lilly (1966) estimated the model constant to be $c = 0.22$ by assuming that the wave number π/h lies in the inertial subrange in an isotropic turbulence problem. However, Deardorff (1970), in his channel flow simulation, has found that the constant must be modified downward by about 50%. Later in this work, this constant will be assessed, based on our numerical results.

Another model, which is similar, at least in the numerical complexity, to the above model is the vorticity model, where K is proportional to the magnitude of the local vorticity:

$$K = (ch)^2(\bar{\omega}_i\bar{\omega}_i)^{1/2} \tag{2-15}$$

where $\bar{\omega}_i$ is given by

$$\bar{\omega}_i = \varepsilon_{ijk}\frac{\partial\bar{u}_k}{\partial x_j} \tag{2-16}$$

In a recent simulation of isotropic turbulence (Kwak, et al., 1975), both models were used and no major differences were found. Based on this experience, we shall use Smagorinsky's model throughout this work.

Since dissipation due to molecular interaction is much smaller than dissipation due to turbulence, the term $\partial^2\bar{u}_i/\partial x_j\partial x_j$ appearing in Eq. (2-6) will be excluded. To maintain incompressibility, we shall use a Poisson equation instead of Eq. (2-7). This equation is derived by taking the divergence of Eq. (2-6) and using Eq. (2-7) to eliminate some of the terms.

After all these modifications the model equations are reduced to the following set:

$$\frac{\partial \bar{u}_i}{\partial t} = -\frac{\partial}{\partial x_j}\left(\overline{\bar{u}_i \bar{u}_j}\right) - \frac{\partial}{\partial x_i}\bar{p} + \frac{\partial}{\partial x_j}\tau_{ij} = s_i \tag{2-17}$$

$$\frac{\partial^2 \bar{p}}{\partial x_i \partial x_i} = -\frac{\partial}{\partial x_i}\frac{\partial}{\partial x_j}\left(\overline{\bar{u}_i \bar{u}_j}\right) + \frac{\partial}{\partial x_i}\frac{\partial}{\partial x_j}\tau_{ij} = q \tag{2-18}$$

CHAPTER 3

FINITE-DIFFERENCE FORMULATION

A. General Considerations

The major difficulty arising in the solution of the averaged set of equations formulated in Chapter 2 is treatment of the term $\partial/\partial x_j\ (\overline{\bar{u}_i\bar{u}_j})$. One approach suggested by Leonard (1974) is first to expand $\overline{\bar{u}_i\bar{u}_j}$ in a Taylor series around $\bar{u}_i\bar{u}_j$. If a symmetrical filter is used in the definition

$$\frac{\partial}{\partial x_j}\,(\overline{\bar{u}_i\bar{u}_j}) = \frac{\partial}{\partial x_j}\int g(\underline{x}-\underline{x}')\ \bar{u}_i(\underline{x}')\ \bar{u}_j(\underline{x}')\ d\underline{x}' \tag{3-1}$$

the result is

$$\frac{\partial}{\partial x_j}\,(\overline{\bar{u}_i\bar{u}_j}) = \frac{\partial}{\partial x_j}\,(\bar{u}_i\bar{u}_j) + \frac{\Delta^2}{\gamma}\,\frac{\partial^2}{\partial x_\ell \partial x_\ell}\,\frac{\partial}{\partial x_j}\,(\bar{u}_i\bar{u}_j) + O(\Delta^4) \tag{3-2}$$

where Δ is the averaging length scale, and the constant γ depends on the particular filtering function $g(\underline{x})$. For example, a Gaussian filter defined by

$$g(\underline{x}) = \left[\left(\frac{6}{\pi}\right)^{1/2}\frac{1}{\Delta}\right]^3 \exp(-6\ |\underline{x}|^2/\Delta^2) \tag{3-3}$$

gives the value $\gamma = 24$. The second term of the RHS of Eq. (3-2) is the so-called "Leonard term." As we shall see, this term contributes substantially in controlling the proper energy transfer among the eddy scales, and therefore should be accounted for in the numerical calculations.

In general, any finite-difference scheme which is applied to the incompressible Navier-Stokes equations must have certain integral conservation properties, if longtime integrations are required. The minimum requirements are mass, momentum, and energy conservation, which means that in the absence of dissipation and truncation errors caused by the time-differencing scheme, the method should have the following properties:

$$\sum_p (D)_i \, u_i = 0 \tag{3-4}$$

$$\frac{\partial}{\partial t} \sum_p u_i = 0 \qquad i = 1,2,3 \tag{3-5}$$

$$\frac{\partial}{\partial t} \sum_p u_i u_i = 0 \tag{3-6}$$

where $\sum_p$ is the sum over all mesh points in an infinite (or periodic) domain, and $(D)_i$ is the finite-difference operator for the first derivative in the ith direction. Mass conservation is controlled by a Poisson equation, and a discussion of this property will be given in section C of this chapter. It can be shown easily that conditions (3-5) and (3-6) impose the following requirements on the advective term:

$$\sum_p (D)_j \, (u_i u_j) = 0 \qquad i = 1,2,3 \tag{3-7}$$

$$\sum_p u_i (D)_j \, (u_i u_j) = 0 \tag{3-8}$$

In the past, two common second-roder schemes have been used to implement these requirements. The first one uses a regular mesh configurations where the variables u_i, p are defined in the same location. This scheme is given by

$$\frac{\partial}{\partial x_j} (u_i u_j) = \frac{1}{2}\left[(D_o)_j (u_i u_j) + u_i (D_o)_j u_j + u_j (D_o)_j u_i\right] + O(h^2) \tag{3-9}$$

where $(D_o)_j$ is the central-difference operator defined by (one dimension)

$$(D_o) \, u_n = (u_{n+1} - u_{n-1})/2h \tag{3-10}$$

The second method uses a staggered-mesh configuration with the variables u_i, p defined as shown in Fig. 3-1. We will give the formulas for this case later.

It was shown by Leonard (1974) that if the averaged equations are used and the term $\partial/\partial x_j\ (\overline{\bar{u}_i\bar{u}_j})$ is expanded as in Eq. (3-2), the Leonard term is nonconservative, and preliminary estimates have shown that this term has a significant part in energy extraction from large scales. However, the term $\partial/\partial x_j\ (\bar{u}_i\bar{u}_j)$ is conservative. Since the Leonard is of $O(h^2)$, a straightforward approach to retain it in a numerical calculation is to use a fourth-order finite-difference scheme for the term $\partial/\partial x_j\ (\bar{u}_i\bar{u}_j)$ and a second-order scheme for

$$\frac{\Delta^2}{\gamma}\frac{\partial^2}{\partial x_\ell \partial x_\ell}\frac{\partial}{\partial x_j}(\bar{u}_i\bar{u}_j) \quad .$$

One possible realization which maintains properties (3-7) and (3-8) for the term $\partial/\partial x_j\ (\bar{u}_i\bar{u}_j)$ is as follows.

The fourth-order scheme for the term $\partial/\partial x_j\ (\bar{u}_i\bar{u}_j)$ is obtained by Richardson's extrapolation (Richardson, 1927). By applying the operator defined by Eq. (3-9) to a mesh with 2h spacing, and then combining the scheme derived for h with that for 2h with weights 4/3 and -1/3 , respectively, we have

$$\begin{aligned}\frac{\partial}{\partial x_j}(\bar{u}_i\bar{u}_j) = {} & \frac{4}{3}\left\{\frac{1}{2}\left[(D_o)_{j,h}(\bar{u}_i\bar{u}_j) + \bar{u}_i(D_o)_{j,h}\,\bar{u}_j + \bar{u}_j(D_o)_{j,h}\,\bar{u}_i\right]\right\} \\ & - \frac{1}{3}\left\{\frac{1}{2}\left[(D_o)_{j,2h}(\bar{u}_i\bar{u}_j) + \bar{u}_i(D_o)_{j,2h}\,\bar{u}_j + \bar{u}_j(D_o)_{j,2h}\,\bar{u}_i\right]\right\} + O(h^4)\end{aligned} \tag{3-11}$$

In order to get the Leonard term, the Laplacian $\partial^2/\partial x_\ell \partial x_\ell$ is approximated by the second-order operator $(D_+D_-)_i$, where for one dimension we have

$$(D_+)\ u_n = (u_{n+1} - u_n)/h \tag{3-12}$$

$$(D_-)\ u_n = (u_n - u_{n-1})/h \tag{3-13}$$

$$(D_+D_-)\ u_n = (u_{n+1} - 2u_n + u_{n-1})/h^2 \tag{3-14}$$

The finite-difference scheme for the Poisson equation in this realization is given by

$$\left[({}_4D_o{}_4D_o)_x + ({}_4D_o{}_4D_o)_y + ({}_4D_o{}_4D_o)_z\right] p = q \qquad (3\text{-}15)$$

where ${}_4D_o$ is the fourth-order central-difference operator defined by (one dimension)

$$({}_4D_o)u_n = (-u_{n+2} + 8u_{n+1} - 8u_{n-1} + u_{n-2})/12h \qquad (3\text{-}16)$$

This method has been used successfully in a recent numerical simulation of turbulence (Kwak, et al., 1975). However, it has two major drawbacks:

1. The scheme extends four points in the major directions away from the point to which it is applied. This makes the method inconvenient to apply in problems with boundary conditions that are not periodic.
2. It gives poor resolution for high wave-numbers in the solution of the Poisson equation, as we shall see in section C of this chapter.

In the following, a new finite-difference scheme is proposed, which removes some of these difficulties. The scheme is compact, it uses information from adjacent points only, and the Poisson solver follows the exact solution more closely. In addition, a reduction in computation time is achieved.

B. The Space-Differencing Scheme

Consider the one-dimensional advective term

$$\frac{d}{dx}(\overline{\bar{u}\bar{u}}) = \frac{d}{dx}(\bar{u}\bar{u}) + \frac{\Delta^2}{\gamma}\frac{d^2}{dx^2}\frac{d}{dx}(\bar{u}\bar{u}) \qquad (3\text{-}17)$$

If we choose $\Delta^2/\gamma = h^2/6$, we can approximate this term by the central-difference operator D_o with fourth-order error term:

$$\frac{d}{dx}(\bar{u}\bar{u}) + \frac{h^2}{6}\frac{d^2}{dx^2}\frac{d}{dx}(\bar{u}\bar{u}) = D_0(\bar{u}\bar{u}) + O(h^4) \tag{3-18}$$

One can interpret this result as follows. The usual central-difference operator, which is second-order accurate for the first derivative, is fourth-order accurate for the entire advective term, provided an appropriate filtering function is chosen. The coefficient $h^2/6$ corresponds to a 2h-width filter, i.e., the filter width Δ is twice the width of the mesh size h.

This idea can be extended to higher dimensions, but the scheme turns out to introduce instabilities due to energy nonconservation. To overcome this difficulty, a staggered-mesh configuration is used. For two dimensions the variables are defined at the points shown in Fig. 3-1. The x-momentum equation is enforced on control volumes surrounding the points (i+1/2,j), the y-momentum equation about (i,j+1/2), and the Poisson equation for the pressure about the points (i,j). Using this configuration we define a new finite-difference operator to represent the advective term. This follows the idea of Eq. (3-18), i.e., the use of a lower-order finite-difference scheme, having a truncation error that matches the Leonard term, to represent the entire advective term to a higher order of accuracy. If $f = \bar{u}_i\bar{u}_j$, this operator is given by

$$\frac{\partial}{\partial x}\bar{f}_{i,j,k} \simeq \alpha D_x f_{i,j,k} + \frac{1-\alpha}{4} D_x(f_{i,j+1/2,k} + f_{i,j-1/2,k} + f_{i,j,k+1/2} + f_{i,j,k-1/2}) \tag{3-19}$$

where

$$D_x f_{i,j,k} = (f_{i+1/2,j,k} - f_{i-1/2,j,k})/h \tag{3-20}$$

To make it clear, we expand the advective terms of the two-dimensional case.

x-momentum equation:

$$\frac{\partial}{\partial x}\,(\overline{\bar{u}\bar{u}})_{i+1/2,j} \simeq \alpha D_x(\bar{u}\bar{u})_{i+1/2,j} + \frac{1-\alpha}{2}\,D_x\left[(\bar{u}\bar{u})_{i+1/2,j+1/2} + (\bar{u}\bar{u})_{i+1/2,j-1/2}\right] \tag{3-21}$$

$$\frac{\partial}{\partial y}\,(\bar{u}\bar{v})_{i+1/2,j} \simeq \alpha D_y(\bar{u}\bar{v})_{i+1/2,j} + \frac{1-\alpha}{2}\,D_y\left[(\bar{u}\bar{v})_{i+1,j} + (\bar{u}\bar{v})_{i,j}\right] \tag{3-22}$$

y-momentum equation:

$$\frac{\partial}{\partial x}\,(\bar{v}\bar{u})_{i,j+1/2} \simeq \alpha D_x(\bar{v}\bar{u})_{i,j+1/2} + \frac{1-\alpha}{2}\,D_x\left[(\bar{v}\bar{u})_{i,j+1} + (\bar{v}\bar{u})_{i,j}\right] \tag{3-23}$$

$$\frac{\partial}{\partial y}\,(\bar{v}\bar{v})_{i,j+1/2} \simeq \alpha D_y(\bar{v}\bar{v})_{i,j+1/2} + \frac{1-\alpha}{2}\,D_y\left[(\bar{v}\bar{v})_{i+1/2,j+1/2} + (\bar{v}\bar{v})_{i-1/2,j+1/2}\right] \tag{3-24}$$

Since in the staggered-mesh configuration not all variables are available at points where they are needed, averages are to be taken from adjacent points. For example,

$$(\bar{u}\bar{v})_{i+1/2,j+1/2} \simeq (\bar{u}_{i+1/2,j} + \bar{u}_{i+1/2,j+1})(\bar{v}_{i,j+1/2} + \bar{v}_{i+1,j+1/2})/4 \tag{3-25}$$

Using these averages in the proposed scheme, and expanding in a Taylor series about the points to which the scheme is applied, we obtain the following (two representative terms are given; other terms can be obtained by analogy):

finite-difference scheme of $\frac{\partial}{\partial x}(\overline{\bar{u}\bar{u}}) = 2\bar{u}\bar{u}_x +$

$$+ \frac{h^2}{12}\Big[6\bar{u}_x\bar{u}_{xx} + 4\bar{u}\bar{u}_{xxx} + 3(1-\alpha)(\bar{u}\bar{u}_{xyy}$$

$$+ \bar{u}\bar{u}_{xzz} + \bar{u}_x\bar{u}_{yy} + \bar{u}_x\bar{u}_{zz} + \bar{u}_y\bar{u}_{xy} + \bar{u}_z\bar{u}_{xz})\Big] + 0(h^4)$$

(3-26)

finite-difference scheme of $\frac{\partial}{\partial y}(\overline{\bar{u}\bar{v}}) = \bar{u}\bar{v}_y + \bar{u}_y\bar{v} +$

$$+ \frac{h^2}{12}\Big[(3\alpha+1)(\frac{3}{2}\bar{u}_y\bar{v}_{xx} + \frac{3}{2}\bar{u}\bar{v}_{xxy} + \frac{3}{2}\bar{u}_y\bar{v}_{yy}$$

$$+ \frac{1}{2}\bar{u}\bar{v}_{yyy} + 2\bar{u}_{yyy}\bar{v} + 3\bar{u}_{yy}\bar{v}_y)$$

$$+ \frac{3}{2}(1-\alpha)(\bar{u}_{xy}\bar{v}_x + \bar{u}_x\bar{v}_{xy} + \bar{u}_{xxy}\bar{v} + \bar{u}_{xx}\bar{v}_y$$

$$+ \bar{u}_y\bar{v}_{zz} + \bar{u}\bar{v}_{zzy} + \bar{v}_z\bar{u}_{yz} + \bar{u}_z\bar{v}_{yz} + \bar{v}\bar{u}_{zzy}$$

$$+ \bar{v}_y\bar{u}_{zz})\Big] + 0(h^4) \qquad (3\text{-}27)$$

The exact expansion of the desired terms is

$$\frac{\partial}{\partial x}(\overline{\bar{u}\bar{u}}) = 2\bar{u}\bar{u}_x + \frac{\Delta^2}{\gamma}\Big[6\bar{u}_x\bar{u}_{xx} + 2\bar{u}\bar{u}_{xxx} + 2\bar{u}\bar{u}_{xyy} + 2\bar{u}\bar{u}_{xzz}$$

$$+ 2\bar{u}_x\bar{u}_{yy} + 2\bar{u}_x\bar{u}_{zz} + 2\bar{u}_y\bar{u}_{xy} + 2\bar{u}_z\bar{u}_{xz}\Big] \qquad (3\text{-}28)$$

$$\frac{\partial}{\partial y}(\overline{\bar{u}\bar{v}}) = \bar{u}\bar{v}_y + \bar{u}_y\bar{v} + \frac{\Delta^2}{\gamma}\Big[\bar{u}_y\bar{v}_{xx} + \bar{u}\bar{v}_{xxy} + 3\bar{u}_y\bar{v}_{yy}$$

$$+ \bar{u}\bar{v}_{yyy} + \bar{u}_{yyy}\bar{v} + 3\bar{u}_{yy}\bar{v}_y + 2\bar{u}_{xy}\bar{v}_x + 2\bar{u}_x\bar{v}_{xy} + \bar{u}_{xxy}\bar{v}$$

$$+ \bar{u}_{xx}\bar{v}_y + \bar{u}_y\bar{v}_{zz} + \bar{u}\bar{v}_{zzy} + 2\bar{v}_z\bar{u}_{yz} + 2\bar{u}_z\bar{v}_{yz} + \bar{v}\bar{u}_{zzy} + \bar{v}_y\bar{u}_{zz}\Big] \tag{3-29}$$

By comparing the finite-difference scheme, Eqs. (3-26) and (3-27), to the exact expansion of the advective term, Eqs. (3-28) and (3-29), it can be seen that for $\alpha \neq 1$ all terms of the finite-difference scheme occur in the exact expansion with different multiplicative constants. In other words, the proposed scheme contains a Leonard term, with filtering properties which depend on the numerical constant α. It is impossible to find a simple expression for this equivalent filter in terms of α, but one can put upper and lower bounds for Δ^2/γ for any value of α. For example, if $\alpha = 1/3$, the scheme represents a filter with

$$\frac{h^2}{24} < \frac{\Delta^2}{\gamma} < \frac{h^2}{3} \quad ,$$

or, in terms of the Gaussian filter, the width of the filter is between h and $2\sqrt{2}\,h$ with most of the terms corresponding to $\Delta = \sqrt{2}\,h$. When $\alpha = 1$, the scheme reduces to the staggered-mesh scheme first introduced by Fromm (1963).

Other terms appearing in the governing equations are finite-differenced in the usual way, for example,

$$\left(\frac{\partial p}{\partial x}\right)_{i+1/2,j,k} = (P_{i+1,j,k} - P_{i,j,k})/h \tag{3-30}$$

The eddy-viscosity coefficient K is evaluated at the same place as the pressure p (see Fig. 3-1).

The complete expansion of the filtered advective term according to Eq. (3-19) is given in Appendix D.

C. The Finite-Difference Poisson Equation

The present work revealed the fact that, in the incompressible case, the finite-difference scheme for the Poisson equation cannot be chosen independently. The difference method used in the equations of motion dictate a particular scheme for the Poisson equation. Otherwise, a nonstable solution is obtained due to a rapid growth of kinetic energy. This is true even if a higher-order method is used for the Poisson equation.

To exemplify this fact, consider Euler's equation.

$$\frac{du_i}{dt} = -\frac{1}{\rho}\frac{\partial p}{\partial x_i} \tag{3-31}$$

where d/dt is the substantial derivative. Multiply Eq. (3-31) by u_i and integrate over all space:

$$\frac{1}{2}\int \frac{d}{dt}(u_i u_i)\, d\underline{x} = -\frac{1}{\rho}\int u_i \frac{\partial p}{\partial x_i}\, d\underline{x} \tag{3-32}$$

Integration by parts of the RHS of Eq. (3-32) gives

$$-\frac{1}{\rho}\int u_i \frac{\partial p}{\partial x_i}\, d\underline{x} = -\frac{1}{\rho}(u_i p)\Big|_\infty + \frac{1}{\rho}\int p \frac{\partial u_i}{\partial x_i}\, d\underline{x} \tag{3-33}$$

Since the contribution of $u_i p$ at infinity is zero, and $\partial u_i/\partial x_i = 0$ for an incompressible fluid, we have

$$\frac{1}{2}\int \frac{d}{dt}(u_i u_i)\, d\underline{x} = 0 \tag{3-34}$$

or, the kinetic energy per unit mass is conserved. The finite-difference form of the RHS of Eq. (3-32) is

$$-\frac{1}{\rho}\sum_p u_i (D_i p) \tag{3-35}$$

We use the finite-difference analog of integration by parts to expand this term:

$$-\frac{1}{\rho}\sum_p u_i (D_i p) = -\frac{1}{\rho}(u_i p)\Big|_\infty + \frac{1}{\rho}\sum_p p(D_i u_i) \tag{3-36}$$

Each term in the RHS of Eq. (3-36) is equal to zero and energy is conserved.

The use of integration by parts in a finite-difference form is consistent only if the operators of the expressions $(D_i p)$ and $(D_i u_i)$ are identical. Therefore, a choice of an operator for the pressure-gradient term $(D_i p)$ in the equations of motion forces us to choose the same operator for the divergence term $(D_i u_i)$, which brings us to the conclusion that the proper Poisson operator should be in the form

$$\frac{\partial^2}{\partial x_i^2} \sim D_i D_i \tag{3-37}$$

To derive the Poisson operator for a staggered-mesh, one additional fact has to be taken into account, namely, that the variables u_i are out of phase by half the mesh size relative to the pressure p. Since a computational cell (see Fig. 3-1) is defined as

$$\begin{aligned} u(I,J,K) &= u_{i+1/2,j,k} \\ v(I,J,K) &= v_{i,j+1/2,k} \\ w(I,J,K) &= w_{i,j,k+1/2} \\ p(I,J,K) &= p_{i,j,k} \end{aligned} \tag{3-38}$$

we find that a second-order operator for $\partial p/\partial x$, which appears in the equations of motion, is given by

$$\left(\frac{\partial p}{\partial x}\right)_{i+1/2,j,k} \sim \Big[p(I+1,J,K) - p(I,J,K)\Big]/h = (D_+)_x\, p \tag{3-39}$$

and a second-order divergence operator for $\partial u/\partial x$ is given by

$$\left(\frac{\partial u}{\partial x}\right)_{i,j,k} \sim \Big[u(I,J,K) - u(I-1,J,K)\Big]/h = (D_-)_x u \tag{3-40}$$

Therefore, a consistent second-order Poisson operator is given by

$$\left(\frac{\partial}{\partial x}\frac{\partial p}{\partial x}\right)_i \sim \left[P(I+1,J,K) - 2p(I,J,K) + p(I-1,J,K)\right]/h^2 = (D_+D_-)_x p \tag{3-41}$$

and the entire finite-difference Poisson equation is then

$$\left[(D_+D_-)_x + (D_+D_-)_y + (D_+D_-)_z\right] p = q \tag{3-42}$$

It is possible to derive higher-order operators for $\partial p/\partial x$ and $\partial u/\partial x$ compatible with each other. For example, a fourth-order Poisson operator is derived from the following pair:

$$\left(\frac{\partial p}{\partial x}\right)_{i+1/2,j,k} \sim \left[-p(I+2,J,K) + 27p(I+1,J,K) - 27p(I,J,K) + p(I-1,J,K)\right]/24h \tag{3-43}$$

$$\left(\frac{\partial u}{\partial x}\right)_{i,j,k} \sim \left[-u(I+1,J,K) + 27u(I,J,K) - 27u(I-1,J,K) + u(I-2,J,K)\right]/24h \tag{3-44}$$

and the Poisson operator is given by

$$\left(\frac{\partial}{\partial x}\frac{\partial p}{\partial x}\right)_i \sim \left[p(I+3,J,K) - 54p(I+2,J,K) + 783p(I+1,J,K) - 1460p(I,J,K) + 783p(I-1,J,K) - 54p(I-2,J,K) + p(I-3,J,K)\right]/576h^2 \tag{3-45}$$

If we define the RHS of Eqs. (3-43) and (3-44), respectively, as $({}_4D_+)_x p$ and $({}_4D_-)_x u$, the finite-difference Poisson equation will have the symbolic form

$$\left[({}_4D_{+4}D_-)_x + ({}_4D_{+4}D_-)_y + ({}_4D_{+4}D_-)_z\right] p = q \tag{3-46}$$

In order to assess the relative accuracy of these operators, it is customary to compare them with the exact Fourier transform. Fourier transforming the various one-dimensional finite-difference Poisson operators and the continuous operator $\partial^2/\partial x^2$ and plotting the transformed coefficients versus the nondimensional wave number kh, Fig. 3-2, one can see the relative distortion introduced in the solution by the different schemes. The fourth-order regular-mesh curve represents Eq. (3-15). As is seen, the staggered-mesh configuration shows a substantial advantage over the regular mesh. For $kh > 0.25$ the difference between the fourth-order regular mesh and the exact Fourier method tends to grow sharply, while the staggered-mesh curves trace the exact solution much more closely.

In this work, we shall use the second-order Poisson operator on a staggered mesh. Although inferior to its fourth-order counterpart, it has the advantage that the scheme extends only one point away from the point to which it is applied.

The actual solution of the Poisson equation is by means of a direct method. The discrete Fourier transform of Eq. (3-42) is given by

$$-\frac{4}{h^2}\left[\sin^2\frac{\pi i}{N} + \sin^2\frac{\pi j}{N} + \sin^2\frac{\pi k}{N}\right]\hat{p} = \hat{q}\ , \quad i,j,k=-\frac{N}{2},\ldots,\frac{N}{2}-1 \tag{3-47}$$

To obtain p, we first transform q into $\hat{q}$, then solve for $\hat{p}$ according to Eq. (3-47), and finally inverse transform $\hat{p}$ to obtain p. The fast Fourier transform algorithm (FFT) is used in the numerical realization. For further details of FFT methods see Cochran, et al. (1967) and Appendix C.

D. The Time-Differencing Scheme

The basic equations of motion can be reduced to the form

$$\frac{\partial \overline{u}_i}{\partial t} = s_i \tag{3-48}$$

where s_i is a complicated nonlinear function evaluated at each time step for every mesh point, by one of the methods described in the previous sections.

This equation, which is parabolic with respect to time, can be solved by methods which are analogous to methods for first-order ordinary differential equations. The existing methods can be classified according to the following criteria: accuracy, stability, one step or multistep, implicit or explicit methods. For extensive treatment of this subject the reader is referred to the book by Gear (1971).

For the present problem two additional criteria were considered, namely, the number of evaluations of s_i per time step, and the amount of storage required. These features are characteristic of problems of large volume and long computation time.

Two commonly used methods, which are second-order accurate and require only one function evaluation per time step, are the leapfrog and the Adams-Bashforth methods. Both are multistep methods and require storage for two time steps. The leapfrog method is given by

$$\bar{u}_i^{(n+1)} = \bar{u}_i^{(n-1)} + 2\,\Delta t\, s_i^{(n)} \tag{3-49}$$

with truncation error

$$-\frac{1}{6}\,\Delta t^2\,\frac{\partial^3 \bar{u}_i}{\partial t^3} \tag{3-50}$$

and the Adams-Bashforth method is given by

$$\bar{u}_i^{(n+1)} = \bar{u}_i^{(n)} + \Delta t(3s_i^{(n)} - s_i^{(n-1)})/2 \tag{3-51}$$

with truncation error

$$-\frac{5}{12}\,\Delta t^2\,\frac{\partial^3 \bar{u}_i}{\partial t^3} \tag{3-52}$$

A linear-stability analysis shows that the Adams-Bashforth method is more stable than the leapfrog method (Lilly, 1965).

In this work we use the Adams-Bashforth method. The time step is chosen to give a Courant number of $N_c = 0.25$ where

$$N_c = \frac{U_{max}\Delta t}{\Delta x} \tag{3-53}$$

U_{max} is the magnitude of the maximum velocity appearing in the problem.

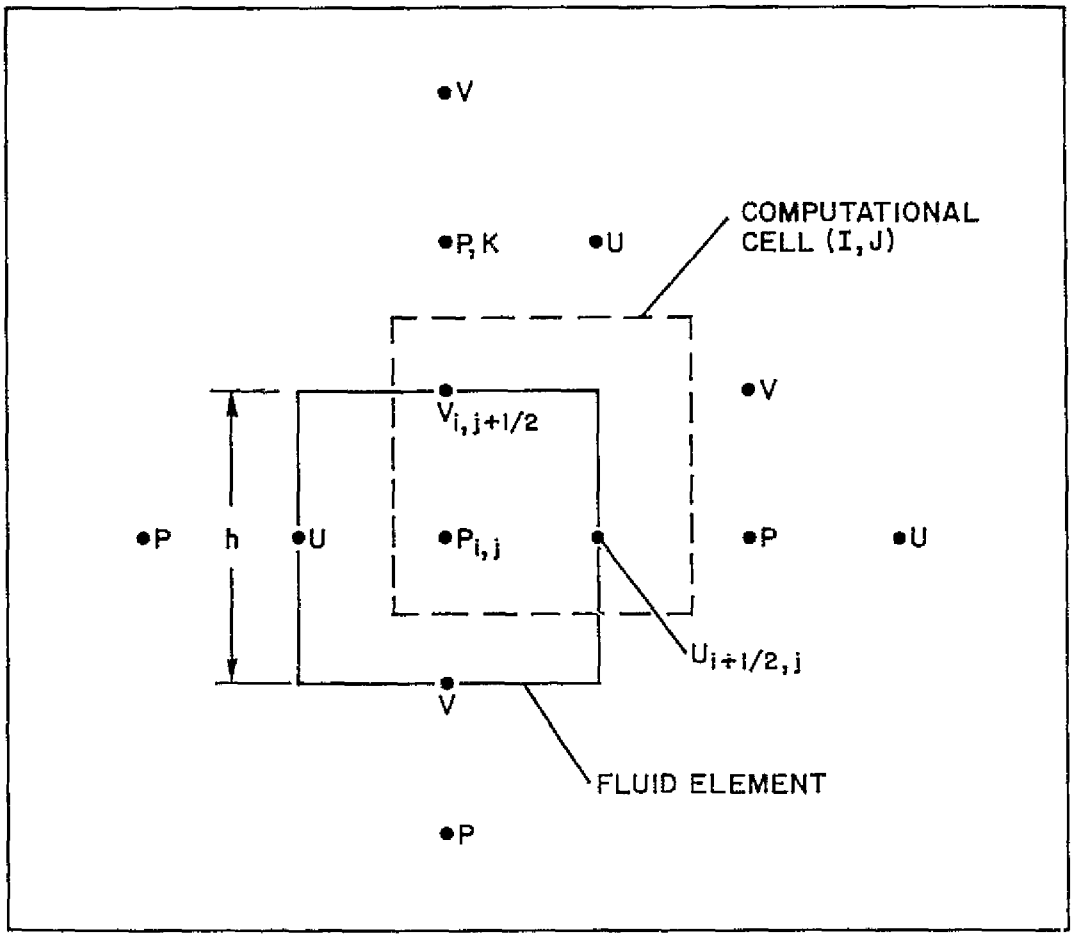

Fig. 3-1. Staggered mesh configuration in two-dimensions.

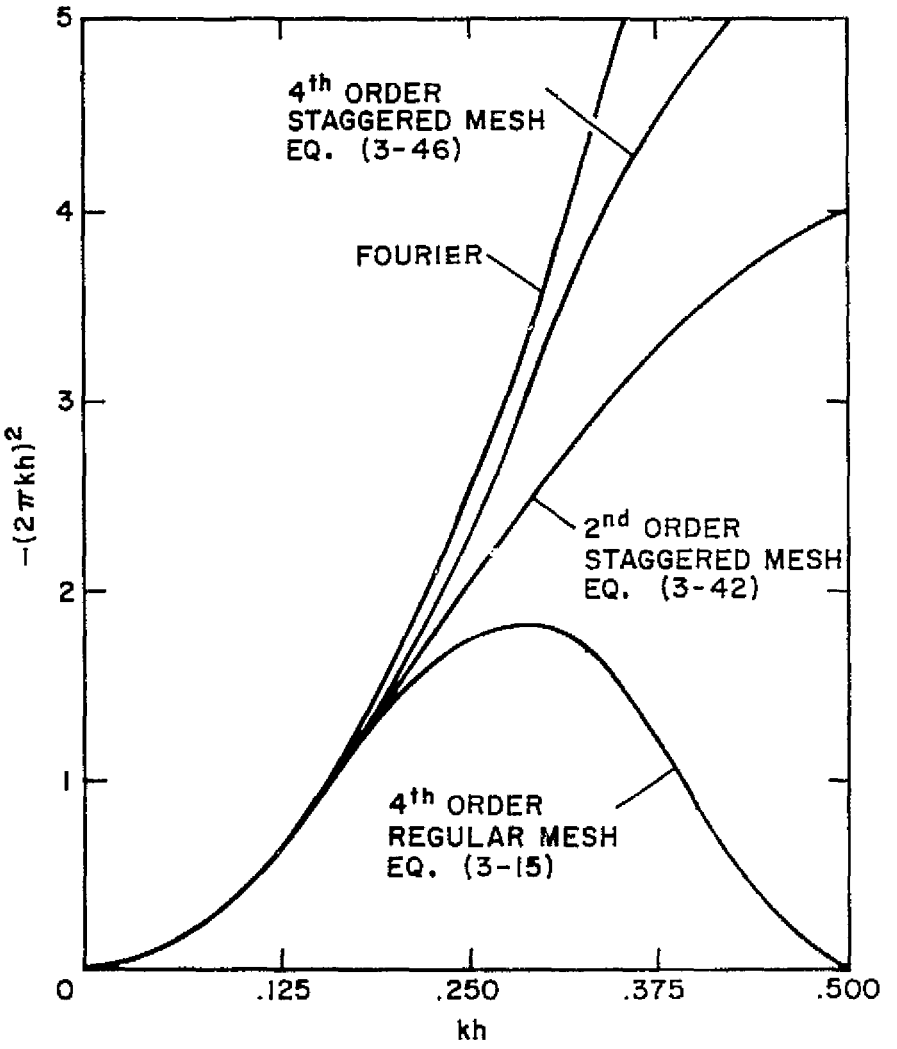

Fig. 3-2. Comparison of second and fourth order Poisson operators to the exact Fourier transform.

CHAPTER 4

DECAY OF ISOTROPIC TURBULENCE

A. General Description

The decay of isotropic trubulence has been chosen as the first problem for numerical simulation. A random-velocity field which satisfies certain correlation and energy properties is specified within a box, and the evolution of this field is observed at later times. This problem, although not of great practical importance, has several attractive properties:

1. There exist experimental data to compare with.
2. The physical processes involved are the simplest of any turbulent flow. Because the mean velocity is zero production terms in the turbulent kinetic energy equation are identically zero and the only processes involved are energy transfer among the wave-numbers and dissipation. Notwithstanding, all terms in the governing equation are used, and can be assessed.
3. Boundary conditions are simple. It is assumed that the domain of numerical integration is sufficiently large compared to any characteristic length associated with the flow field (for example, the integral scale), so that correlations at distances comparable to the size of the box are practically zero. This property allows us to choose convenient periodic conditions for the boundaries.

It should be noted at this point that this problem has also inherent limitations. Since the experimentalists measured only certain gross properties, such as the shape of the three-dimensional energy spectrum and the rate of energy decay, it is obvious that only these properties can be compared with numerical results. Many of the details available in the numerical simulation are averaged out. It is believed, however, that the properties we are comparing with experimental data are the most important ones for this flow, and that, if simulations predict these properties correctly, they represent an actual turbulent flow field closely enough.

Decay of isotropic turbulence also serves as a means of finding the proper value for the model constant c appearing in the subgrid scale model. It is chosen to fit experimental data as close as possible. Another method of determining c from a purely computational experiment is being pursued by Clark (ongoing Ph.D. research, Stanford University).

B. The Experimental Results

The experiment which has been chosen to be simulated is due to Comte-Bellot and Corrsin (1971). Measurements are given for an isotropic turbulent field which is generated in a wind tunnel behind a grid of bars. The Reynolds number based on the Taylor microscale λ and RMS turbulent velocity level is in the range of $Re_\lambda = 60$ to 70, which corresponds to low levels of turbulence. Measurements are taken at three stations downstream in the mean flow direction. Using Taylor's hypothesis, the spatial locations can be regarded as temporal stations with respect to the evolution of homogeneous turbulence with the following relation:

$$\Delta x = U_0 \, \Delta t \tag{4-1}$$

where U_0 is the mean velocity.

At these stations the three-dimensional energy spectrum $E(k,t)$ is given, where $E(k,t)$ is defined as the integral over a spherical shell of radius k of the trace of the spectrum tensor $\Phi_{ij}(\underline{k})$, which is the Fourier transform of the correlation tensor $R_{ij}(\underline{r})$ defined by

$$R_{ij}(\underline{r}) = \langle u_i(\underline{x},t) \, u_j(\underline{x}+\underline{r},t) \rangle \tag{4-2}$$

$\langle \, \rangle$ is an appropriate average (see Tennekes and Lumley, 1972, Chapter 8). In Fourier space this function is given by

$$E(k) = 2\pi k^2 \langle u_i(\underline{k}) \, u_i^*(\underline{k}) \rangle_{\text{spherical shell}} \tag{4-3}$$

It should be noted that the integral of the three-dimensional energy spectrum over the entire wave-number range is equal to the kinetic energy per unit mass

$$\int_0^\infty E(k)dk = \langle u_i(\underline{x})\ u_i(\underline{x}) \rangle /2 \qquad (4\text{-}4)$$

Our aim is to start the numerical simulation with initial conditions that correspond to the experimental data at the first station, then to integrate the equations of motion for the interval of time between stations one and two, and examine and compare numerical results with experimental data for the second station. Two main properties are chosen for comparison, namely, rate of decay of turbulent kinetic energy, and the shape of the three-dimensional energy spectrum. These properties are basic for this problem. Rate of decay shows how good our model for the subgrid scale dissipation is. The shape of the energy spectrum shows how accurately transfer and redistribution of energy among different waves are treated and is an indication of how well the nonlinear terms are represented by the numerical scheme.

Since experimental data are regarded as representing the instantaneous field, while our method filters out the small-scale motion, it is required to filter the experimental data, so that a common basis for comparison is achieved. As was shown in Chapter 3 the proposed numerical scheme for the advective term is representing a filter with two bounds on Δ^2/γ. For a Gaussian filter we have $h < \Delta < 2\sqrt{2}\ h$ with most of the terms corresponding to $\Delta = \sqrt{2}\ h$. If we choose the Gaussian filter with width of $\sqrt{2}\ h$ as representing the filtering process, then the three-dimensional energy spectrum at each station of the experiment would be

$$\overline{E}(k,t) = [\hat{g}(k)]^2\ E(k,t) = \exp(-k^2h^2/6)E(k,t) \qquad (4\text{-}5)$$

This is the energy of the large scales of motion. For a 16^3 mesh problem with $h=2$ cm, the filtered energy spectrum for the first station in the experiment includes about 40% of the turbulence energy.

C. The Initial Velocity Field

The Fourier transform of an isotropic turbulence field of an incompressible fluid should satisfy at least four requirements:

1. incompressibility

$$k_i \bar{u}_i(\underline{k}) = 0 \tag{4-6}$$

2. real field

$$\bar{u}_i(\underline{k}) = \left[\bar{u}_i(-\underline{k})\right]^* \tag{4-7}$$

3. isotropy

$$\langle \bar{u}_i(\underline{k})\ \bar{u}_j(\underline{k})\rangle = 0 \qquad i \neq j \tag{4-8}$$

4. given energy spectrum

$$\bar{u}_i(\underline{k})\ \bar{u}_i^*(\underline{k}) = \bar{E}(k)/2\pi k^2 \tag{4-9}$$

In a numerical simulation, a modification should be made in Eq. (4-6) to account for the representation of derivatives by finite differences. In order to arrive at this modification in a simple way, consider the one-dimensional case. The finite-difference analog to the divergence operator $\partial/\partial x$, which is used in the present work, is $(D_-)_x$, where

$$(D_-)_x\ \bar{u} = (\bar{u}_i - \bar{u}_{i-1})/h \tag{4-10}$$

The Fourier transforms of these operators are

$$\partial/\partial x \xrightarrow{FT} i\ k_x \tag{4-11}$$

$$(D_-)_x \xrightarrow{DFT} \left[(1-\cos\frac{2\pi m}{N}) + i\ \sin\frac{2\pi m}{N}\right]/h \tag{4-12}$$

where N is the number of mesh points in the discrete case, and $m=k_x/2\pi$. The Fourier operator associated with a continuous derivative is a pure imaginary number, while in the discrete case it is a complex number, which depends on the finite-difference scheme used. Therefore, the finite-difference form of the incompressibility condition should be modified to

$$k_i'(\underline{k})\ \bar{u}_i(\underline{k}) = 0 \tag{4-13}$$

where k_i' is a complex vector field dependent on the finite-difference divergence operator D_i . This assures the numerical divergenceless condition in real space,

$$D_i \bar{u}_i(\underline{x}) = 0 \tag{4-14}$$

A method of generating a field which satisfies Eqs. (4-7), (4-8), (4-9), and (4-13) is described in detail in Appendix B. The generated field is periodic in space, since a spectral method is used to generate it.

D. Results and Discussion

In Figs. 4-1 and 4-2 numerical simulation of decay of turbulent energy and three-dimensional energy spectra are compared to experiment for the case of isotropic turbulence with mean velocity of $U_0 = 10^3$ cm/sec behind a grid of bars of diameter $M = 5.08$ cm. The best fit to the experiment was obtained with model constant $c = 0.24$ and numerical constant $\alpha = 1/3$.

Figures 4-3 and 4-4 show the dependence of energy decay and energy spectrum on the numerical constant α . While energy decay differs only slightly for different values of α , the energy spectrum exhibits an irregular distribution in the $\alpha = 1$ case, where energy piles up in the region of high wave-numbers. This case is the staggered-mesh scheme used by Harlow and Welch (1965), Deardorff (1970), and others. The proposed scheme with $\alpha = 1/3$ shows a more regular behavior, which suggests that the Leonard term, which is included implicitly in this scheme, has an important effect on the correct transfer and distribution of energy, and should be included in the numerical scheme for proper simulation, especially in problems in which the energy is spread over a wide range of wave-numbers. This conclusion agrees with that of Kwak, et al. (1975). It is interesting to note that the staggered-mesh scheme with $\alpha = 1$ contains implicitly part of the Leonard term, as can be seen from Eqs. (3-26) and (3-27), and was included in the past in simulations which used this scheme.

Sensitivity to the model constant is shown in Figs. 4-5 and 4-6. The effect of changing c acts mostly on the high wave-number region. The chosen value of $c = 0.24$ is 10% higher than Lilly's theoretical estimate of $c = 0.22$ (Lilly, 1966) and more than twice the value used by Deardorff in the channel simulation; he ran cases with $c = 0.06$ to 0.17 and chose $c = 0.1$ to be a representative value (Deardorff, 1970). Later, in a paper devoted entirely to the problem of the magnitude of c, (Deardorff, 1971), the author suggested that the large difference between his numerical estimates and the value given by Lilly is due to the large-scale valocity shear presented in his flow. Kwak, et al. (1975) have found this constant to be $c = .41$.

Figure 4-7 shows the skewness defined by

$$\bar{S} = \langle \partial^3 \bar{u}/\partial x^3 \rangle \,/\, \langle \partial^2 \bar{u}/\partial x^2 \rangle^{3/2} \qquad (4\text{-}15)$$

for different values of α. This function, which starts practically from zero, reaches a maximum value and then declines monotonically. The maximum value for $\bar{S}$ is in the range based on theoretical estimates (Batchelor, 1953, p. 172). However, $\bar{S}$ depends on the high wave-number part of the spectrum and our result cannot be fairly compared with experiment.

In this chapter a numerical simulation of isotropic turbulence has been shown to be feasible and to give acceptable results. Computation time for a 16^3 mesh-point problem is about two minutes on the CDC 7600 computer. In the following chapters we shall use this method with constants $c = 0.24$ and $\alpha = 1/3$ to simulate homogeneous turbulence in the presence of shear and system rotation.

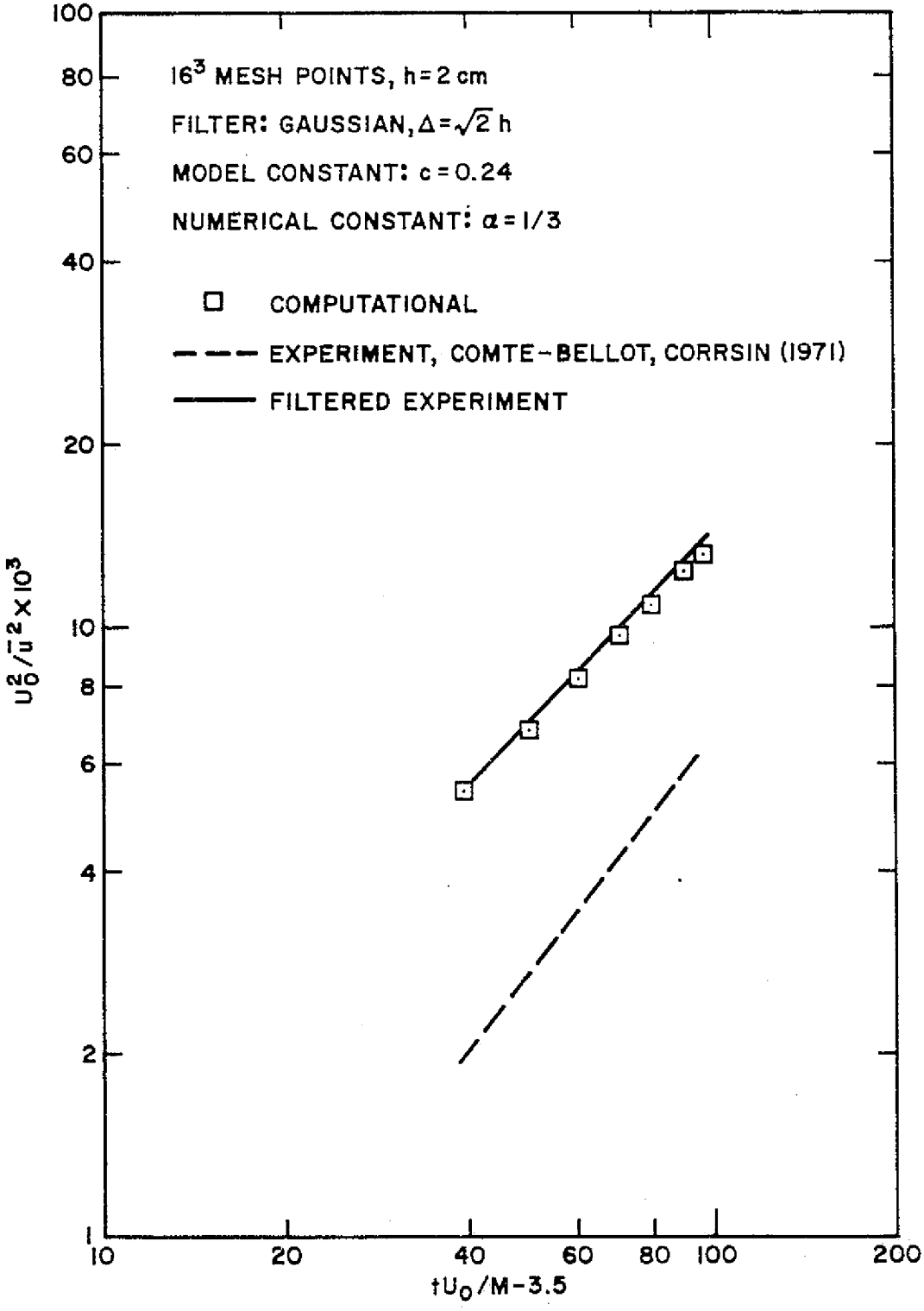

Fig. 4-1. Rate of energy decay of isotropic turbulence.

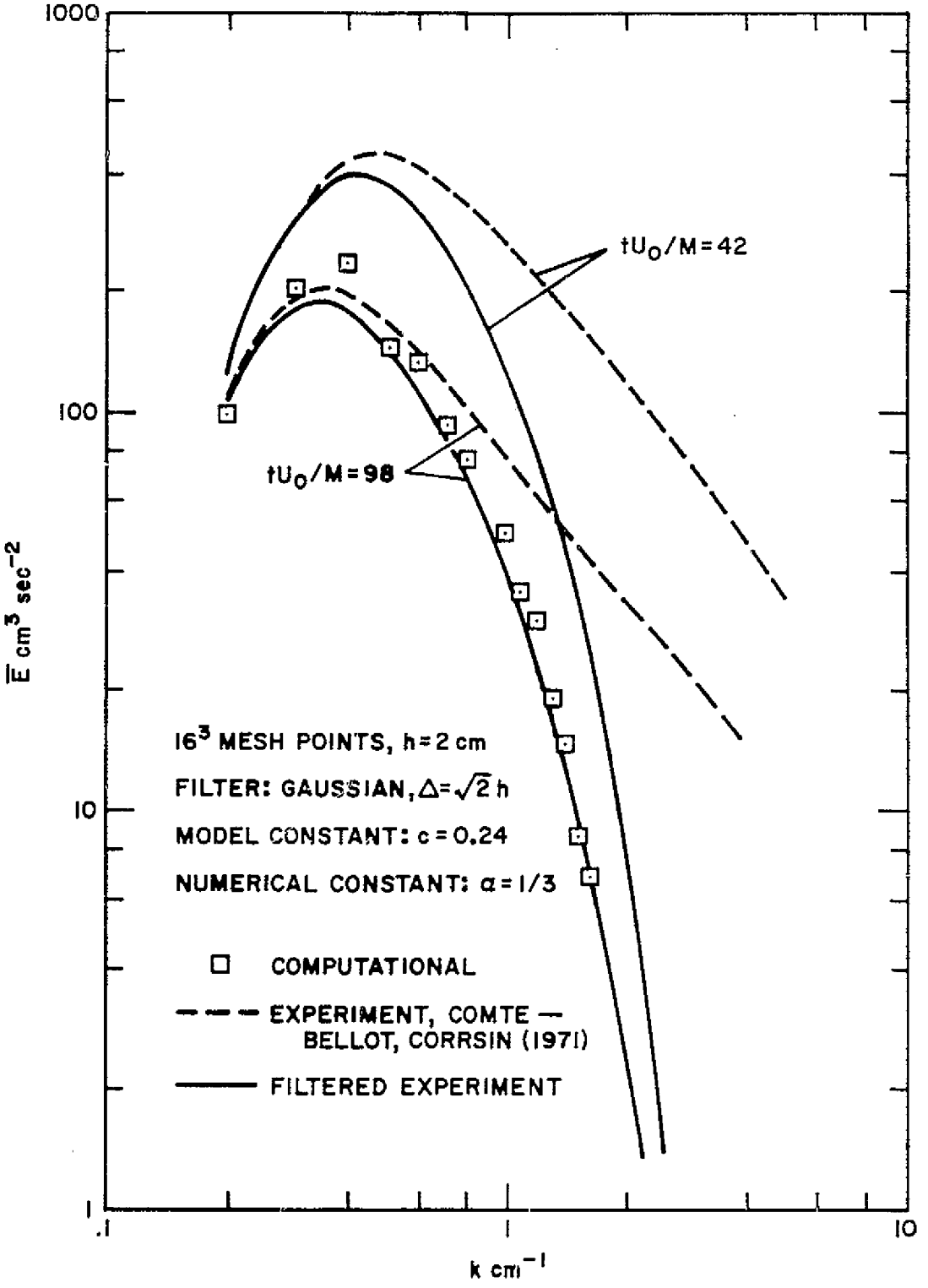

Fig. 4-2. Three-dimensional energy spectra of isotropic turbulence.

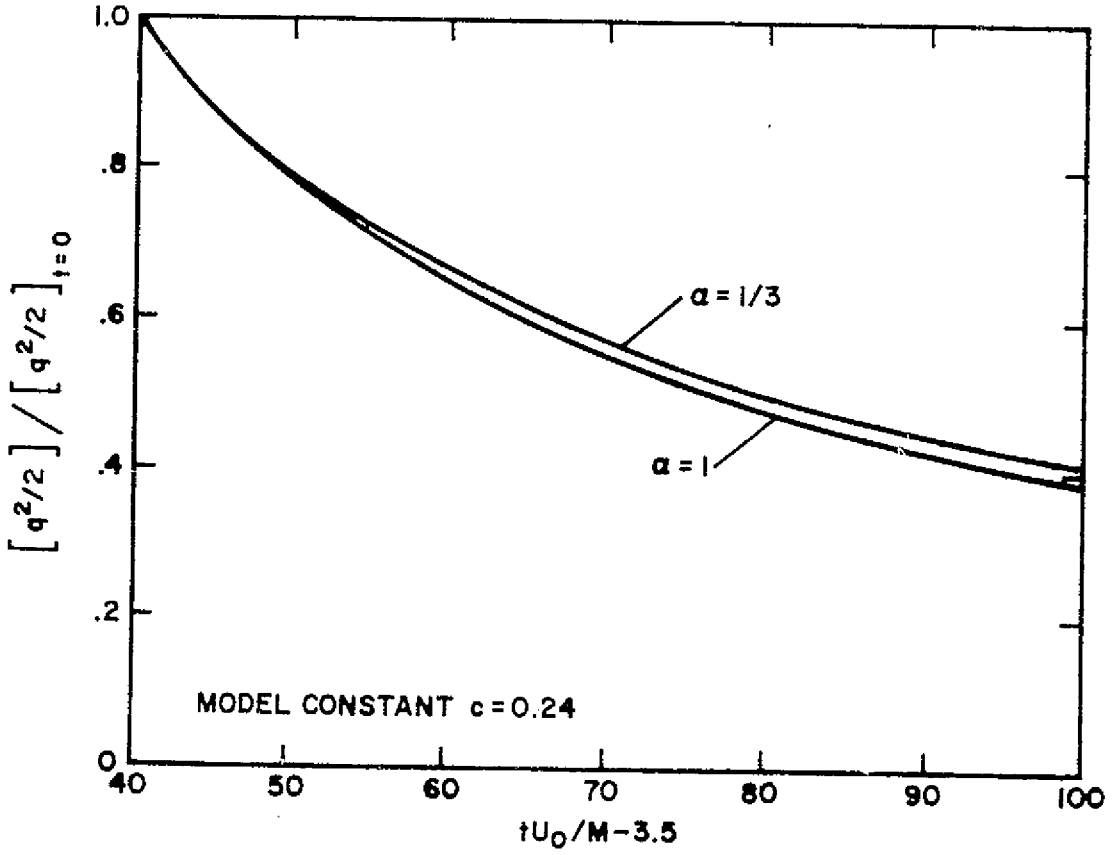

Fig. 4-3. Dependence of rate of energy decay on numerical constant.

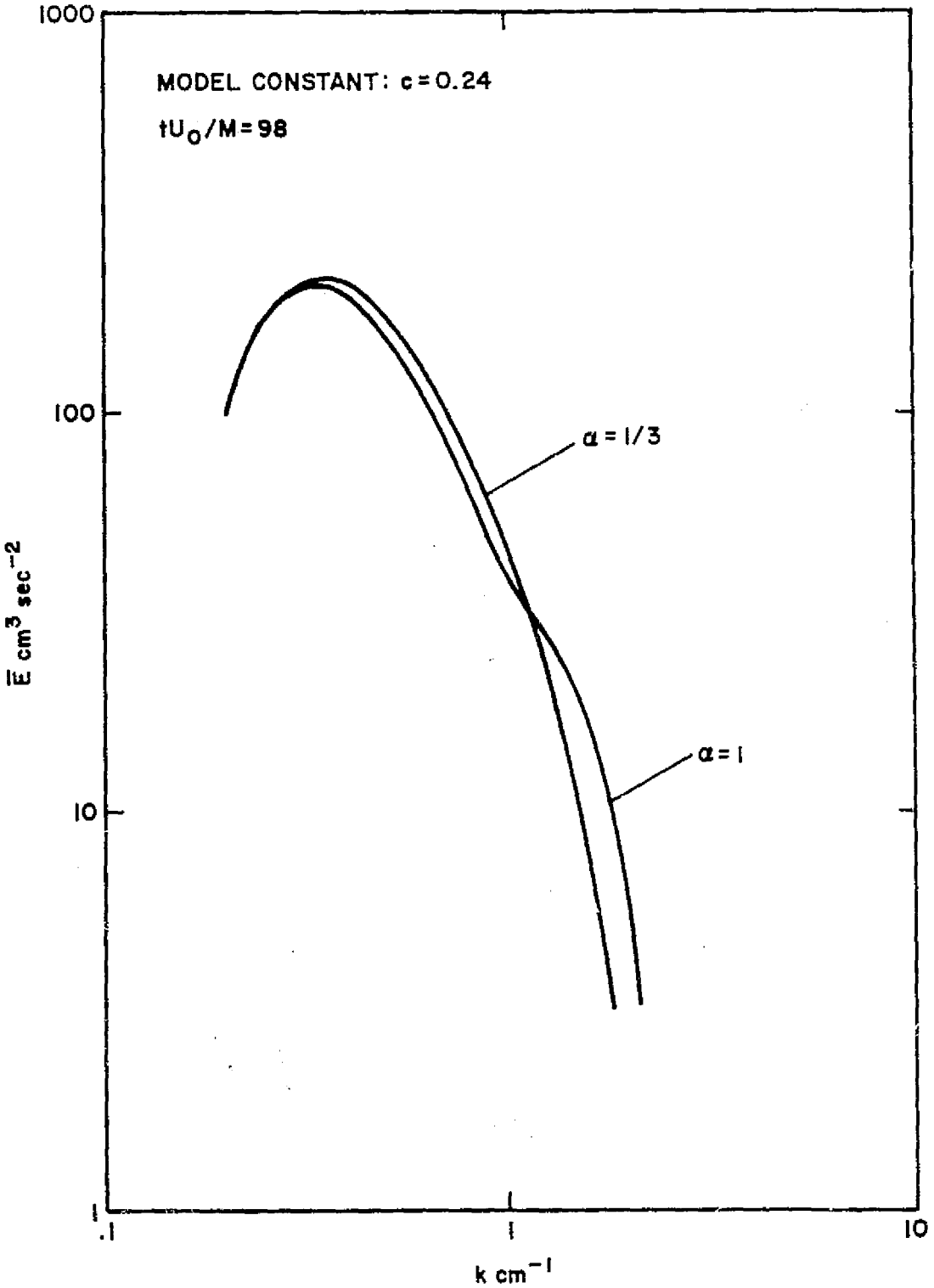

Fig. 4-4. Dependence of energy spectrum on numerical constant.

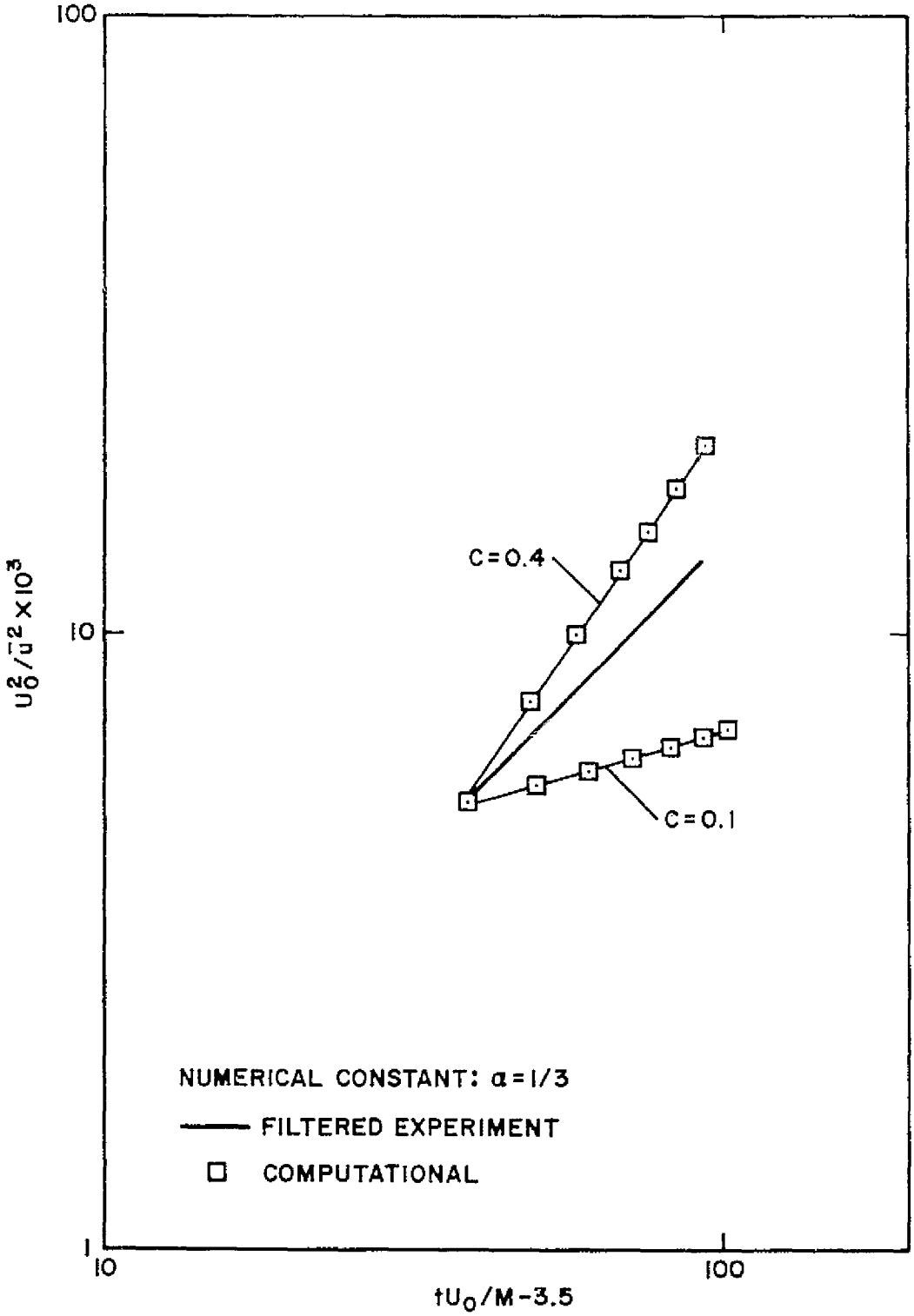

Fig. 4-5. Rate of energy decay for various model constants.

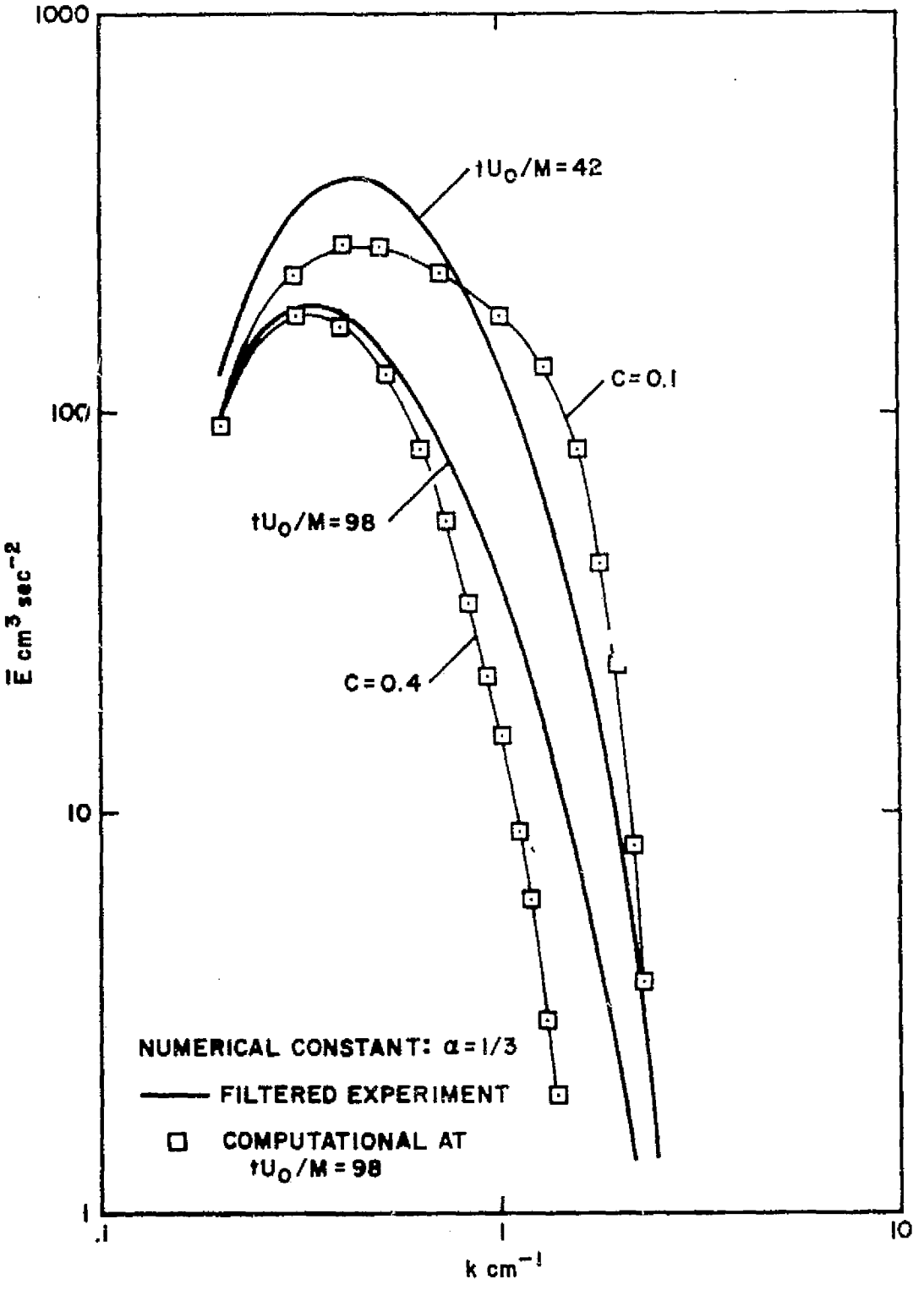

Fig. 4-6. Energy spectra for various model constants.

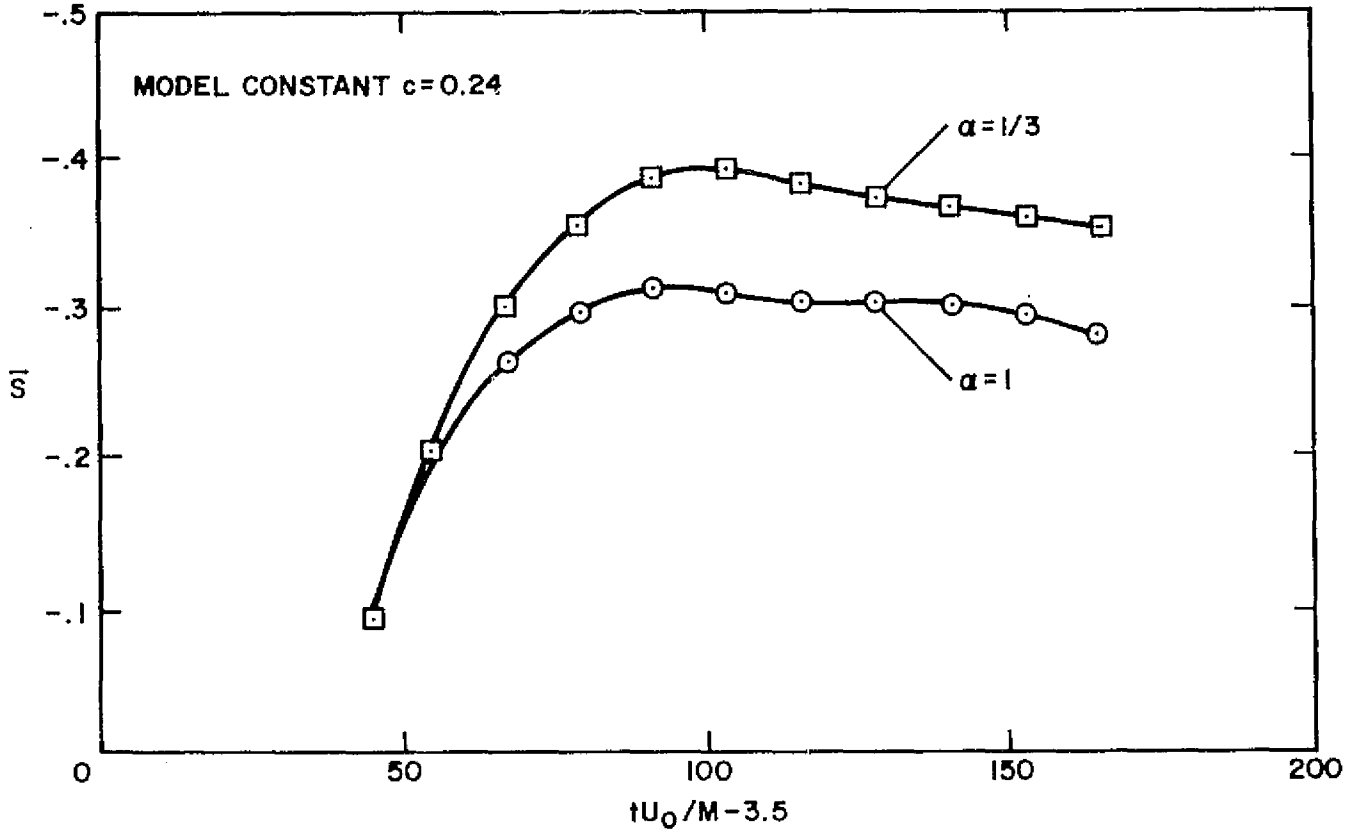

Fig. 4-7. Skewness for different numerical constants.

CHAPTER 5

HOMOGENEOUS TURBULENT SHEAR FLOW

A. General Description

Most natural and technological flows are shear flows. In shear flows most of the energy is contained in the mean (time-averaged) velocity field. When the flow is turbulent, there is a coupling between the mean velocity and the turbulent fluctuations, and the flow characteristics are determined largely by this irteraction. In contrast to an isotropic turbulent field with zero mean flow, in which turbulence levels are reduced by dissipation, as was shown in Chapter 4, turbulence levels in shear flows can be maintained or even increased by an energy-transfer mechanism which subtracts energy from mean flow and feeds it into the turbulence in preferred directions. This effect tends to make turbulence anisotropic. Another characteristic of shear flows is the growth of length scales in the direction of shear.

The simplest turbulent shear flow is the spatially homogeneous flow. Numerical results will be compared with two experiments. The first experiment is due to Champagne, Harris, and Corrsin (1970) (referred to later as CHC flow) and the second is due to Harris (1974). Both experiments were conducted in a wind tunnel. The shear flow was generated by a row of parallel, equal-width channels having adjustable internal resistances. A schematic sketch of the mean flow is shown in Fig. 5-1. In the first experiment, measurements were taken between the nondimensional lengths $x/H = 8.5$ and $x/H = 10.5$, where x is the downstream coordinate, and H is the height of the tunnel ($H = 1$ ft). The mean velocity gradient was $\Gamma = 12.9\ \mathrm{sec}^{-1}$ with a tunnel centerline speed of 40.7 ft/sec. This setup was limited in performance and left only two feet for experimentation. In the second experiment the same setup was used, but the mean velocity gradient has been increased to $44\ \mathrm{sec}^{-1}$. If data are referred to a dimensionless stretched coordinate $\tilde{x} = (x/U_c)\,\Gamma$, the high- and low-shear experiments appear as a continuation of each other. Thus, the high-shear case can be regarded as low-shear data extended to distance $x/H = 35$.

The purpose of these experiments was to confirm previous hypotheses made by Corrsin (1963) concerning development of anisotropy with downstream distances, which implies asymptotic nonstationarity of the flow in a frame of reference convected with the mean flow. Another characteristic that was found in the experiments was a growth in length scales in the mean flow direction. The data will be presented when needed for comparison with calculation.

In the numerical simulation we will try to assess these properties. In addition, the pressure-strain correlation tensor T_{ij} will be computed. The pressure-strain term is responsible for the intercomponent energy transfer. According to Rotta (1951,1962), it destroys shear stresses, thus helps in redistribution of turbulence among the different components. Numerical results will be compared to Rotta's estimates.

B. Mathematical Formulation

The mathematical representation of a spatially homogeneous turbulent shear flow is given by

$$\langle U \rangle_{xz} = \Gamma y + U_c \tag{5-1}$$

$$\langle V \rangle = 0 \tag{5-2}$$

$$\langle W \rangle = 0 \tag{5-3}$$

$$\langle P \rangle = 0 \tag{5-4}$$

where U,V,W,P are instantaneous velocity components and pressure, which include the mean flow, Γ is the mean velocity gradient, $\langle\ \rangle_{ij}$ are averages over planes defined by ij coordinates, and $\langle\ \rangle$ are averages over the entire space.

It is advantageous to change coordinates to a convective frame traveling in the x direction with centerline velocity U_c. The mean field in this frame is shown in Fig. 5-2. Let u,v,w, and p be the turbulence components defined as deviations from the mean flow. To

obtain the equations for the turbulence, we subtract the mean flow out by the following transformation:

$$u = U - \Gamma y \tag{5-5}$$

$$v = V \tag{5-6}$$

$$w = W \tag{5-7}$$

$$p = P \tag{5-8}$$

Substitution of these definitions in the Navier-Stokes equations for U,V,W,P (molecular viscosity is neglected) gives

$$\frac{\partial u}{\partial t} = -\frac{1}{\rho}\frac{\partial p}{\partial x} - \frac{\partial}{\partial x_j}\left[(u+\Gamma y)u_j\right] - \Gamma\frac{\partial}{\partial x}(yu) \tag{5-9}$$

$$\frac{\partial v}{\partial t} = -\frac{1}{\rho}\frac{\partial p}{\partial y} - \frac{\partial}{\partial x_j}(vu_j) - \Gamma\frac{\partial}{\partial x}(yv) \tag{5-10}$$

$$\frac{\partial w}{\partial t} = -\frac{1}{\rho}\frac{\partial p}{\partial z} - \frac{\partial}{\partial x_j}(wu_j) - \Gamma\frac{\partial}{\partial x}(yw) \tag{5-11}$$

$$\frac{\partial^2 p}{\partial x_i \partial x_i} = -\frac{\partial}{\partial x_i}\frac{\partial}{\partial x_j}(u_i u_j) - 2\Gamma\frac{\partial}{\partial x}\frac{\partial}{\partial x_j}(yu_j) \tag{5-12}$$

In order to maintain these equations in a conservative form, no further simplifications should be made by means of the continuity equation. Using the averaging operator according to Chapter 2, we get

$$\frac{\partial \overline{u}}{\partial t} = -\frac{1}{\rho}\frac{\partial \overline{p}}{\partial x} - \frac{\partial}{\partial x_j}\left[\overline{(u+\Gamma y)u_j}\right] - \Gamma\frac{\partial}{\partial x}(\overline{yu}) \tag{5-13}$$

$$\frac{\partial \overline{v}}{\partial t} = -\frac{1}{\rho}\frac{\partial \overline{p}}{\partial y} - \frac{\partial}{\partial x_j}(\overline{vu_j}) - \Gamma\frac{\partial}{\partial x}(\overline{yv}) \tag{5-14}$$

$$\frac{\partial \overline{w}}{\partial t} = -\frac{1}{\rho}\frac{\partial \overline{p}}{\partial z} - \frac{\partial}{\partial x_j}(\overline{wu_j}) - \Gamma\frac{\partial}{\partial x}(\overline{yw}) \tag{5-15}$$

$$\frac{1}{\rho}\frac{\partial^2\overline{p}}{\partial x_i \partial x_i} = -\frac{\partial}{\partial x_i}\frac{\partial}{\partial x_j}(\overline{u_i u_j}) - 2\Gamma\frac{\partial}{\partial x}\frac{\partial}{\partial x_j}(\overline{y u_j}) \tag{5-16}$$

If we set $u = \overline{u} + u'$ and lump all subgrid components into the term $\frac{\partial}{\partial x_j}\tau_{ij}$, we obtain

$$\frac{\partial\overline{u}}{\partial t} = -\frac{\partial\overline{p}}{\partial x} - \frac{\partial}{\partial x_j}[\overline{(\overline{u}+\Gamma y)\overline{u}_j}] - \Gamma\frac{\partial}{\partial x}(\overline{y\overline{u}}) + \frac{\partial}{\partial x_j}\tau_{xj} \tag{5-17}$$

$$\frac{\partial\overline{v}}{\partial t} = -\frac{\partial\overline{p}}{\partial y} - \frac{\partial}{\partial x_j}(\overline{\overline{v}\overline{u}_j}) - \Gamma\frac{\partial}{\partial x}(\overline{y\overline{v}}) + \frac{\partial}{\partial x_j}\tau_{yj} \tag{5-18}$$

$$\frac{\partial\overline{w}}{\partial t} = -\frac{\partial\overline{p}}{\partial z} - \frac{\partial}{\partial x_j}(\overline{\overline{w}\overline{u}_j}) - \Gamma\frac{\partial}{\partial x}(\overline{y\overline{w}}) + \frac{\partial}{\partial x_j}\tau_{zj} \tag{5-19}$$

$$\frac{\partial^2\overline{p}}{\partial x_i \partial x_i} = -\frac{\partial}{\partial x_i}\frac{\partial}{\partial x_j}(\overline{\overline{u}_i\overline{u}_j}) - 2\Gamma\frac{\partial}{\partial x}\frac{\partial}{\partial x_j}(\overline{y\overline{u}_j}) + \frac{\partial}{\partial x_i}\frac{\partial}{\partial x_j}\tau_{ij} \tag{5-20}$$

All functionals of the form $\partial/\partial x_j\ (\overline{y\overline{u}_j})$ are treated numerically in the same manner as the advective term $\partial/\partial x_j\ (\overline{\overline{u}_i\overline{u}_j})$, thus capturing implicitly the Leonard term that arises whenever a product of quantities is averaged. τ_{ij} is assumed to be proportional to the rate-of-strain tensor of the filtered turbulence components:

$$\tau_{ij} = K\left(\frac{\partial\overline{u}_i}{\partial x_j} + \frac{\partial\overline{u}_j}{\partial x_i}\right) \tag{5-21}$$

K is given by Eq. (2-14), and we choose the model constant to be $c = 0.24$, as for the isotropic case (Chapter 4), on the assumption that the subgrid scales are nearly isotropic even in the presence of mean shear. It should be noted that τ_{ij} now contains terms of the type $\overline{u_i' y}$ i.e., averages containing the product of the subgrid scale turbulence and the mean flow. These represent interactions of the mean flow with the subgrid scale turbulence to produce resolvable scale fluctuations. Little is

known about these terms or their effects, and in using the same value of c as in the isotropic case we are tacitly assuming that they are negligible. This point deserves further investigation but will not be pursued here.

a. Boundary conditions

Since Eqs. (5-17) to (5-20) contain turbulence components only, and we assume that the computational domain is sufficiently large compared to the characteristic length scales of the flow, we shall assume $\bar{u}_i$, $\bar{p}$ to be periodic with respect to the computational domain. Although convenient for numerical implementation, this assumption has some limitations, in particular in shear flows. As we shall see, there is a growth of length scales in the direction of mean shear. As time goes on, these scales become comparable in size to the computational region, and periodicity assumption is questionable. In the present simulation we start with a field with $\lambda/H = 0.1$, where λ is the Taylor microscale, and H is the length of the computational domain. Computation is terminated when this ratio becomes ~ 0.2 . For longer simulations one must increase the computational box, at least in the shear direction, if periodic conditions are to be retained.

b. Initial conditions

The initial turbulence velocity field is chosen to be isotropic, with identical energy distribution to that of the case described in Chapter 4 . The turbulence level is adjusted to $\langle \bar{u}_i^2 \rangle^{1/2}/U_c \sim 0.022$, which is approximately the initial value reported in the CHC experiment.

c. Computational time steps

The time steps are chosen to give a Courant number of $N_c = 0.25$ with respect to the mesh size h and the largest mean velocity U_{max} presented in the flow field. For $U_{max} = U_o/2 = 6.45$ ft/sec and $h = 6.25 \times 10^{-2}$ ft, we find that $\Delta t = 0.25\ h/U_{max} = 2.422 \times 10^{-3}$ sec. Using the Taylor hypothesis for the convective velocity $U_c = 40.7$ ft/sec, the following relation holds:

10 time steps $\longleftrightarrow$ 1 ft

These quantities will be used throughout the numerical simulation of the present and the following chapter.

C. Results and Discussion

a. Comparison with experiments

Figures 5-3 and 5-4 compare numerical simulation to experiments. The first figure compares the turbulent levels in different directions. As in the experiment, the $\bar{v}$ and $\bar{w}$ components, which are perpendicular to the shear direction, decay monotonically with distance, while the level of $\bar{u}$, the component in the shear direction, behaves differently. At first it decays, then it levels off and starts to grow. The growth of $\bar{u}$ in the CHC experiment is not clear enough, but it is shown clearly in the extended experiment made by Harris. Numerical results confirm the experimental evidence which shows that in the presence of mean shear, energy is extracted from the mean shear and fed into preferred turbulence components. This growth makes the flow nonstationary in a reference frame convected with the centerline velocity U_c.

Note that the computed results show faster growth than the experimental results. To bring the computations into agreement with experiment would require increasing the subgrid scale constant c which is inconsistent with what Deardorff (1970) and Schumann (1973) found. Furthermore, the neglected interaction between the mean flow and the subgrid scale fluctuations should be a production term and would tend to reduce the subgrid scale constant. Thus, although the computed trends agree with experiment, the results do differ quantitatively and the most obvious possible causes would change the results in the wrong direction. The remaining possibility, i.e., that the difference is due to improper initial conditions, is also not likely to be correct as an isotropic initial condition should yield the smallest growth rate for a given turbulence level.

The second figure compares the Reynolds shear stress $-\langle \bar{u}\bar{v} \rangle$. As we shall see later, this shear stress acts together with the mean shear to create a production term for the turbulence in the x direction. This term is important also in two-dimensional turbulence modeling. As is shown, computed results agree quite well with experiment. These comparisons, although limited, bring us to the conclusion that the numerical simulation properly represents the main features of an actual shear flow.

b. Additional numerical results

In Figs. 5-5 to 5-11 additional information is extracted from the numerical simulation. Some of this information is either difficult or impossible to obtain experimentally. Examples in the first category are spatial correlations and length scales, and in the second category are pressure-strain correlations and the "return to isotropy" simulation. This information extends considerably the existing data set for shear flows and can be of help in two-dimensional turbulence modeling. A detailed description of these data follow.

Figure 5-5 shows the development of total turbulent kinetic energy $\bar{u}_i\bar{u}_i$ with time (or distance). Since the initial field is isotropic, energy starts to decay at an equivalent rate as in the case of isotropic turbulence with zero mean flow (Chapter 4). As anisotropy develops, enough energy is extracted from the mean flow to compensate for dissipation, and to allow the net energy to increase. There is no reason to believe that the growth will not remain indefinitely; the steady mean field implies that it is being pumped in such a way as to maintain its energy.

Figure 5-6 shows the development of turbulent levels in each direction.

Figure 5-7 shows the three components of shear stress $-\langle \bar{u}_i\bar{u}_j \rangle$ (normalized on the RMS values of $\bar{u}_i$ and $\bar{u}_j$). Ideally, initial conditions for these terms should be zero, if the field is truly isotropic. Practically, it is difficult to achieve this requirement in a 16^3 problem. Nevertheless, the flow adjusts itself after a short period (about thirty steps) and the terms $-\langle \bar{u}\bar{w} \rangle$ and $-\langle \bar{v}\bar{w} \rangle$ are reduced to zero (within an error band of 0.01). The value of $-\langle \bar{u}\bar{v} \rangle$, on the other hand, grows to an approximate value of 0.5.

Figure 5-8 shows the development of length scales $\bar{\lambda}_j$ in each direction. The length scale in the shear direction grows considerably, while in the other directions there is not a significant change. Although experimental data for the length scales exist in the CHC experiment, comparison can be made qualitatively only. The reason is the large difference in the initial length scales of the experiment ($\lambda \sim .016$ ft) and the numerical simulation ($\bar{\lambda} \sim .10$ ft). This difference comes mainly from the fact that in the numerical simulation we are using filtered rather than instantaneous quantities, and there is a considerable difference between $(\partial u/\partial x)^2$ and $(\partial \bar{u}/\partial x)^2$ which occur in the definitions of λ and $\bar{\lambda}$, respectively.

The explanation for the observed behavior of the turbulence quantities and length scales that we prefer is that small nearly circular, eddies with their vorticity in the z direction combine to form elongated eddies with their major axes in the x direction. Such a process, similar to the vortex-pairing process put forward by the USC group (Winant and Browand, 1974) would lead to an increase in $<\bar{u}^2>$, a decrease in $<\bar{v}^2>$, an increase in $\bar{\lambda}_x$, and a constant $\bar{\lambda}_y$. It will also decrease $<\bar{\omega}_z^2>$, which was observed but is not shown in the figures.

Figure 5-9 shows nine components of spatial correlations. The most significant change occurs in the $R_{11}(x,0,0)$ component. The reason for that is the growth of length scales in the x direction which makes the flow correlated over larger distances. It should be noted that the least changes occure in the z direction, which means that most of the interaction takes place in the (x-y) directions.

Figure 5-10 shows the development of the pressure-strain correlation tensor T_{ij}, where

$$T_{ij} = < \bar{p}\left(\frac{\partial \bar{u}_i}{\partial x_j} + \frac{\partial \bar{u}_j}{\partial x_i}\right) > \qquad (5\text{-}22)$$

In an isotropic field of turbulence these terms should be identically zero. As can be seen, the initial values, as with the stresses $-<\bar{u}_i\bar{u}_j>$, are not zero, and a period of adjustment should be allowed before any conclusion can be drawn from the simulation. In the present case we

shall refer to data at time step $L = 100$, where the T_{ij} show regular behavior, and the length scales have not increased so much as to invalidate the periodic boundary conditions used in this simulation. More details on T_{ij} will be given later in this section.

Figure 5-11 shows a "return to isotropy" simulation from a sheared state. As the mean shear is turned off, the flow returns to isotropy in a peculiar way. When the amount of anisotropy is large, there is a transfer of energy between $\bar{u}$ and $\bar{v}$ which causes initially an increase in the $\bar{v}$ component. When the anisotropy diminishes, dissipation effects take over and all three components decrease toward isotropy. No such effect is observed in the $\bar{w}$ component, which suggests that most of the interaction and energy exchange is two-dimensional. This can be explined physically by the rotation of the elongated eddies that were formed by pairing. (In the absence of strain an elongated vortex will rotate.)

c. Pressure-strain correlation T_{ij}

The energy and stress balance equations for a homogeneous shear flow are given (Hinze, 1959, p. 252) by

$$\frac{\partial}{\partial t} \langle \frac{1}{2} \bar{u}^2 \rangle = \langle -\bar{u}\bar{v} \rangle \Gamma + T_{11} + D_{sgs} \tag{5-23}$$

$$\frac{\partial}{\partial t} \langle \frac{1}{2} \bar{v}^2 \rangle = \qquad + T_{22} + D_{sgs} \tag{5-24}$$

$$\frac{\partial}{\partial t} \langle \frac{1}{2} \bar{w}^2 \rangle = \qquad + T_{33} + D_{sgs} \tag{5-25}$$

$$\frac{\partial}{\partial t} \langle -\bar{u}\bar{v} \rangle = \langle \bar{v}^2 \rangle \Gamma - T_{12} + D_{sgs} \tag{5-26}$$

D_{sgs} stands for a subgrid dissipation term which will not be specified explicitly here. T_{ij} is defined in Eq. (5-22).

Initially, when the flow is nearly isotropic, T_{ij} is identically zero. As time elapses, the term $\langle \bar{v}^2 \rangle \Gamma$ in Eq. (5-26), which is positive definite, causes a positive increase in the stress term $\langle -\bar{u}\bar{v} \rangle$. This, in turn, increases the turbulence level of $\langle \bar{u}^2 \rangle$ in Eq. (5-23), thus making

the flow anisotropic. When the field is anisotropic, the terms T_{ij} are no longer zero. The values of T_{ij} grow in a way which tends to equalize the velocity levels and reduce the shear stresses. Qualitatively, the values of T_{ij} should be as follows:

$$T_{11} < 0 \quad , \quad T_{22} > 0 \quad , \quad T_{33} > 0 \quad , \quad T_{12} > 0 \tag{5-27}$$

This is indeed what we find in Fig. 5-10.

Because of the importance of the term T_{ij} , and the extreme difficulty of measuring it, it has long been a subject of model estimation. One of the simplest and most popular models is Rotta's estimate (1951, 1962), where he assumed that the pressure-strain correlation tensor is proportional to the amount of anisotropy presented in the flow:

$$T_{ij} = -A\, D\, b_{ij} \tag{5-28}$$

where D is the isotropic dissipation given by

$$-D = \frac{\partial}{\partial t}(q^2/2) \tag{5-29}$$

and b_{ij} is the anisotropy tensor defined by

$$b_{ij} = (R_{ij} - q^2\, \delta_{ij}/3)/q^2 \tag{5-30}$$

$$(R_{ij} = \langle \bar{u}_i \bar{u}_j \rangle , \; q^2 = R_{ii})$$

This model has been checked with data obtained from the "return to isotropy" simulation (Fig. 5-11). The results (for $L = 280$) are as follows:

a. component T_{11} gives a constant $A = 2.3$
b. component T_{22} gives a constant $A = 3.8$
c. component T_{33} gives a constant $A = 1.4$

These results agree with estimates made by Norris and Reynolds (Reynolds, 1975). They recommend a value of $A = 5/2$, which is the average value of what we find for the separate components of T_{ij}.

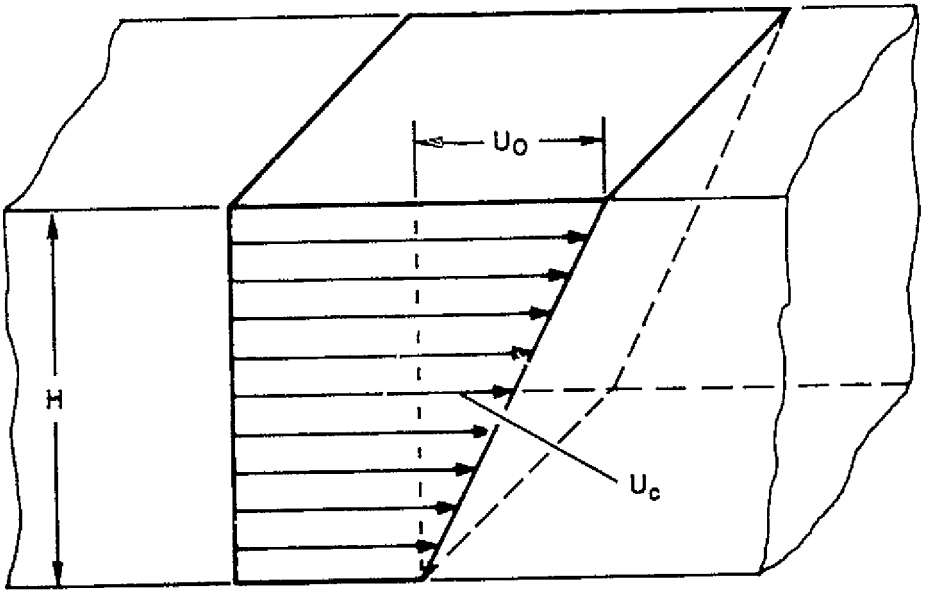

Fig. 5-1. Schematic sketch of the homogeneous turbulent shear flow.

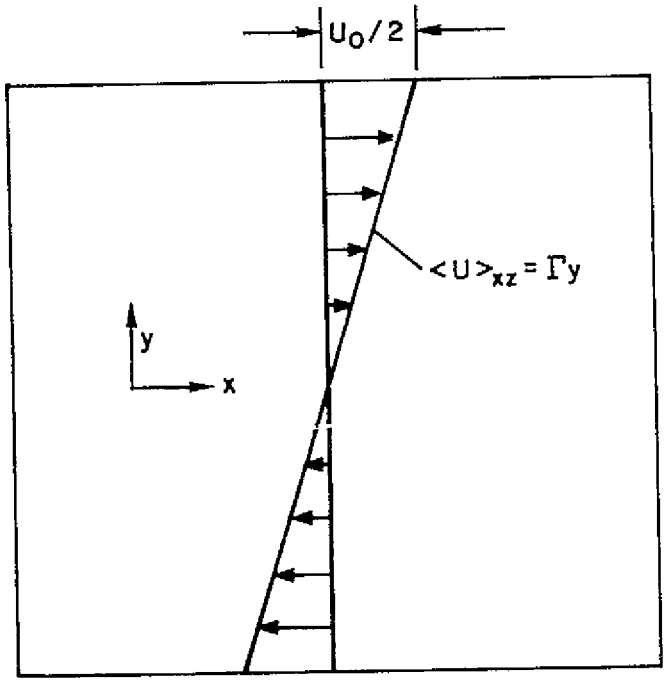

Fig. 5-2. Mean velocity in a convective frame.

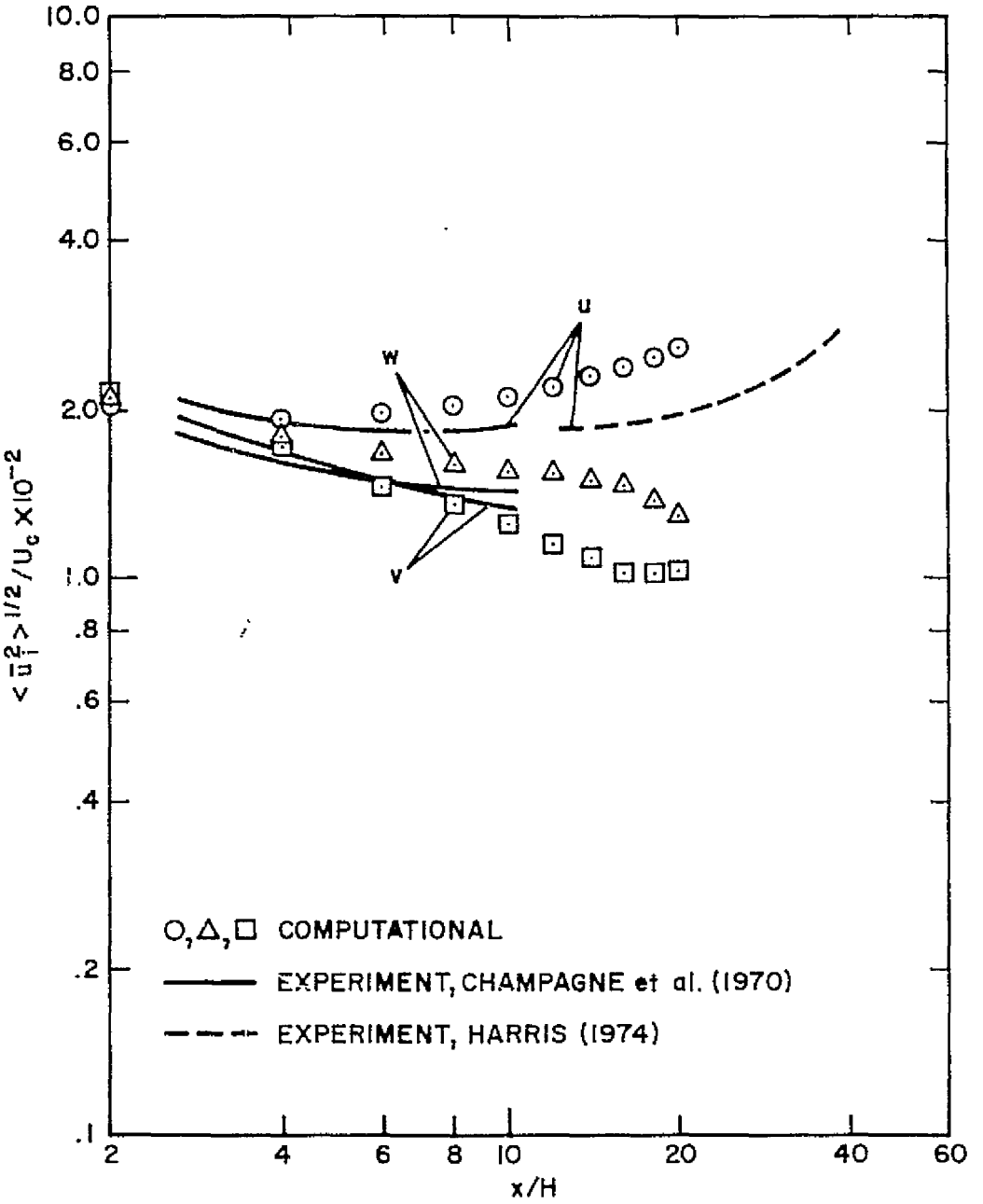

Fig. 5-3. Turbulence levels in homogeneous shear flow, comparison with experiment.

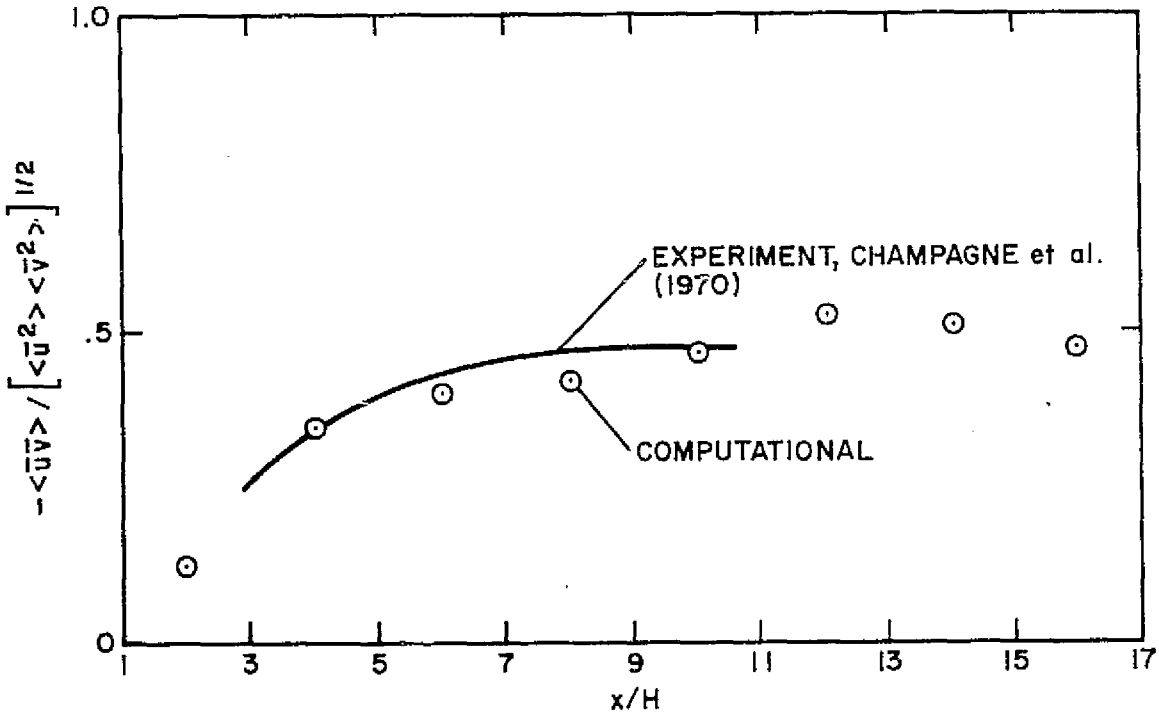

Fig. 5-4. Shear stress in homogeneous shear flow, comparison with experiment.

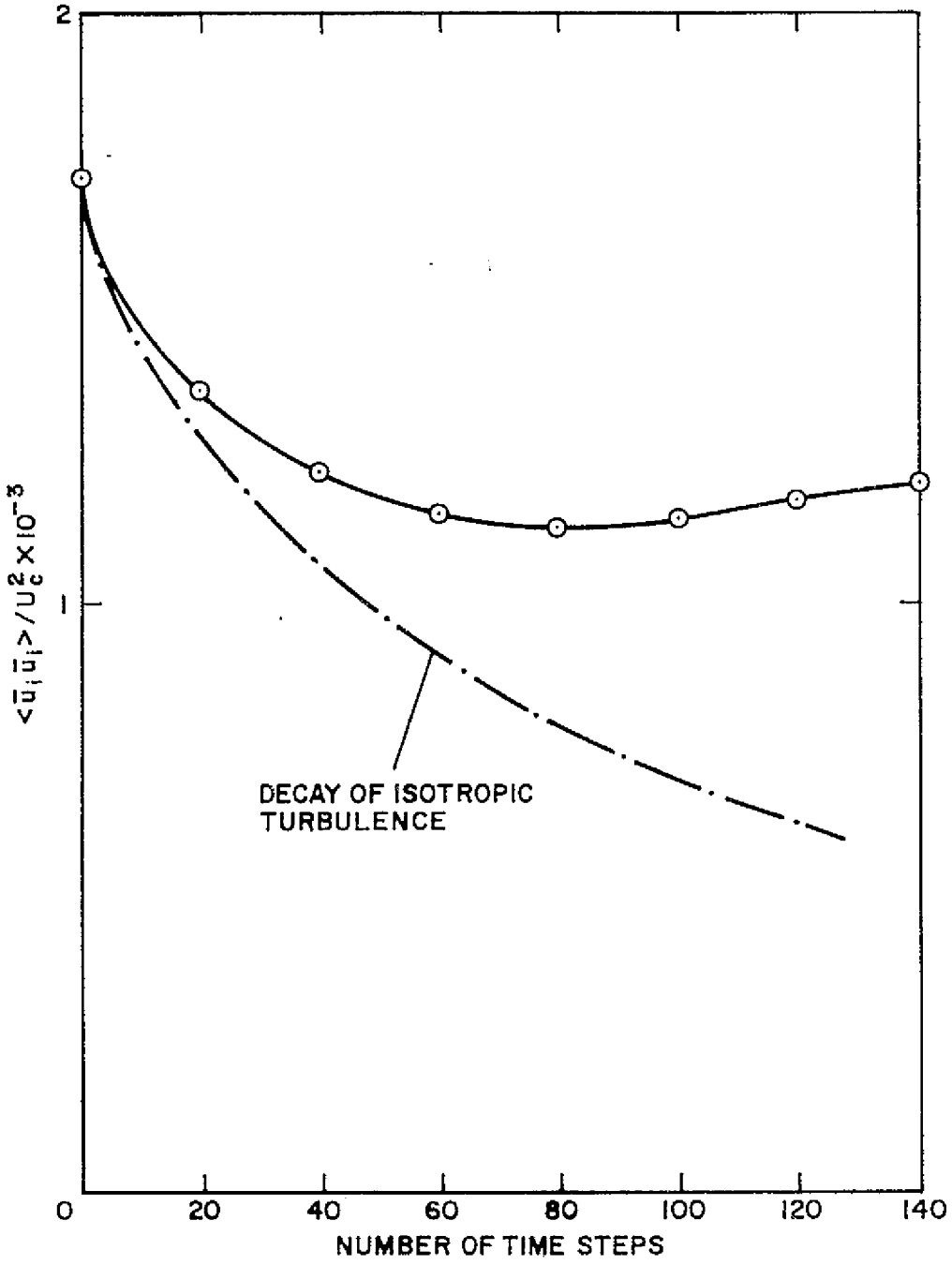

Fig. 5-5. Development of turbulent kinetic energy in homogeneous shear flow.

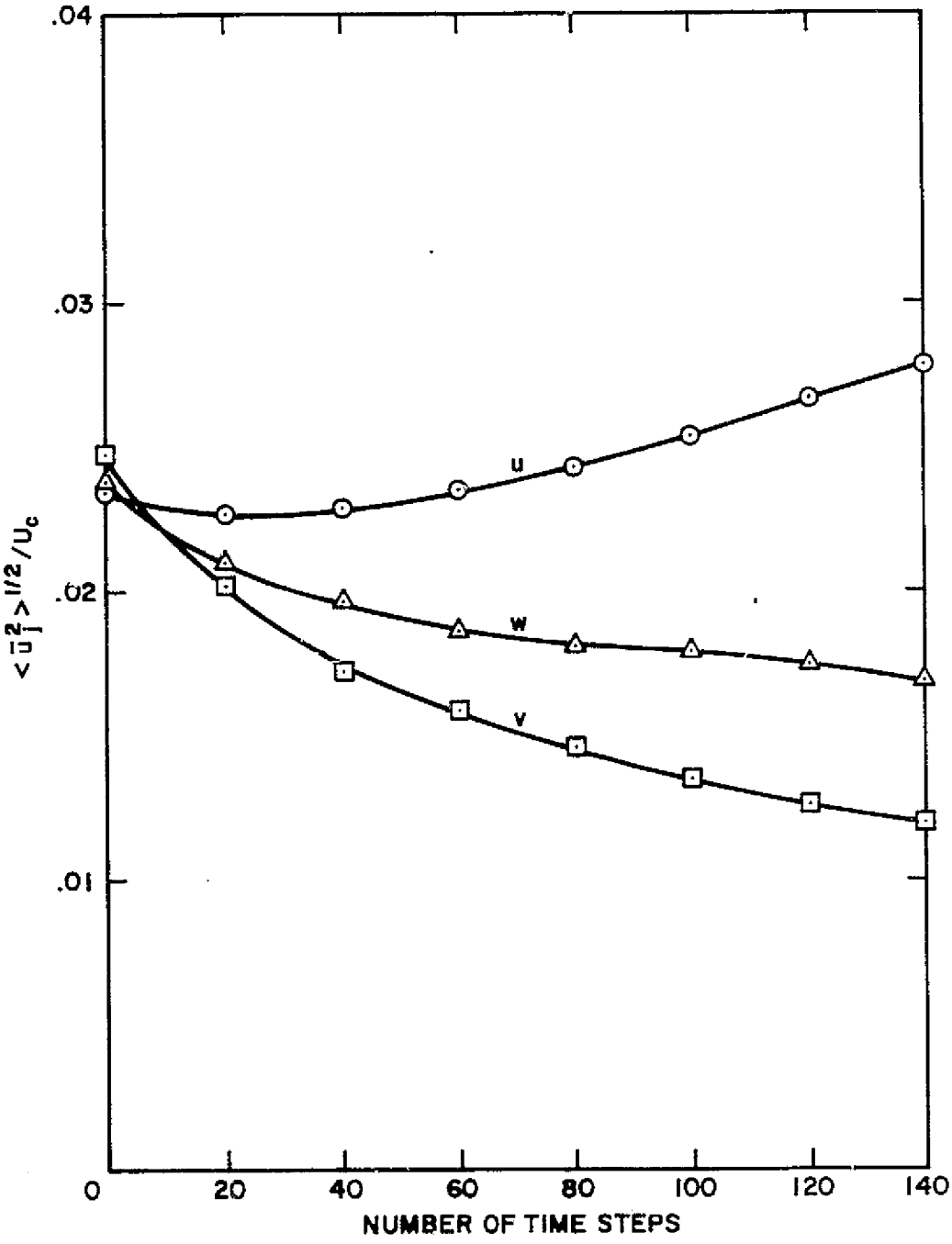

Fig. 5-6. Development of turbulence levels in homogeneous shear flow.

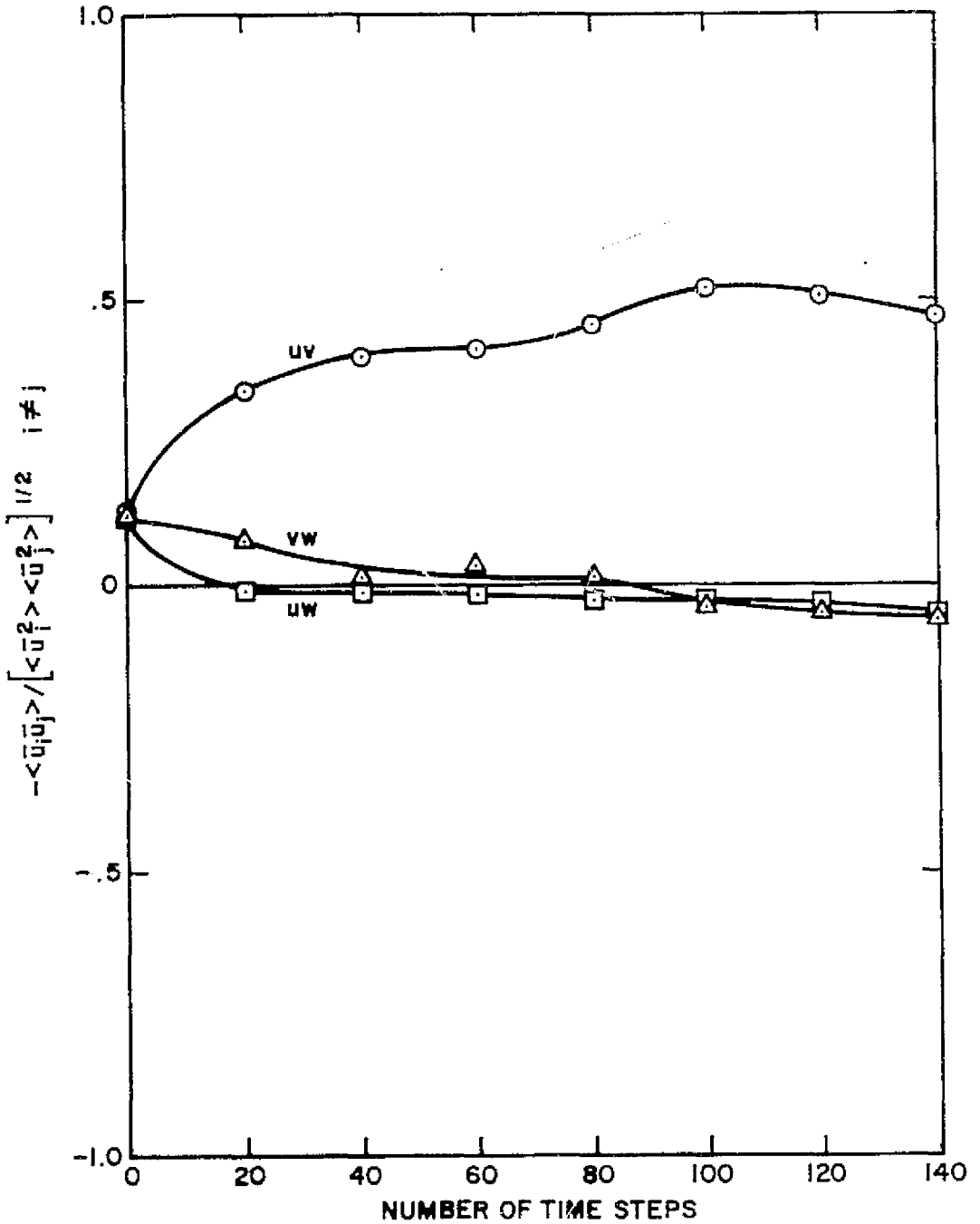

Fig. 5-7. Development of shear stresses in homogeneous shear flow.

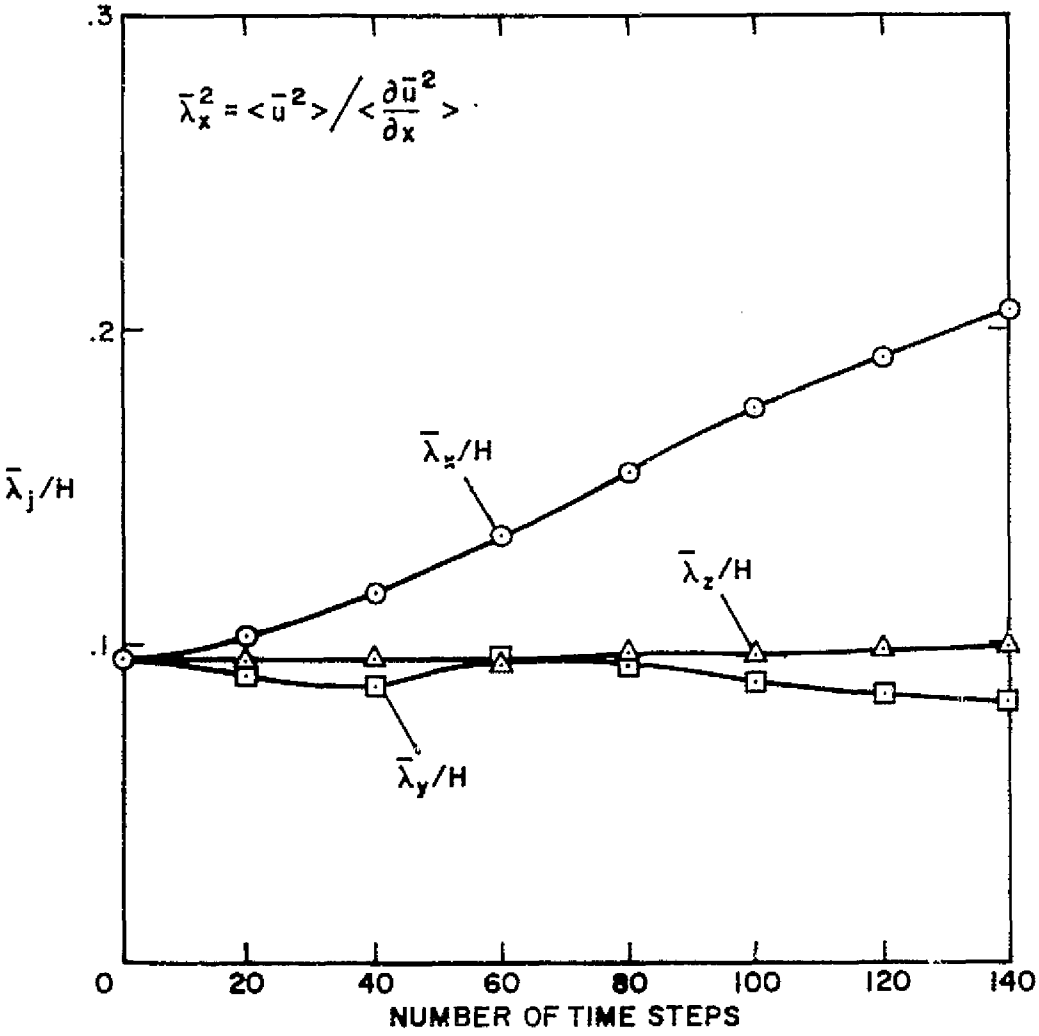

Fig. 5-8. Development of length scales in homogeneous shear flow.

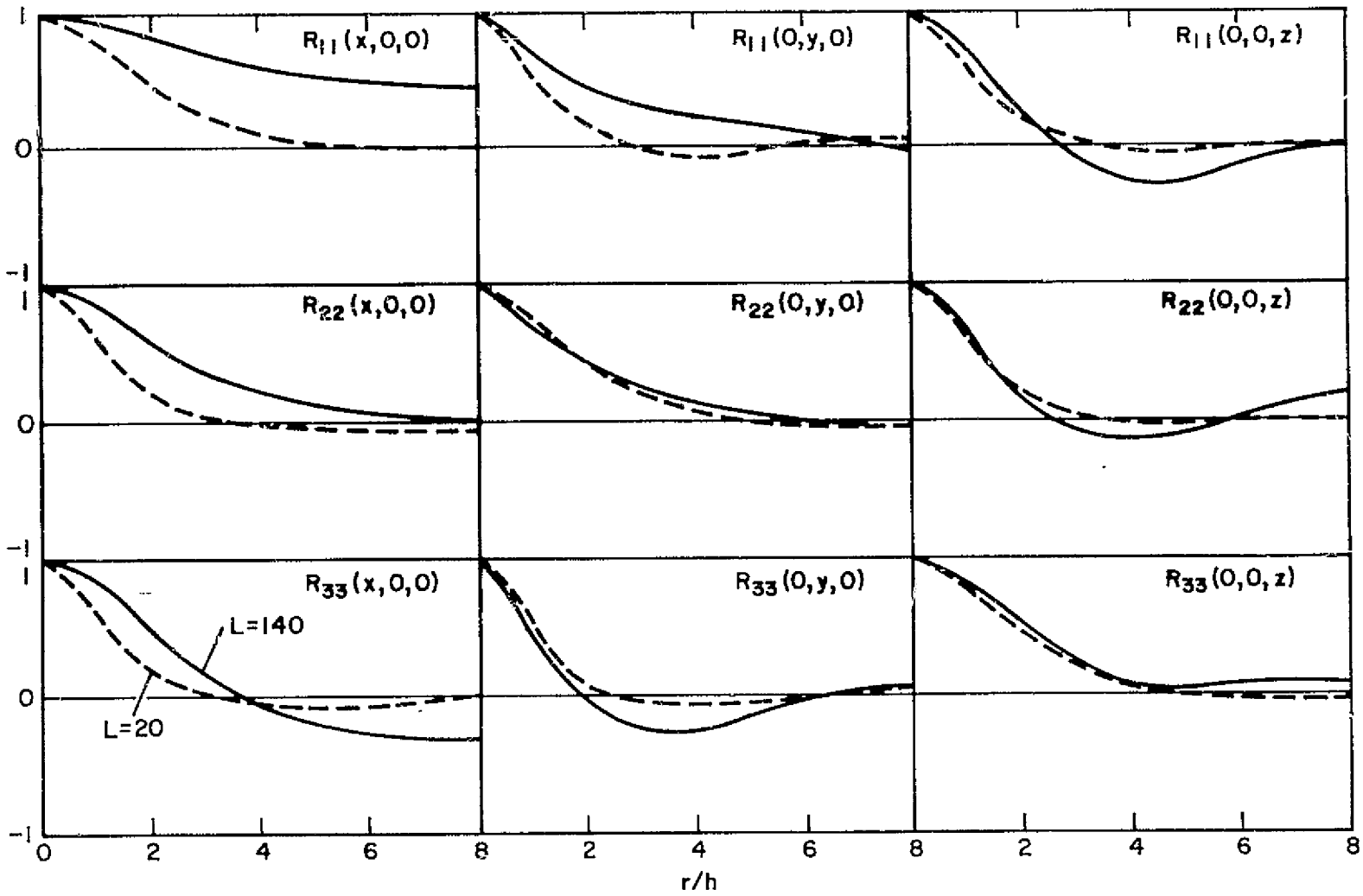

Fig. 5-9. Spatial correlations in homogeneous shear flow.

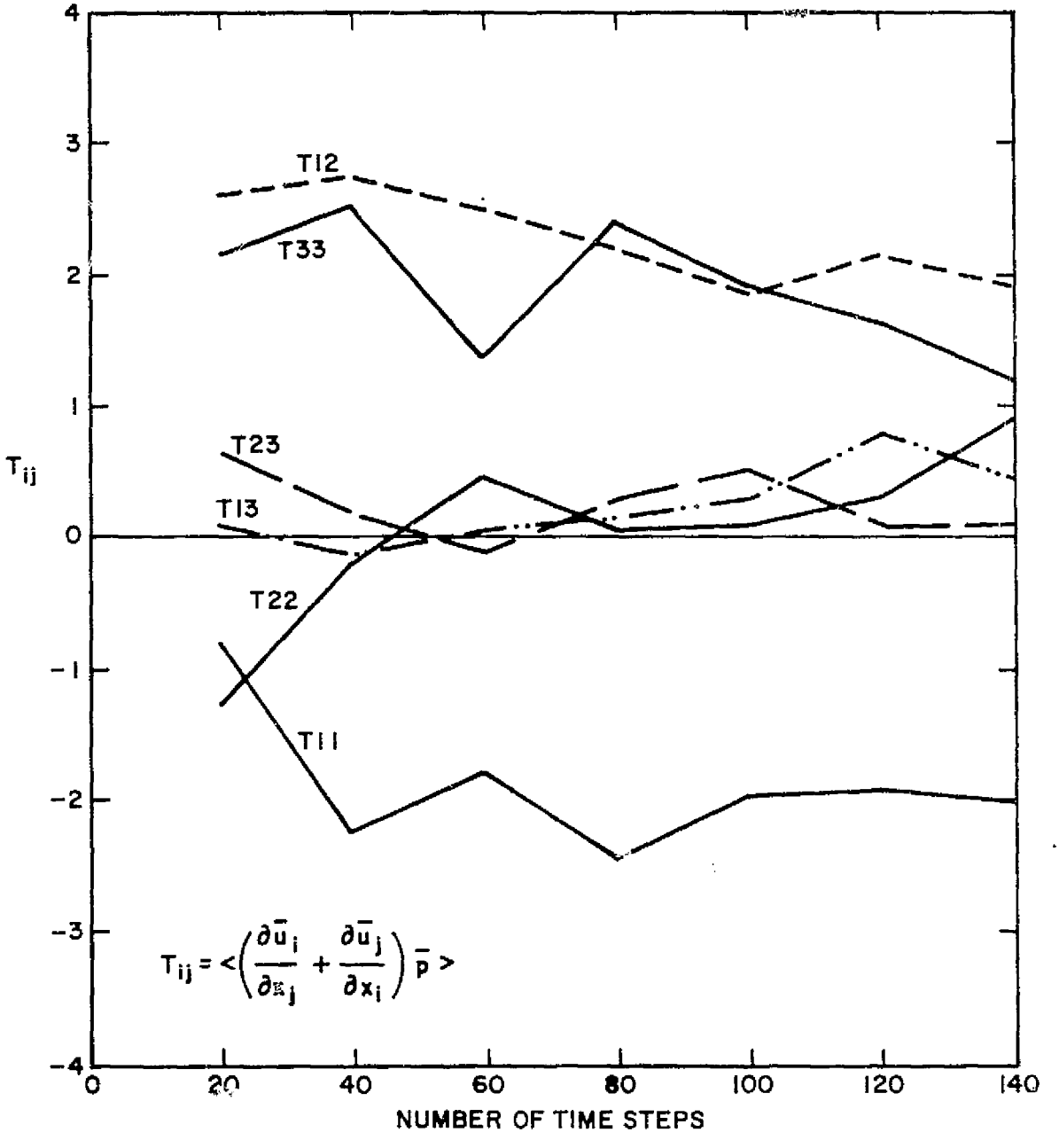

Fig. 5-10. Development of pressure-strain correlations in homogeneous shear flow.

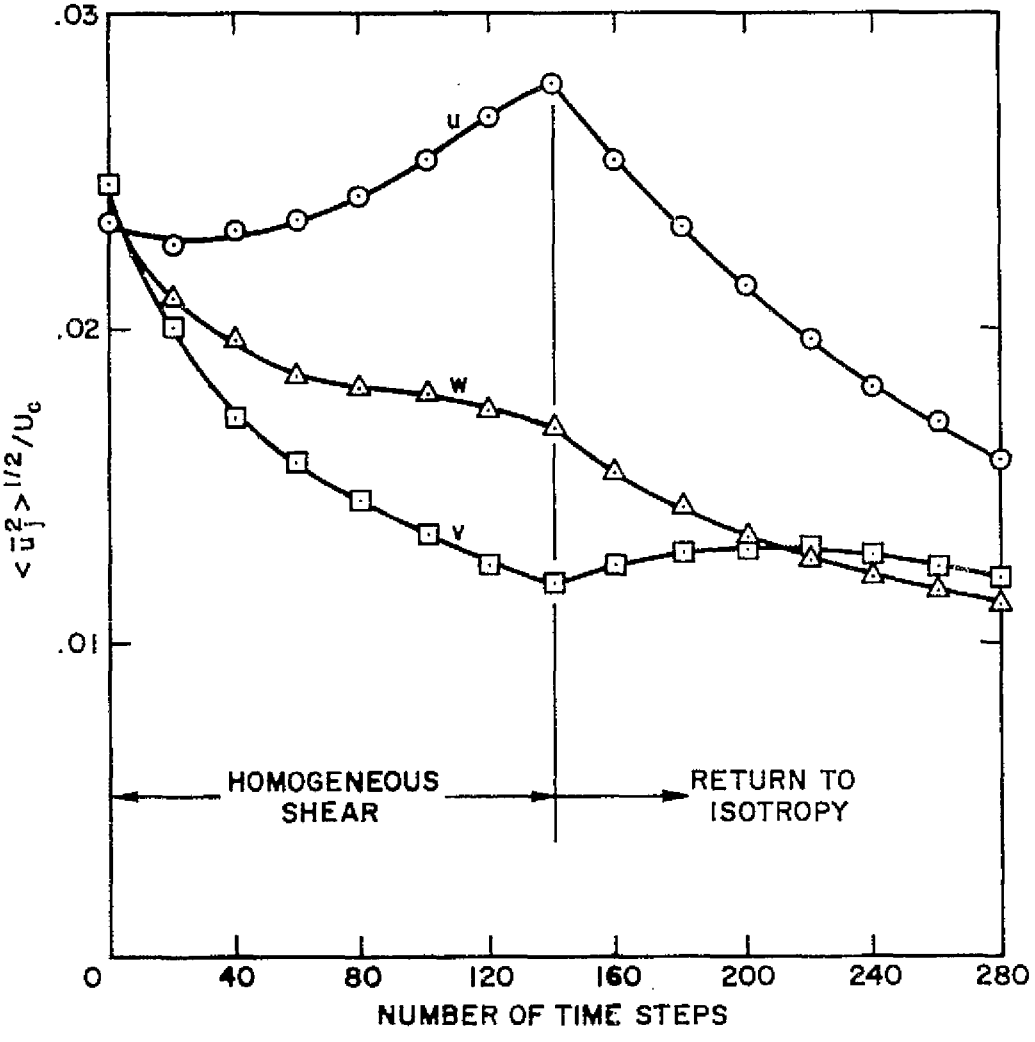

Fig. 5-11. Return to isotropy from homogeneous shear.

CHAPTER 6

HOMOGENEOUS TURBULENT SHEAR FLOW WITH SYSTEM ROTATION

A. General Description

The third problem to be simulated adds one more parameter to the flow field. Homogeneous turbulent shear flow is examined in the presence of system rotation. This problem is of interest in two important fields. The first one is atmospheric turbulence where the flow field is in a rotating frame of the earth, and the second is the internal flow of turbomachines. Rotation has an effect on the stability of turbulence. It has been shown by experiments (Halleen and Johnston, 1967) that, depending on the magnitude and direction of rotation, either augmentation or suppression of turbulence intensities results. Johnston (1974) investigated the effects of rotation on boundary layers in turbomachine rotors and proposed a relation for the mixing-length ratio ℓ/ℓ_0 (used in two-dimensional turbulence modeling) which is based on the local gradient Richardson number defined by

$$Ri = \frac{-2\Omega(\Gamma - 2\Omega)}{\Gamma^2} \tag{6-1}$$

in the form

$$\ell/\ell_0 = 1 - \beta \; Ri \tag{6-2}$$

where ℓ is defined by

$$\ell = \langle \bar{u}\bar{v} \rangle^{1/2} / \Gamma \tag{6-3}$$

Based on experiments, β was found to be in the range of 2 to 6.

Since our simulation represents a small region of the flow field away from solid boundaries or other interfaces, we do not claim that this simulation represents a real flow such as exhibited in an interior of a turbomachine; therefore, comparison with available experiments should be made carefully, if at all, at this stage. On the other hand, the experiments are involved and results are affected by effects other than rotation, as can be seen from the scattered data of the experiments (Fig. 6-6),

while the numerical simulation is "clean" in the sense that we are testing the exclusive effect of rotation on the flow.

In the following, numerical results will be given for different Ri numbers and will be compared to experiment, and a simple explanation will be given for the stabilizing effect of rotation on the turbulence.

B. Mathematical Formulation

The equations of motion relative to a frame which is rotating in a constant angular velocity Ω are given (Batchelor 1967, p. 144) by

$$\frac{\partial \underline{U}}{\partial t} + \underline{U} \cdot \nabla \underline{U} = -\frac{1}{\rho} \nabla P - 2\underline{\Omega} \times \underline{U} - \underline{\Omega} \times (\underline{\Omega} \times \underline{U}) \tag{6-4}$$

$$\nabla \cdot \underline{U} = 0 \tag{6-5}$$

The term $-2\underline{\Omega} \times \underline{U}$ is the Coriolis force, which is perpendicular to both $\underline{U}$ and $\underline{\Omega}$, and $-\underline{\Omega} \times (\underline{\Omega} \times \underline{U})$ is a centrifugal force, which can be written also as

$$-\frac{1}{2} \nabla (\underline{\Omega} \times \underline{X})^2 \tag{6-6}$$

This term can be added to the pressure term $-1/\rho \nabla P$ to form a generalized pressure P^*:

$$P^* = P + \frac{1}{2} \rho (\underline{\Omega} \times \underline{X})^2 \tag{6-7}$$

In Cartesian tensor notation the equations of motion read

$$\frac{\partial U_i}{\partial t} + \frac{\partial}{\partial x_j} (U_i U_j) = -\frac{1}{\rho} \frac{\partial P^*}{\partial x_i} - 2 \varepsilon_{ijk} \Omega_j U_k \tag{6-8}$$

$$\frac{\partial U_i}{\partial x_i} = 0 \tag{6-9}$$

Let $\underline{\Omega} = (0,0,\Omega)$, and the velocity field be defined as

$$\langle U \rangle_{xz} = \Gamma y \tag{6-10}$$

$$\langle V \rangle = 0 \tag{6-11}$$

$$\langle W \rangle = 0 \tag{6-12}$$

We define also a mean pressure

$$\langle P \rangle_{xz} = -\rho \Omega \Gamma y^2 \tag{6-13}$$

To obtain the equations of turbulence, we subtract the mean values from the instantaneous field:

$$u = U - \Gamma y \tag{6-14}$$

$$v = V \tag{6-15}$$

$$w = W \tag{6-16}$$

$$p = P^* + \rho \Omega \Gamma y^2 \tag{6-17}$$

Substitution of these definitions in Navier-Stokes equations for U, V, W, P^*, Eqs. (6-8) and (6-9), gives

$$\frac{\partial u}{\partial t} = -\frac{1}{\rho}\frac{\partial p}{\partial x} - \frac{\partial}{\partial x_j}[(u+\Gamma y)u_j] - \Gamma \frac{\partial}{\partial x}(yu) + 2\Omega v \tag{6-18}$$

$$\frac{\partial v}{\partial t} = -\frac{1}{\rho}\frac{\partial p}{\partial y} - \frac{\partial}{\partial x_j}(vu_j) - \Gamma \frac{\partial}{\partial x}(yv) - 2\Omega u \tag{6-19}$$

$$\frac{\partial w}{\partial t} = -\frac{1}{\rho}\frac{\partial p}{\partial z} - \frac{\partial}{\partial x_j}(wu_j) - \Gamma \frac{\partial}{\partial x}(yw) \tag{6-20}$$

$$\frac{\partial^2 p}{\partial x_i \partial x_i} = -\frac{\partial}{\partial x_i}\frac{\partial}{\partial x_j}(u_i u_j) - 2\Gamma \frac{\partial}{\partial x}\frac{\partial}{\partial x_j}(yu_j) + 2\Omega\left(\frac{\partial v}{\partial x} - \frac{\partial u}{\partial y}\right) \tag{6-21}$$

Following the same procedure of averaging described in Chapter 5, Eqs. (5-13) to (5-20), we get the conservative form of the filtered equations of motion relative to a rotating frame.

$$\frac{\partial \bar{u}}{\partial t} = -\frac{\partial \bar{p}}{\partial x} - \frac{\partial}{\partial x_j}\left[(\bar{u}+\Gamma y)\bar{u}_j\right] - \Gamma\frac{\partial}{\partial x}\overline{(y\bar{u})} + \frac{\partial}{\partial x_j}\tau_{xj} + 2\Omega\bar{v} \tag{6-22}$$

$$\frac{\partial \bar{v}}{\partial t} = -\frac{\partial \bar{p}}{\partial x} - \frac{\partial}{\partial x_j}\overline{(\bar{v}\bar{u}_j)} - \Gamma\frac{\partial}{\partial x}\overline{(y\bar{v})} + \frac{\partial}{\partial x_j}\tau_{yj} - 2\Omega\bar{u} \tag{6-23}$$

$$\frac{\partial \bar{w}}{\partial t} = -\frac{\partial \bar{p}}{\partial z} - \frac{\partial}{\partial x_j}\overline{(\bar{w}\bar{u}_j)} - \Gamma\frac{\partial}{\partial x}\overline{(y\bar{w})} + \frac{\partial}{\partial x_j}\tau_{zj} \tag{6-24}$$

$$\frac{\partial^2 \bar{p}}{\partial x_i \partial x_i} = -\frac{\partial}{\partial x_i}\frac{\partial}{\partial x_j}\overline{(\bar{u}_i\bar{u}_j)} - \Gamma\frac{\partial}{\partial x}\frac{\partial}{\partial x_j}\overline{(y\bar{u}_j)} + 2\Omega\left(\frac{\partial \bar{v}}{\partial x} - \frac{\partial \bar{u}}{\partial y}\right) + \frac{\partial}{\partial x_i}\frac{\partial}{\partial x_j}\tau_{ij} \tag{6-25}$$

Again, we use periodic conditions for the turbulent components $\bar{u}_i$, $\bar{p}$. Initial conditions are isotropic with the same energy spectrum as for the case given in Chapter 5.

C. Results

Four different values for Ω were used in the simulation:

$$\Omega = \left\{-1.33,\ -.591,\ .727,\ 3.22\right\}$$

which correspond to gradient Richardson numbers:

$$Ri = \left\{.25,\ .1,\ -.1,\ -.25\right\}$$

The mean velocity gradient was kept as in the case of $\Omega = 0$ in Chapter 5, $\Gamma = 12.9\ Sec^{-1}$. Figures 6-1 to 6-5 show the dependence of the total turbulent energy $<\bar{u}_i\bar{u}_i>$, the shear stress $-<\bar{u}\bar{v}>$, and the turbulence levels $<\bar{u}_i^2>^{1/2}$ on Ri. As can be seen, turbulent intensities and shear stresses are higher for larger rotations (or smaller Ri numbers) and vice versa, which means that rotation either stabilizes or destabilizes the turbulent field, depending on the magnitude and direction of Ω. With regard to the turbulence levels, the most profound change occurs in the $\bar{v}$ component, where rotation changes its behavior entirely from a decaying mode for $Ri = .25$ to a rapidly growing mode for $Ri = -.25$.

It is interesting to note that for $Ri = -.25$, turbulence levels of $\bar{u}$ and $\bar{v}$ are almost identical (a simple explanation will be given later in this chapter).

Figure 6-6 shows the dependence of mixing-length ratio on the local gradient Richardson number, as was evaluated from experiments (Johnston, 1974). As was mentioned before, this experiment is quite complicated and data are scattered, which makes any interpretation difficult, at best. Contrary to the experiment, which is conducted in stead-state conditions, our simulation exhibits nonstationarity. Nevertheless, if we analyze data from time step $L = 100$, at which time the flow has developed (but not too much to invalidate the periodic conditions), we find that $\beta \sim 1.7$ which is in the lower range of experimental results (Fig. 6-6).

In an attempt to obtain simple correlations, we have plotted $<\bar{u}\bar{v}>$ and $<\bar{u}\bar{v}>^{1/2}$ (which is proportional to the mixing length) versus both Ω and Ri . The best fit was obtained with $<\bar{u}\bar{v}>^{1/2}$ versus Ri and is shown in Fig. 6-7. We find

$$<\bar{u}\bar{v}>^{1/2} \sim C_1 - C_2 Ri \tag{6-26}$$

where $C_1 \sim .5$ and $C_2 \sim .04t^{-2}$

D. Interpretation of Results

Simple shearing motion can be viewed as a superposition of a pure straining motion and a rigid rotation. When simple shear and rigid rotation are applied together, there is a value of rotation which cancels the rotational part of the shear and thus reduces the flow to a pure strain, the principal axes of which are at 45° to the (x–y) axes. The case of simple shearing motion in a rotating frame is similar. Let us write Eq. (6-8) in the form

$$\frac{\partial U_i}{\partial t} + U_j\,(\mathcal{S}_{ij} + \mathcal{R}_{ij}) + U_j\,\rho_{ij} = -\frac{1}{\rho}\frac{\partial P^*}{\partial x_i} \tag{6-27}$$

where

$$\mathcal{S}_{ij} = \frac{1}{2}\left(\frac{\partial U_i}{\partial x_j} + \frac{\partial U_j}{\partial x_i}\right) \tag{6-28}$$

$$\mathcal{R}_{ij} = \frac{1}{2}\left(\frac{\partial U_i}{\partial x_j} - \frac{\partial U_j}{\partial x_i}\right) \tag{6-29}$$

$$\rho_{ij} = 2\,\varepsilon_{ikj}\,\Omega_k \tag{6-30}$$

For simple shear with $\partial U/\partial y = \Gamma$ and $\Omega_k = (0,0,\Omega)$ we have in two dimensions

$$\mathcal{S}_{ij} = \begin{pmatrix} 0 & \Gamma/2 \\ \Gamma/2 & 0 \end{pmatrix} \tag{6-31}$$

$$\mathcal{R}_{ij} = \begin{pmatrix} 0 & \Gamma/2 \\ -\Gamma/2 & 0 \end{pmatrix} \tag{6-32}$$

$$\rho_{ij} = \begin{pmatrix} 0 & -2\Omega \\ 2\Omega & 0 \end{pmatrix} \tag{6-33}$$

It is easy to see that if $\Gamma/2 = 2\Omega$, then $\mathcal{R}_{ij} = -\rho_{ij}$ and the motion reduces to pure strain with principal axes at 45°.

The general form of the turbulent shear stress tensor for pure strain in the principal axes (two dimensions) is given by

$$\langle \bar{u}_i \bar{u}_j \rangle = \begin{pmatrix} \langle \bar{u}^2 \rangle & 0 \\ 0 & \langle \bar{v}^2 \rangle \end{pmatrix} \tag{6-34}$$

If we rotate this tensor 45°, we obtain

$$\frac{1}{2}\begin{pmatrix} \langle \bar{u}^2 \rangle + \langle \bar{v}^2 \rangle & \langle \bar{u}^2 \rangle - \langle \bar{v}^2 \rangle \\ \langle \bar{u}^2 \rangle - \langle \bar{v}^2 \rangle & \langle \bar{u}^2 \rangle + \langle \bar{v}^2 \rangle \end{pmatrix} \tag{6-35}$$

with the result that the terms on the diagonal are equal. If we examine the case of pure shear in a rotating frame with $\Gamma/2 = 2\Omega$ or $\Omega = 3.22$ (Ri = -.25), we find that within computational accuracy the diagonal elements of $\langle \bar{u}_i \bar{u}_j \rangle$ are equal, or $\langle \bar{u}^2 \rangle^{1/2} = \langle \bar{v}^2 \rangle^{1/2}$, as can be seen from Figs. 6-3 and 6-4.

This view also leads to a simple picture of turbulence production. If we focus strictly on the production terms, then the three most important equations for the turbulent velocities may be written:

$$\frac{d<\bar{u}^2>}{dt} = -2<\bar{u}_1^2>\mathcal{S}_{11} - 2<\bar{u}\bar{v}>\mathcal{S}_{12} - 2<\bar{u}\bar{v}>\mathbb{R}_{12} \tag{6-36}$$

$$\frac{d<\bar{v}^2>}{dt} = -2<\bar{v}^2>\mathcal{S}_{22} - 2<\bar{u}\bar{v}>\mathcal{S}_{12} + 2<\bar{u}\bar{v}>\mathbb{R}_{12} \tag{6-37}$$

$$\frac{d<\bar{u}\bar{v}>}{dt} = -<\bar{u}\bar{v}>(\mathcal{S}_{11} + \mathcal{S}_{22}) - (<\bar{u}^2> + <\bar{v}^2>)\mathcal{S}_{12} - (<\bar{v}^2> - <\bar{u}^2>)\mathbb{R}_{12} \tag{6-38}$$

where $\mathbb{R}_{12} = \mathbb{R}_{12} + \rho_{12}$ and we have noted that $\mathcal{S}_{12} = \mathcal{S}_{21}$, $\mathbb{R}_{12} = -\mathbb{R}_{21}$. Without loss of generality we can choose the principal axes to be along the coordinate directions so that

$$\mathcal{S}_{12} = 0 \ , \ 2\mathcal{S}_{11} = -2\mathcal{S}_{22} = s \ , \ 2\mathbb{R}_{12} = r \tag{6-39}$$

and Eqs. (6-36) to (6-38) reduce to

$$\frac{d<\bar{u}^2>}{dt} = s<\bar{u}^2> - r<\bar{u}\bar{v}> \tag{6-40}$$

$$\frac{d<\bar{v}^2>}{dt} = -s<\bar{v}^2> + r<\bar{u}\bar{v}> \tag{6-41}$$

$$\frac{d<\bar{u}\bar{v}>}{dt} = -r(<\bar{v}^2> - <\bar{u}^2>)/2 \tag{6-42}$$

The kinetic energy obeys the equation

$$\frac{d}{dt}(<\bar{u}^2> + <\bar{v}^2>) = s(<\bar{u}^2> - <\bar{v}^2>) \tag{6-43}$$

so that there is no production of turbulent kinetic energy if the turbulence is isotropic. If, however, $<\bar{u}^2> > <\bar{v}^2>$, there will be growth caused by the fact that $<\bar{u}^2>$ grows faster than $<\bar{v}^2>$ decays.

Thus, if the turbulence is anisotropic, there will be production, and the production is in such a direction as to increase both the energy and the anisotropy.

It is interesting to note the effect of rotation on production. Equations (6-40) to (6-42) are linear ordinary differential equations in $<\bar{u}^2>$, $<\bar{v}^2>$, and $<\bar{u}\bar{v}>$ and thus have exponential solutions. Seeking solutions of the form e^{at}, we find

$$a = 0 \quad , \quad \pm\sqrt{s^2 - r^2} \tag{6-44}$$

Thus, we see that the greatest production results when $r = 0$, i.e., for pure strain (corresponding to $Ri = -.25$). Any rotation inhibits the production and, in fact, for $r > s$ there is no production at all. When $r = s$, the growth is algebraic.

Physically, rotation mixes the components, i.e., it transfers some of the $\bar{u}$ component to the $\bar{v}$ component. In so doing, it reduces the anisotropy and, indirectly, inhibits the production of turbulent kinetic energy.

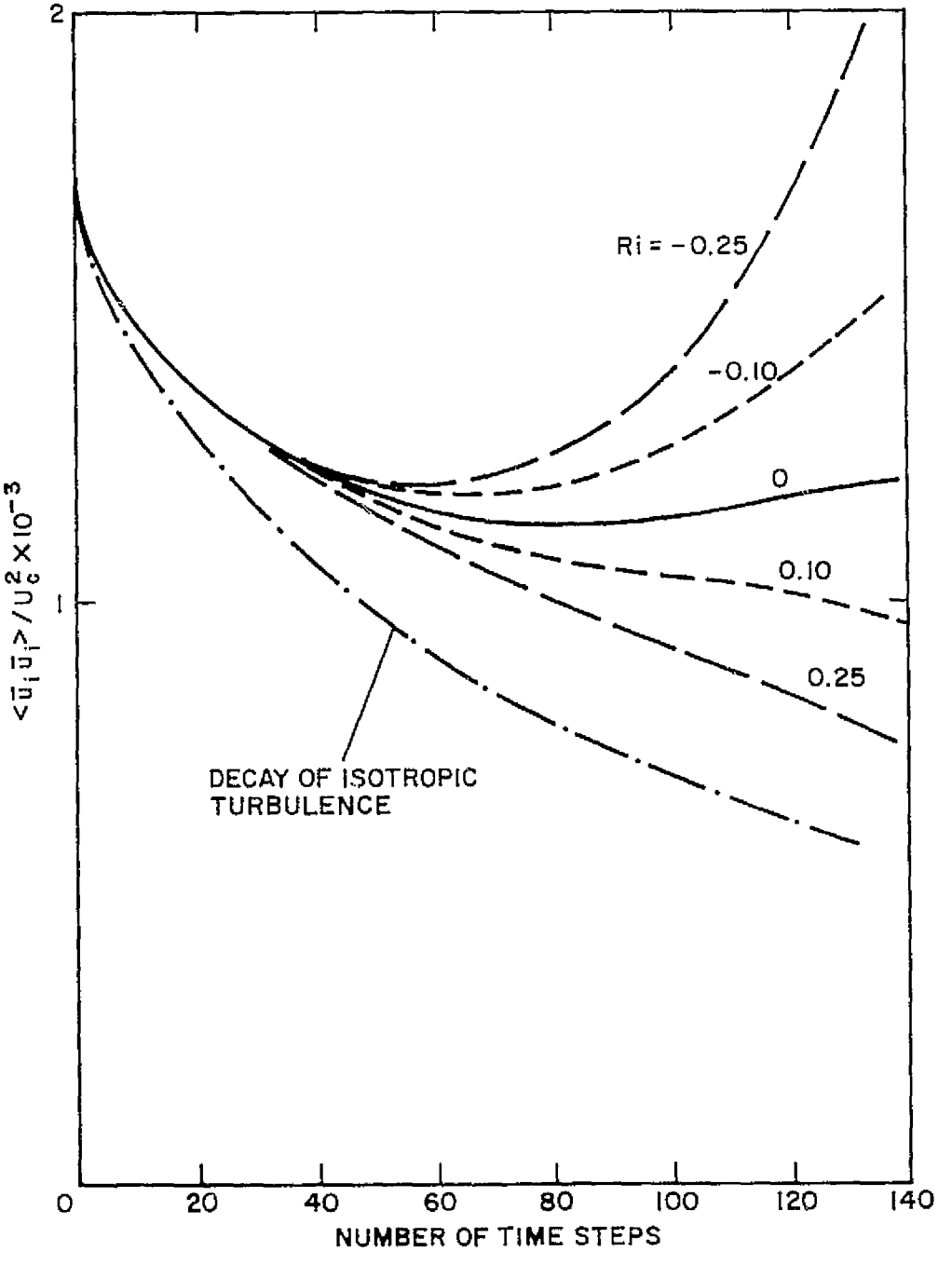

Fig. 6-1. Turbulent kinetic energy for different gradient Richardson numbers.

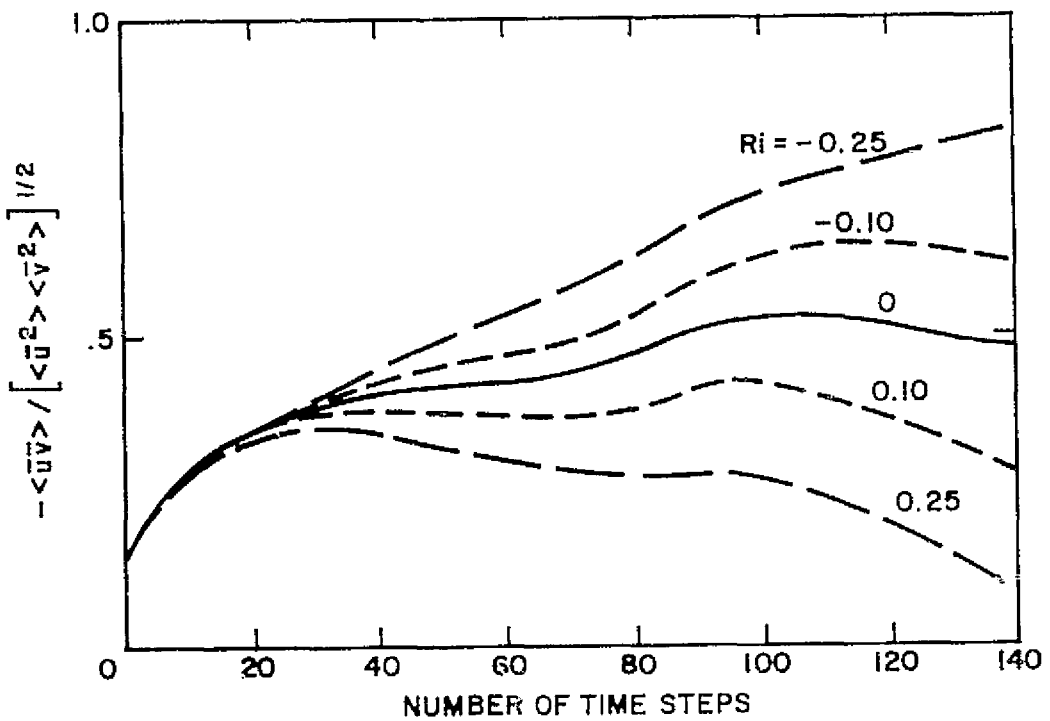

Fig. 6-2. Shear stresses for different gradient Richardson numbers.

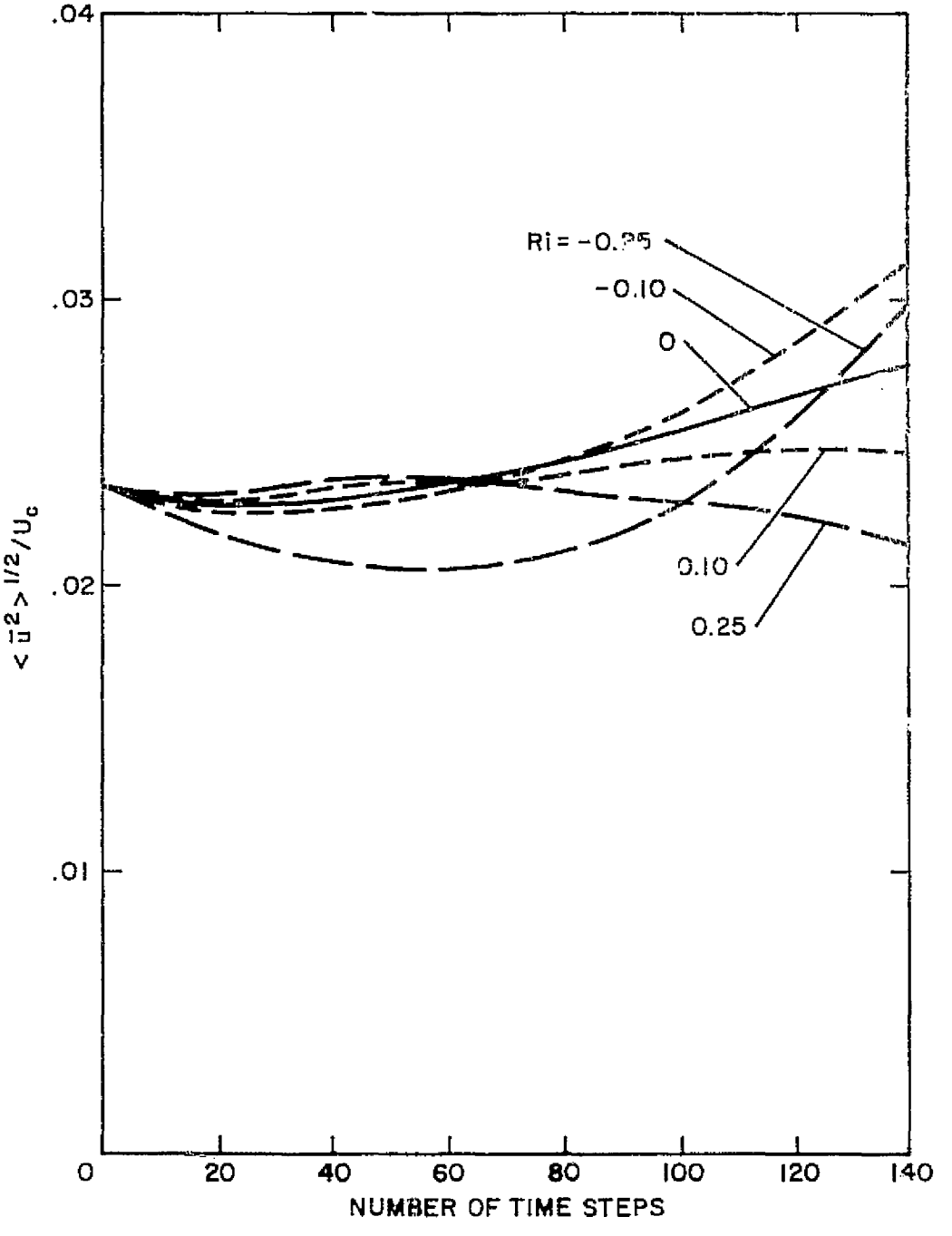

Fig. 6-3. Turbulence level of u for different gradient Richardson numbers.

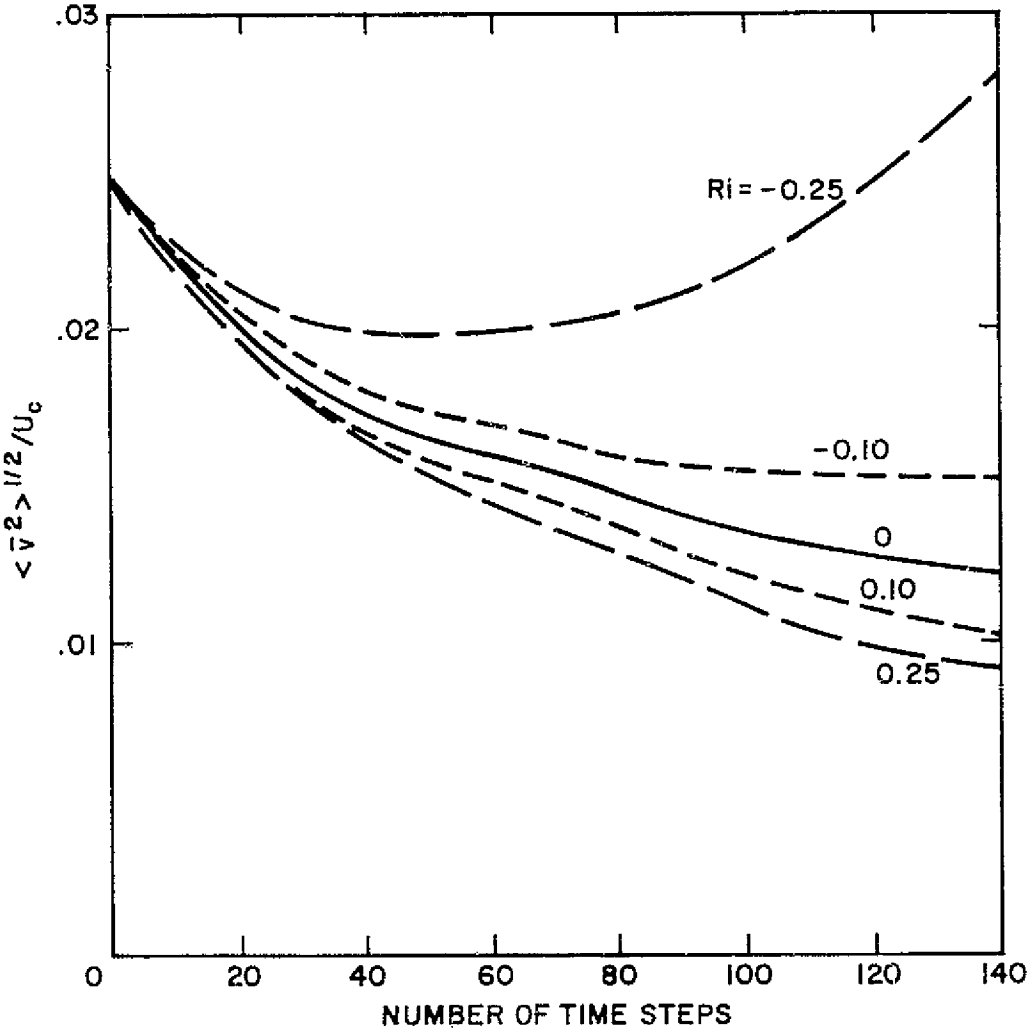

Fig. 6-4. Turbulence level of v for different gradient Richardson numbers.

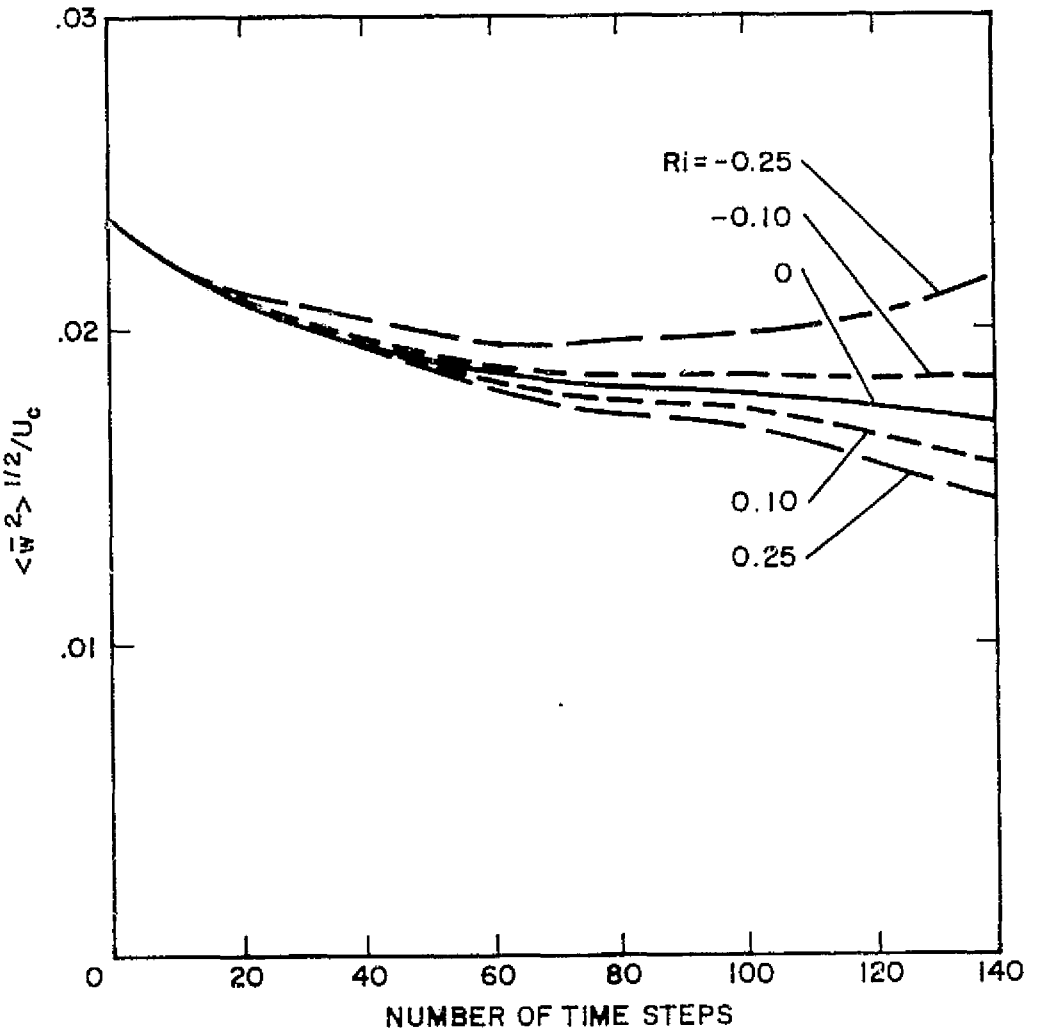

Fig. 6-5. Turbulence level of w for different gradient Richardson numbers.

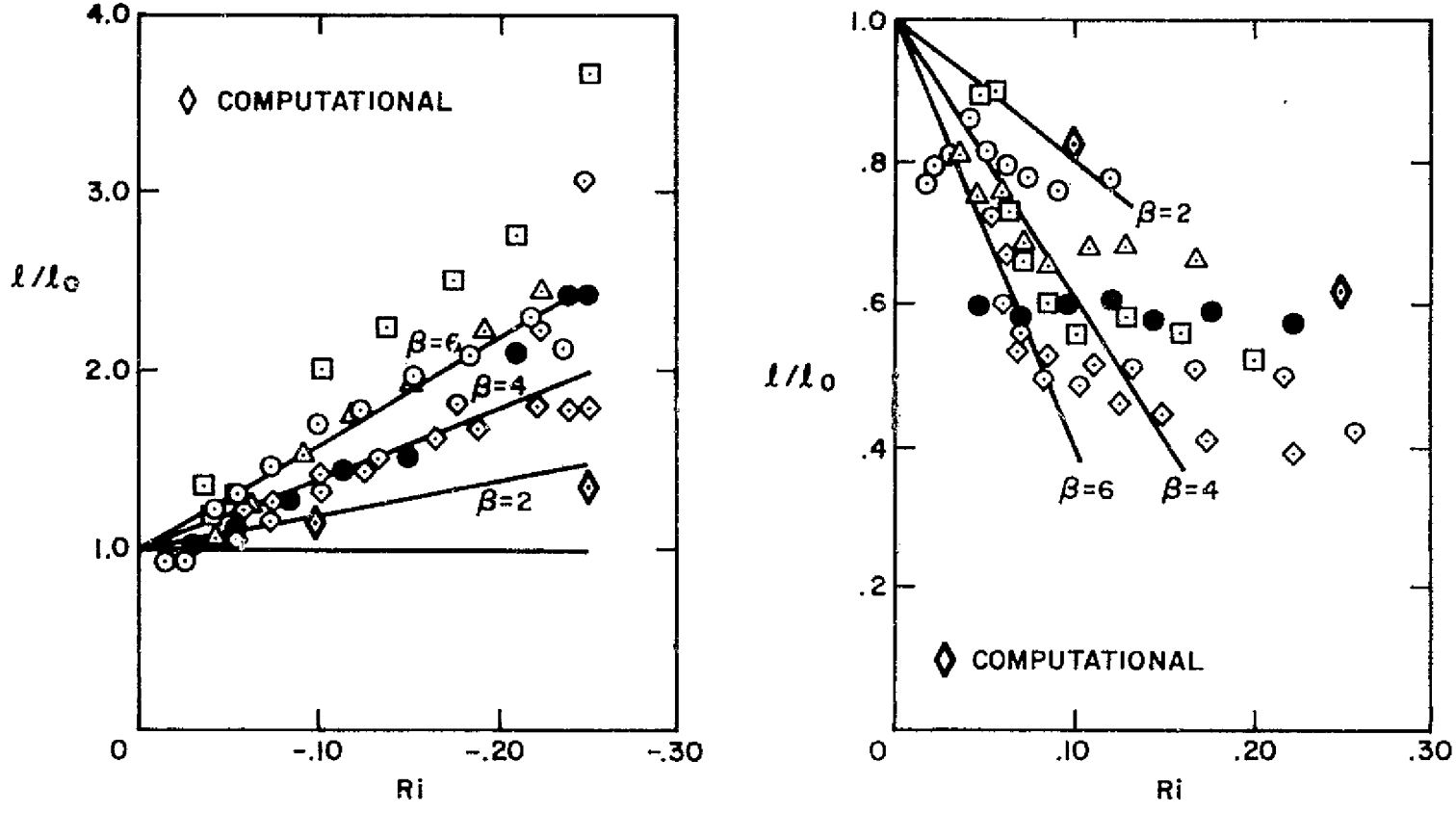

Fig. 6-6. Mixing length ratio versus gradient Richardson number. Data from Johnston (1974).

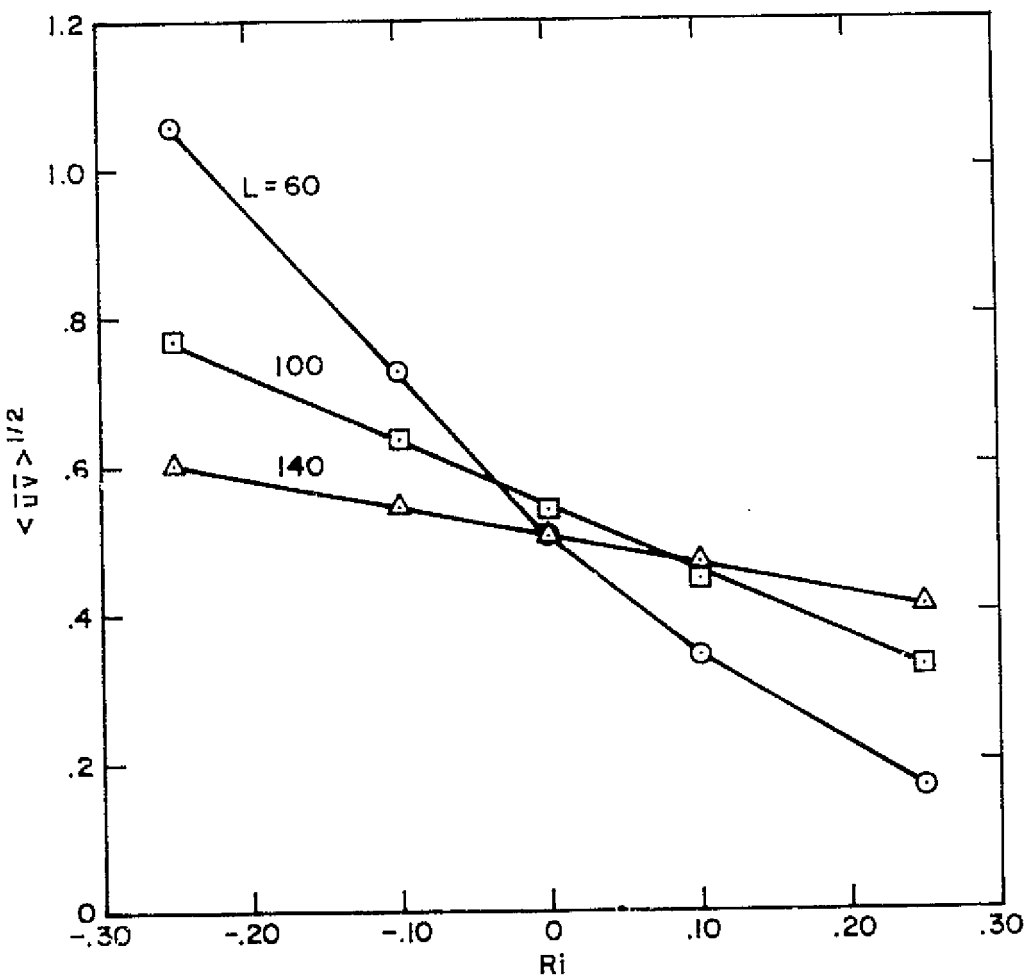

Fig. 6-7. $<\bar{u}\bar{v}>^{1/2}$ versus gradient Richardson number at various time steps.

CHAPTER 7

SUMMARY

A. Conclusions

Three-dimensional time-dependent numerical simulations of simple turbulent flows using the filtered incompressible Navier-Stokes equations with the simple formulation of Smagorinsky for the subgrid scale eddy coefficient prove to give very reasonable results. Although the number of degrees of freedom of 16^3 mesh points is limited, with respect to resolution, it was shown that useful information can be extracted from these simulations, which contain much of the physics of these flows. Furthermore, the approach is convenient and reasonably economical with regard to speed and capacity of available computers.

The proposed numerical scheme for the filtered advective term, which contains a Leonard term implicitly, was shown to be important for proper energy transfer down the wave-number scale and is recommended for use in future investigations, in particular when long time integrations are needed and when the turbulent energy is spread over a wide range of wave numbers (high Reynolds numbers).

The imposed periodic conditions for the turbulence, which have been used in all of our examples, have advantages as well as disadvantages. The advantages are twofold. First, the mathematical problem is well posed on the boundaries, and does not introduce errors into the domain of numerical integration. Second, periodic conditions allow the use of rapid routines in the solution of the Poisson equation. The disadvantage is that turbulent length scales must be kept small compared to the computational dimension, and in problems where these scales grow, numerical simulation cannot be carried out for long times without invalidating this requirement.

B. Recommendations

Based on the experience gained in this work the following recommendations are proposed for future work in this field:

1. Improvement of initial conditions to allow better control on the statistics of the velocity and pressure fields such as stresses $<\bar{u}_i\bar{u}_j>$ and pressure-strain correlations T_{ij} .
2. Extension of boundary conditions to allow other conditions than periodic. For example, treatment of a rotational-irrotational interface and a solid boundary.
3. Extension of the computational region, at least in important directions such as the shear direction in a homogeneous shear problem, to allow longer integration periods. This will require the use of peripheral equipment.
4. Simulation of other basic flows for which experimental data exist such as vortex pairing and far field solutions of jets and wakes.

This work is one of many efforts made in recent years the aim of which is to explore the basic problems of turbulent flow simulations, and it is believed that eventually it will bring about the solution of actual problems on the engineering level.

APPENDIX A

THE FILTERING OPERATOR AND ITS PROPERTIES

The filtered function $\overline{f}(\underline{x})$ is obtained as the convolution integral of the function $f(\underline{x})$ with a filtering function $g(\underline{x})$

$$\overline{f}(\underline{x}) = g(\underline{x}) * f(\underline{x}) = \int_{\text{all space}} g(\underline{x}-\underline{x}')\, f(\underline{x}')\, d\underline{x}' \qquad \text{(A-1)}$$

$\underline{x}$. $\underline{x}'$ are position vectors whose components in a Cartesian system are x, y, z and x', y', z', respectively, and $d\underline{x}'$ is the volume element $dx'\, dy'\, dz'$.

The only requirement on the filtering function $g(\underline{x})$ is that it is Fourier transformable, which means that it should be square integrable. Since

$$\mathcal{F}\left\{\frac{\partial}{\partial x_i}\left[g(\underline{x}) * f(\underline{x})\right]\right\} = i\, k_i\, \hat{g}(\underline{k})\, \hat{f}(\underline{k}) \qquad \text{(A-2)}$$

and

$$\mathcal{F}\left[\frac{\partial g(\underline{x})}{\partial x_i} * f(\underline{x})\right] = i\, k_i\, \hat{g}(\underline{k})\, \hat{f}(\underline{k}) \qquad \text{(A-3)}$$

and also

$$\mathcal{F}\left[g(\underline{x}) * \frac{\partial f(\underline{x})}{\partial x_i}\right] = i\, k_i\, \hat{g}(\underline{k})\, \hat{f}(\underline{k}) \qquad \text{(A-4)}$$

then

$$\frac{\partial}{\partial x_i}(g\, f) = \frac{\partial g}{\partial x_i} * f = g * \frac{\partial f}{\partial x_i} \qquad \text{(A-5)}$$

and an important conclusion can be drawn:

$$\overline{\frac{\partial f}{\partial x_i}} = \frac{\partial}{\partial x_i}\, \overline{f} \qquad \text{(A-6)}$$

The filtering function used in this work for averaging the Navier-Stokes equations is the Gaussian filter defined by

$$g(\underline{x}) = \left[\left(\frac{6}{\pi}\right)^{1/2} \frac{1}{\Delta}\right]^3 \exp\left(-6|\underline{x}|^2/\Delta^2\right) \tag{A-7}$$

the Fourier transform of which is

$$\hat{g}(\underline{k}) = \exp\left(-\Delta^2|\underline{k}|^2/24\right) \tag{A-8}$$

Other functions can be used as well. For example, the running mean filter is defined by

$$g(\underline{x}) = \begin{cases} \dfrac{1}{\Delta^3} & |\underline{x}| \leq \text{box of sides } \Delta \\ 0 & |\underline{x}| > \text{box of sides } \Delta \end{cases} \tag{A-9}$$

its Fourier transform is given by

$$\hat{g}(\underline{k}) = \prod_{i=1}^{3} \frac{\sin(k_i\Delta/2)}{k_i\,\Delta/2} \tag{A-10}$$

This filter has been used by Deardorff (1970). For a detailed discussion of the properties of these filters see Kwak, et al. (1975).

APPENDIX B

GENERATION OF INITIAL VELOCITY FIELD FOR ISOTROPIC TURBULENCE SIMULATION

The initial velocity field for isotropic turbulence simulation should satisfy the following requirements (to simplify, we shall drop the averaging symbol ($\bar{\ }$))

$$k_i'(\underline{k})\ u_i(\underline{k}) = 0 \tag{B-1}$$

$$u_i(\underline{k}) = \left[u_i(-\underline{k})\right]^* \tag{B-2}$$

$$< u_i(\underline{k})\ u_j(\underline{k}) > = 0 \qquad i \neq j \tag{B-3}$$

$$u_i(\underline{k})\ u_i^*(\underline{k}) = E(k)/2\pi k^2 \tag{B-4}$$

where k_i' , u_i are complex vector fields, and $\underline{k}$ is the position vector in Fourier space. Let

$$k_i' = (k_i')_R + i\,(k_i')_I \tag{B-5}$$

$$u_i = (u_i)_R + i\,(u_i)_I \tag{B-6}$$

Substituting the last two equations into Eqns. (B-1) and (B-4), and separating real and imaginary parts, we have

$$(k_i')_R(u_i)_R - (k_i')_I(u_i)_I = 0 \tag{B-7}$$

$$(k_i')_R(u_i)_I - (k_i')_I(u_i)_R = 0 \tag{B-8}$$

$$(u_i u_i)_R + (u_i u_i)_I = E(k)/2\pi k^2 \tag{B-9}$$

To satisfy Eq. (B-3), the velocity components should be random.

The required field is generated in two stages. First, two fields ${}_1u_i$, ${}_2u_i$ are generated, with k_i' real and equal to $(k_i')_R$ and $(k_i')_I$, respectively. Second, the fields are combined to give the required field that satisfy Eqs. (B-1) to (B-4).

Let us assume for the moment that we have generated these two fields; then

$$(k_i')_R({}_1u_i) = 0 \tag{B-10}$$

$$(k_i')_I({}_2u_i) = 0 \tag{B-11}$$

$${}_1u_i\ {}_1u_i^* = {}_2u_i\ {}_2u_i^* = E(k)/2\pi k^2 \tag{B-12}$$

Let the desired field be a linear combination of the two fields

$$(u_i)_R = a_1({}_1u_i)_R + a_2({}_2u_i)_R \tag{B-13}$$

$$(u_i)_I = a_3({}_1u_i)_I + a_4({}_2u_i)_I \tag{B-14}$$

Substitute Eqs. (B-13) and (B-14) into (B-7) to (B-9) and use Eqs. (B-10) and (B-11) to get

$$a_2(k_i')_R({}_2u_i)_R - a_3(k_i')_I({}_1u_i)_I = 0 \tag{B-15}$$

$$a_1(k_i')_I({}_1u_i)_R - a_4(k_i')_R({}_2u_i)_I = 0 \tag{B-16}$$

$$\begin{aligned} &a_1^2({}_1u_i\ {}_1u_i)_R + 2a_1a_2({}_1u_i\ {}_2u_i)_R + a_2^2({}_2u_i\ {}_2u_i)_R \\ &+ a_3^2({}_1u_i\ {}_1u_i)_I + 2a_3a_4({}_1u_i\ {}_2u_i)_I + a_4^2({}_2u_i\ {}_2u_i)_I \\ &= E(k)/2\pi k^2 \end{aligned} \tag{B-17}$$

In order to determine the field u_i, we have to determine the constants a_1, a_2, a_3, a_4. This is done by solving the three algebraic equations (B-15) to (B-17) in four unknowns (one is determined arbitrarily), for every value of k_i in the region $k_3 \leq 0$. The other half-space $k_3 > 0$ is obtained by condition (B-2), which makes $u_i(\underline{x})$ real.

The two separate fields are generated as follows: Consider a coordinate system in wave-number space, as shown in Fig. B-1. For any position vector k_i, the vector k_i' is specified. k_i' depends on the specific finite-difference scheme used for the divergence operator; for example, see Eq. (4-12). Let u_i be a vector which lies in a plane P perpendicular to k_i', and which makes an angle ξ with a reference to vector $\underline{t}$, which is the intersection of P and the plane formed by k_i' and $\underline{e}_3$. ξ is chosen randomly in the range $(0,2\pi)$. $u_i u_i$ is chosen to be equal to $E(k)/2\pi k^2$. Let η be another random number in the range $(0,1)$. Decompose $u_i u_i$ into two parts such that

$$(u_i u_i)_R = \eta(u_i u_i) \tag{B-18}$$

$$(u_i u_i)_I = (1-\eta)(u_i u_i) \tag{B-19}$$

Then decompose $(u_i u_i)_R^{1/2}\ \underline{e}_u$ and $(u_i u_i)_I^{1/2}\ \underline{e}_u$ into their components along the vectors $\underline{e}_1$, $\underline{e}_2$, $\underline{e}_3$ according to the formulae

$$(u_1)_R = -(\cos\xi\ \cos\phi\ \cos\theta + \sin\xi\ \sin\theta)(u_i u_i)_R^{1/2} \tag{B-20}$$

$$(u_2)_R = (-\cos\xi\ \cos\phi\ \sin\theta + \sin\xi\ \cos\theta)(u_i u_i)_R^{1/2} \tag{B-21}$$

$$(u_3)_R = (\cos\xi\ \sin\phi)(u_i u_i)_R^{1/2} \tag{B-22}$$

$$(u_1)_I = -(\cos\xi\ \cos\phi\ \cos\theta + \sin\xi\ \sin\theta)(u_i u_i)_I^{1/2} \tag{B-23}$$

$$(u_2)_I = (-\cos\xi\ \cos\phi\ \sin\theta + \sin\xi\ \cos\theta)(u_i u_i)_I^{1/2} \tag{B-24}$$

$$(u_3)_I = (\cos\xi \ \sin\phi \ )(u_i u_i)_I^{1/2} \tag{B-25}$$

This procedure is repeated twice for $(k_i')_R$ and $(k_i')_I$. The subroutine INICON is a realization of this method.

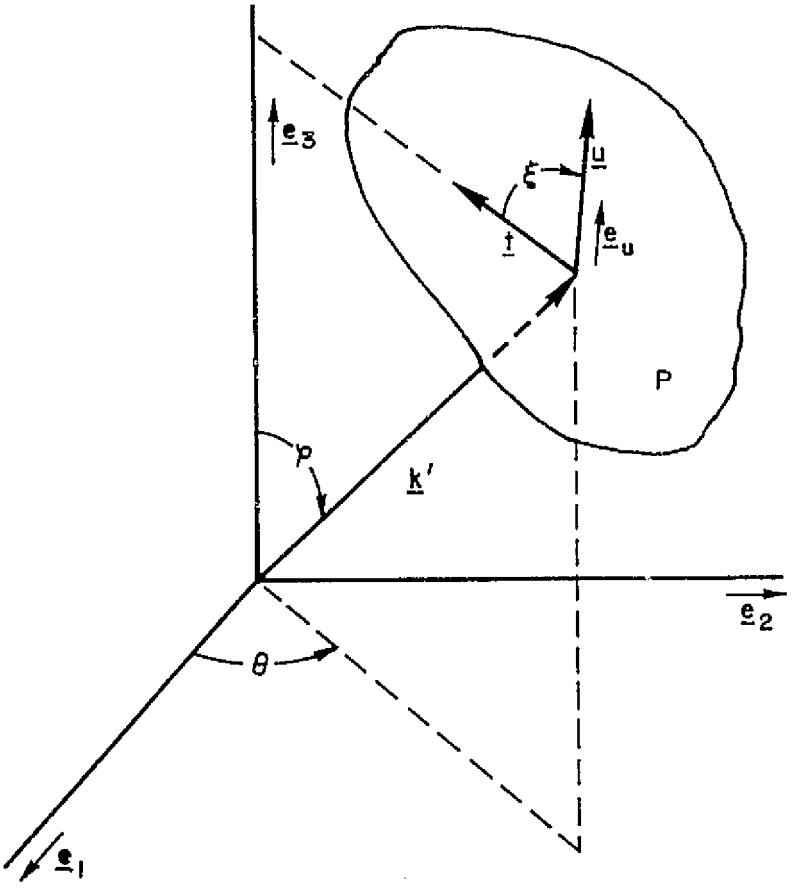

Fig. B-1. Coordinate system for decomposition of $\underline{u}$.

APPENDIX C

THE DISCRETE FOURIER TRANSFORM AND ITS COMPUTATIONAL FORM

The truncated sum of a Fourier expansion up to wave number $N/2$ is given by

$$f(n) = \sum_{m=-N/2}^{N/2-1} F(m) \exp(2\pi i\, mn/N) \qquad n=0,\ldots,N-1 \tag{C-1}$$

The inverse of this transformation is given by

$$F(m) = \frac{1}{N}\sum_{n=0}^{N-1} f(n) \exp(-2\pi i\, nm/N) \qquad m=-N/2,\ldots,N/2-1 \tag{C-2}$$

A more frequently used transform pair is given by the definition

$$f(n) = \sum_{m=0}^{N-1} F(m) \exp(2\pi i\, mn/N) \qquad n=0,\ldots,N-1 \tag{C-3}$$

$$F(m) = \frac{1}{N}\sum_{n=0}^{N-1} f(n) \exp(-2\pi i\, nm/N) \qquad m=0,\ldots,N-1 \tag{C-4}$$

which is used in most fast Fourier transform (FFT) algorithms.

Since exp is a periodic function in N, it is, in general, immaterial whether one set is used or the other. Both will recover the original function after applying a transform followed by an inverse. However, when discrete Fourier transforms are used to solve differential equations, the first pair should be used, otherwise the method will pick up an aliased solution which contains higher frequencies. Nevertheless, it is not required to give up the existing FFT codes, because there is a one to one correspondence between the two definitions.

Consider that $f(n)$, $n=0,\ldots,N-1$ is given. Then, according to Eq. (C-2) we have

$$F(m) = \frac{1}{N}\sum_{n=0}^{N-1} f(n)\ \exp(-2\pi i\, nm/N) \qquad m=-N/2,\ldots,N/2-1 \quad \text{(C-5)}$$

$$= \frac{1}{N}\sum_{n=0}^{N-1} f(n)\ \exp(-2\pi i\, nm'/N) \qquad m' = \begin{cases} m+n & \text{for } -N/2 \le m < 0 \\ m & \text{for } 0 \le m < N/2-1 \end{cases}$$

m' now varies from 0 to $N-1$, as in Eqn. (C-4), but the ordering of $F(m)$ has been changed. As an example, consider the case of $N = 4$. Let

$$f(n) = \left\{ f(0),\ f(1),\ f(2),\ f(3) \right\}$$

The discrete Fourier transform of $f(n)$ using Eqn. (C-2) gives

$$F(m) = \left\{ F(-2),\ F(-1),\ F(0),\ F(1) \right\}$$

while using Eqn. (C-4) the order of $F(m)$ is changed to

$$F(m) = \left\{ F(0),\ F(1),\ F(-2),\ F(-1) \right\}$$

For a detailed description of the fast Fourier transform algorithms the reader should see Cochran, et al. (1967).

C2

APPENDIX D

THE COMPLETE EXPANSION OF THE FILTERED ADVECTIVE TERM FOR THE STAGGERED MESH CONFIGURATION

In the following, a complete expansion of the term $\partial/\partial x_j\ (\overline{\bar{u}_i\bar{u}_j})$ in three dimensions is given for the staggered-mesh configuration which contains implicitly the Leonard term as part of its truncation error (see Chapter 3) (the overbar is dropped from $\bar{u}_i$ in the expansion).

$$
\begin{aligned}
\frac{\partial}{\partial x}(\overline{\bar{u}\bar{u}})_{i+1/2,j,k} = \\
&\frac{\alpha}{4h}\Big[(u_{i+3/2,j,k} + u_{i+1/2,j,k})^2 - (u_{i+1/2,j,k} + u_{i-1/2,j,k})^2\Big] \\
&+ \frac{1-\alpha}{64h}\Big[(u_{i+3/2,j,k} + u_{i+3/2,j+1,k} + u_{i+1/2,j+1,k} + u_{i+1/2,j,k})^2 \\
&\quad - (u_{i+1/2,j,k} + u_{i+1/2,j+1,k} + u_{i-1/2,j+1,k} + u_{i-1/2,j,k})^2 \\
&\quad + (u_{i+3/2,j-1,k} + u_{i+3/2,j,k} + u_{i+1/2,j,k} + u_{i+1/2,j-1,k})^2 \\
&\quad - (u_{i+1/2,j-1,k} + u_{i+1/2,j,k} + u_{i-1/2,j,k} + u_{i-1/2,j-1,k})^2 \\
&\quad + (u_{i+3/2,j,k+1} + u_{i+3/2,j,k} + u_{i+1/2,j,k} + u_{i+1/2,j,k+1})^2 \\
&\quad - (u_{i+1/2,j,k+1} + u_{i+1/2,j,k} + u_{i-1/2,j,k} + u_{i-1/2,j,k+1})^2 \\
&\quad + (u_{i+3/2,j,k} + u_{i+3/2,j,k-1} + u_{i+1/2,j,k-1} + u_{i+1/2,j,k})^2 \\
&\quad - (u_{i+1/2,j,k} + u_{i+1/2,j,k-1} + u_{i-1/2,j,k-1} + u_{i-1/2,j,k})^2\Big]
\end{aligned}
\qquad \text{(D-1)}
$$

$$\frac{\partial}{\partial y}(\overline{\bar{u}\bar{v}})_{i+1/2,j,k} =$$

$$\frac{\alpha}{4h}\Big[(u_{i+1/2,j,k} + u_{i+1/2,j+1,k})(v_{i+1,j+1/2,k} + v_{i,j+1/2,k})$$

$$- (u_{i+1/2,j-1,k} + u_{i+1/2,j,k})(v_{i+1,j-1/2,k} + v_{i,j-1/2,k})\Big]$$

$$+ \frac{1-\alpha}{16h}\Big[(u_{i+3/2,j,k} + u_{i+3/2,j+1,k} + u_{i+1/2,j+1,k} + u_{i+1/2,j,k})v_{i+1,j+1/2,k}$$

$$- (u_{i+3/2,j-1,k} + u_{i+3/2,j,k} + u_{i+1/2,j,k} + u_{i+1/2,j-1,k})v_{i+1,j-1/2,k}$$

$$+ (u_{i+1/2,j,k} + u_{i+1/2,j+1,k} + u_{i-1/2,j+1,k} + u_{i-1/2,j,k})v_{i,j+1/2,k}$$

$$- (u_{i+1/2,j-1,k} + u_{i+1/2,j,k} + u_{i-1/2,j,k} + u_{i-1/2,j-1,k})v_{i,j-1/2,k}\Big]$$

$$+ \frac{1-\alpha}{64h}\Big[(u_{i+1/2,j,k} + u_{i+1/2,j+1,k} + u_{i+1/2,j,k+1} + u_{i+1/2,j+1,k+1})$$

$$\cdot (v_{i+1,j+1/2,k} + v_{i,j+1/2,k} + v_{i+1,j+1/2,k+1} + v_{i,j+1/2,k+1})$$

$$- (u_{i+1/2,j-1,k} + u_{i+1/2,j,k} + u_{i+1/2,j-1,k+1} + u_{i+1/2,j,k+1})$$

$$\cdot (v_{i+1,j-1/2,k} + v_{i,j-1/2,k} + v_{i+1,j-1/2,k+1} + v_{i,j-1/2,k+1})$$

$$+ (u_{i+1/2,j,k-1} + u_{i+1/2,j+1,k-1} + u_{i+1/2,j,k} + u_{i+1/2,j+1,k})$$

$$\cdot (v_{i+1,j+1/2,k-1} + v_{i,j+1/2,k-1} + v_{i+1,j+1/2,k} + v_{i,j+1/2,k})$$

$$- (u_{i+1/2,j-1,k-1} + u_{i+1/2,j,k-1} + u_{i+1/2,j-1,k} + u_{i+1/2,j,k})$$

$$\cdot (v_{i+1,j-1/2,k-1} + v_{i,j-1/2,k-1} + v_{i+1,j-1/2,k} + v_{i,j-1/2,k})\Big] \qquad \text{(D-2)}$$

$$\frac{\partial}{\partial z}(\overline{\bar{u}\bar{w}})_{i+1/2,j,k} =$$

$$\frac{\alpha}{4h}\Big[(u_{i+1/2,j,k} + u_{i+1/2,j,k+1})(w_{i+1,j,k+1/2} + w_{i,j,k+1/2})$$

$$- (u_{i+1/2,j,k-1} + u_{i+1/2,j,k})(w_{i+1,j,k-1/2} + w_{i,j,k-1/2})\Big]$$

$$+ \frac{1-\alpha}{16h}\Big[(u_{i+3/2,j,k+1} + u_{i+3/2,j,k} + u_{i+1/2,j,k} + u_{i+1/2,j,k+1})w_{i+1,j,k+1/2}$$

$$- (u_{i+3/2,j,k} + u_{i+3/2,j,k-1} + u_{i+1/2,j,k-1} + u_{i+1/2,j,k})w_{i+1,j,k-1/2}$$

$$+ (u_{i+1/2,j,k+1} + u_{i+1/2,j,k} + u_{i-1/2,j,k} + u_{i-1/2,j,k+1})w_{i,j,k+1/2}$$

$$- (u_{i+1/2,j,k} + u_{i+1/2,j,k-1} + u_{i-1/2,j,k-1} + u_{i-1/2,j,k})w_{i,j,k-1/2}\Big]$$

$$+ \frac{1-\alpha}{64}\Big[(u_{i+1/2,j,k} + u_{i+1/2,j,k+1} + u_{i+1/2,j+1,k} + u_{i+1/2,j+1,k+1})$$

$$\cdot (w_{i+1,j,k+1/2} + w_{i,j,k+1/2} + w_{i+1,j+1,k+1/2} + w_{i,j+1,k+1/2})$$

$$- (u_{i+1/2,j,k-1} + u_{i+1/2,j,k} + u_{i+1/2,j+1,k-1} + u_{i+1/2,j+1,k})$$

$$\cdot (w_{i+1,j,k-1/2} + w_{i,j,k-1/2} + w_{i+1,j+1,k-1/2} + w_{i,j+1,k-1/2})$$

$$+ (u_{i+1/2,j-1,k} + u_{i+1/2,j-1,k+1} + u_{i+1/2,j,k} + u_{i+1/2,j,k+1})$$

$$\cdot (w_{i+1,j-1,k+1/2} + w_{i,j-1,k+1/2} + w_{i+1,j,k+1/2} + w_{i,j,k+1/2})$$

$$- (u_{i+1/2,j-1,k-1} + u_{i+1/2,j-1,k} + u_{i+1/2,j,k-1} + u_{i+1/2,j,k})$$

$$\cdot (w_{i+1,j-1,k-1/2} + w_{i,j-1,k-1/2} + w_{i+1,j,k-1/2} + w_{i,j,k-1/2})\Big]$$

(D-3)

$$\frac{\partial}{\partial x}(\overline{\bar{v}\bar{u}})_{i,j+1/2,k} =$$

$$\frac{\alpha}{4h}\Big[(v_{i+1,j+1/2,k} + v_{i,j+1/2,k})(u_{i+1/2,j,k} + u_{i+1/2,j+1,k})$$

$$- (v_{i,j+1/2,k} + v_{i-1,j+1/2,k})(u_{i-1/2,j,k} + u_{i-1/2,j+1,k})\Big]$$

$$+ \frac{1-\alpha}{16h}\Big[(v_{i+1,j+1/2,k} + v_{i+1,j+3/2,k} + v_{i,j+3/2,k} + v_{i,j+1/2,k})u_{i+1/2,j+1,k}$$

$$- (v_{i,j+1/2,k} + v_{i,j+3/2,k} + v_{i-1,j+3/2,k} + v_{i-1,j+1/2,k})u_{i-1/2,j+1,k}$$

$$+ (v_{i+1,j-1/2,k} + v_{i+1,j+1/2,k} + v_{i,j+1/2,k} + v_{i,j-1/2,k})u_{i+1/2,j,k}$$

$$- (v_{i,j-1/2,k} + v_{i,j+1/2,k} + v_{i-1,j+1/2,k} + v_{i-1,j-1/2,k})u_{i-1/2,j,k}\Big]$$

$$+ \frac{1-\alpha}{64h}\Big[(v_{i+1,j+1/2,k} + v_{i,j+1/2,k} + v_{i+1,j+1/2,k+1} + v_{i,j+1/2,k+1})$$

$$\cdot (u_{i+1/2,j,k} + u_{i+1/2,j+1,k} + u_{i+1/2,j,k+1} + u_{i+1/2,j+1,k+1})$$

$$- (v_{i,j+1/2,k} + v_{i-1,j+1/2,k} + v_{i,j+1/2,k+1} + v_{i-1,j+1/2,k+1})$$

$$\cdot (u_{i-1/2,j,k} + u_{i-1/2,j+1,k} + u_{i-1/2,j,k+1} + u_{i-1/2,j+1,k+1})$$

$$+ (v_{i+1,j+1/2,k-1} + v_{i,j+1/2,k-1} + v_{i+1,j+1/2,k} + v_{i,j+1/2,k})$$

$$\cdot (u_{i+1/2,j,k-1} + u_{i+1/2,j+1,k-1} + u_{i+1/2,j,k} + u_{i+1/2,j+1,k})$$

$$- (v_{i,j+1/2,k-1} + v_{i-1,j+1/2,k-1} + v_{i,j+1/2,k} + v_{i-1,j+1/2,k})$$

$$\cdot (u_{i-1/2,j,k-1} + u_{i-1/2,j+1,k-1} + u_{i-1/2,j,k} + u_{i-1/2,j+1,k})\Big]$$

(D-4)

$$\frac{\partial}{\partial y}(\overline{\bar{v}\bar{v}})_{i,j+1/2,k} =$$

$$\frac{\alpha}{4h}\left[(v_{i,j+3/2,k} + v_{i,j+1/2,k})^2 - (v_{i,j+1/2,k} + v_{i,j-1/2,k})^2\right]$$

$$+ \frac{1-\alpha}{64h}\Big[(v_{i+1,j+1/2,k} + v_{i+1,j+3/2,k} + v_{i,j+3/2,k} + v_{i,j+1/2,k})^2$$

$$- (v_{i+1,j-1/2,k} + v_{i+1,j+1/2,k} + v_{i,j+1/2,k} + v_{i,j-1/2,k})^2$$

$$+ (v_{i,j+1/2,k} + v_{i,j+3/2,k} + v_{i-1,j+3/2,k} + v_{i-1,j+1/2,k})^2$$

$$- (v_{i,j-1/2,k} + v_{i,j+1/2,k} + v_{i-1,j+1/2,k} + v_{i-1,j-1/2,k})^2$$

$$+ (v_{i,j+1/2,k} + v_{i,j+3/2,k} + v_{i,j+1/2,k+1} + v_{i,j+3/2,k+1})^2$$

$$- (v_{i,j-1/2,k} + v_{i,j+1/2,k} + v_{i,j-1/2,k+1} + v_{i,j+1/2,k+1})^2$$

$$+ (v_{i,j+1/2,k-1} + v_{i,j+3/2,k-1} + v_{i,j+1/2,k} + v_{i,j+3/2,k})^2$$

$$- (v_{i,j-1/2,k-1} + v_{i,j+1/2,k-1} + v_{i,j-1/2,k} + v_{i,j+1/2,k})^2\Big] \qquad \text{(D-5)}$$

$$\frac{\partial}{\partial z}(\overline{\bar{v}\bar{w}})_{i,j+1/2,k} =$$

$$\frac{\alpha}{4h}\Big[(v_{i,j+1/2,k} + v_{i,j+1/2,k+1})(w_{i,j,k+1/2} + w_{i,j+1,k+1/2})$$

$$- (v_{i,j+1/2,k-1} + v_{i,j+1/2,k})(w_{i,j,k-1/2} + w_{i,j+1,k-1/2})\Big]$$

$$+ \frac{1-\alpha}{16h}\Big[(v_{i,j+1/2,k} + v_{i,j+3/2,k} + v_{i,j+3/2,k+1} + v_{i,j+1/2,k+1})w_{i,j+1,k+1/2}$$

$$- (v_{i,j+1/2,k-1} + v_{i,j+3/2,k-1} + v_{i,j+3/2,k} + v_{i,j+1/2,k})w_{i,j+1,k-1/2}$$

$$+ (v_{i,j-1/2,k} + v_{i,j+1/2,k} + v_{i,j+1/2,k+1} + v_{i,j-1/2,k+1})w_{i,j,k+1/2}$$

$$- (v_{i,j-1/2,k-1} + v_{i,j+1/2,k-1} + v_{i,j+1/2,k} + v_{i,j-1/2,k})w_{i,j,k-1/2}\Big]$$

$$+ \frac{1-\alpha}{64h}\Big[(v_{i,j+1/2,k} + v_{i,j+1/2,k+1} + v_{i+1,j+1/2,k} + v_{i+1,j+1/2,k+1})$$

$$\cdot (w_{i,j,k+1/2} + w_{i,j+1,k+1/2} + w_{i+1,j,k+1/2} + w_{i+1,j+1,k+1/2})$$

$$- (v_{i,j+1/2,k-1} + v_{i,j+1/2,k} + v_{i+1,j+1/2,k-1} + v_{i+1,j+1/2,k})$$

$$\cdot (w_{i,j,k-1/2} + w_{i,j+1,k-1/2} + w_{i+1,j,k-1/2} + w_{i+1,j+1,k-1/2})$$

$$+ (v_{i-1,j+1/2,k} + v_{i-1,j+1/2,k+1} + v_{i,j+1/2,k} + v_{i,j+1/2,k+1})$$

$$\cdot (w_{i-1,j,k+1/2} + w_{i-1,j+1,k+1/2} + w_{i,j,k+1/2} + w_{i,j+1,k+1/2})$$

$$- (v_{i-1,j+1/2,k-1} + v_{i-1,j+1/2,k} + v_{i,j+1/2,k-1} + v_{i,j+1/2,k})$$

$$\cdot (w_{i-1,j,k-1/2} + w_{i-1,j+1,k-1/2} + w_{i,j,k-1/2} + w_{i,j+1,k-1/2})\Big]$$

(D-6)

$$\frac{\partial}{\partial x}(\overline{\bar{w}\bar{u}})_{i,j,k+1/2} =$$

$$\frac{\alpha}{4h}\Big[(w_{i+1,j,k+1/2} + w_{i,j,k+1/2})(u_{i+1/2,j,k+1} + u_{i+1/2,j,k})$$

$$- (w_{i,j,k+1/2} + w_{i-1,j,k+1/2})(u_{i-1/2,j,k+1} + u_{i-1/2,j,k})\Big]$$

$$+ \frac{1-\alpha}{16h}\Big[(w_{i+1,j,k+3/2} + w_{i+1,j,k+1/2} + w_{i,j,k+1/2} + w_{i,j,k+3/2})u_{i+1/2,j,k+1}$$

$$- (w_{i,j,k+3/2} + w_{i,j,k+1/2} + w_{i-1,j,k+1/2} + w_{i-1,j,k+3/2})u_{i-1/2,j,k+1}$$

$$+ (w_{i+1,j,k+1/2} + w_{i+1,j,k-1/2} + w_{i,j,k-1/2} + w_{i,j,k+1/2})u_{i+1/2,j,k}$$

$$- (w_{i,j,k+1/2} + W_{i,j,k-1/2} + w_{i-1,j,k-1/2} + w_{i-1,j,k+1/2})u_{i-1/2,j,k}\Big]$$

$$+ \frac{1-\alpha}{64h}\Big[(w_{i+1,j,k+1/2} + w_{i,j,k+1/2} + w_{i+1,j+1,k+1/2} + w_{i,j+1,k+1/2})$$

$$\cdot (u_{i+1/2,j,k+1} + u_{i+1/2,j,k} + u_{i+1/2,j+1,k+1} + u_{i+1/2,j+1,k})$$

$$- (w_{i,j,k+1/2} + w_{i-1,j,k+1/2} + w_{i,j+1,k+1/2} + w_{i-1,j+1,k+1/2})$$

$$\cdot (u_{i-1/2,j,k+1} + u_{i-1/2,j,k} + u_{i-1/2,j+1,k+1} + u_{i-1/2,j+1,k})$$

$$+ (w_{i+1,j-1,k+1/2} + w_{i,j-1,k+1/2} + w_{i+1,j,k+1/2} + w_{i,j,k+1/2})$$

$$\cdot (u_{i+1/2,j-1,k+1} + u_{i+1/2,j-1,k} + u_{i+1/2,j,k+1} + u_{i+1/2,j,k})$$

$$- (w_{i,j-1,k+1/2} + w_{i-1,j-1,k+1/2} + w_{i,j,k+1/2} + w_{i-1,j,k+1/2})$$

$$\cdot (u_{i-1/2,j-1,k+1} + u_{i-1/2,j-1,k} + u_{i-1/2,j,k+1} + u_{i-1/2,j,k})\Big]$$

(D-7)

$$\frac{\partial}{\partial y}(\overline{\bar{w}\bar{v}})_{i,j,k+1/2} =$$

$$\frac{\alpha}{4h}\Big[(w_{i,j,k+1/2} + w_{i,j+1,k+1/2})(v_{i,j+1/2,k} + v_{i,j+1/2,k+1})$$

$$- (w_{i,j-1,k+1/2} + w_{i,j,k+1/2})(v_{i,j-1/2,k} + v_{i,j-1/2,k+1})\Big]$$

$$+ \frac{1-\alpha}{16h}\Big[(w_{i,j,k+1/2} + w_{i,j+1,k+1/2} + w_{i,j+1,k+3/2} + w_{i,j,k+3/2})v_{i,j+1/2,k+1}$$

$$- (w_{i,j-1,k+1/2} + w_{i,j,k+1/2} + w_{i,j,k+3/2} + w_{i,j-1,k+3/2})v_{i,j-1/2,k+1}$$

$$+ (w_{i,j,k-1/2} + w_{i,j+1,k-1/2} + w_{i,j+1,k+1/2} + w_{i,j,k+1/2})v_{i,j+1/2,k}$$

$$- (w_{i,j-1,k-1/2} + w_{i,j,k-1/2} + w_{i,j,k+1/2} + w_{i,j-1,k+1/2})v_{i,j-1/2,k}\Big]$$

$$+ \frac{1-\alpha}{64h}\Big[(w_{i,j,k+1/2} + w_{i,j+1,k+1/2} + w_{i+1,j,k+1/2} + w_{i+1,j+1,k+1/2})$$

$$\cdot (v_{i,j+1/2,k} + v_{i,j+1/2,k+1} + v_{i+1,j+1/2,k} + v_{i+1,j+1/2,k+1})$$

$$- (w_{i,j-1,k+1/2} + w_{i,j,k+1/2} + w_{i+1,j-1,k+1/2} + w_{i+1,j,k+1/2})$$

$$\cdot (v_{i,j-1/2,k} + v_{i,j-1/2,k+1} + v_{i+1,j-1/2,k} + v_{i+1,j-1/2,k+1})$$

$$+ (w_{i-1,j,k+1/2} + w_{i-1,j+1,k+1/2} + w_{i,j,k+1/2} + w_{i,j+1,k+1/2})$$

$$\cdot (v_{i-1,j+1/2,k} + v_{i-1,j+1/2,k+1} + v_{i,j+1/2,k} + v_{i,j+1/2,k+1})$$

$$- (w_{i-1,j-1,k+1/2} + w_{i-1,j,k+1/2} + w_{i,j-1,k+1/2} + w_{i,j,k+1/2})$$

$$\cdot (v_{i-1,j-1/2,k} + v_{i-1,j-1/2,k+1} + v_{i,j-1/2,k} + v_{i,j-1/2,k+1})\Big]$$

(D-8)

$$\frac{\partial}{\partial z}(\overline{\bar{w}\bar{w}})_{i,j,k+1/2} =$$

$$\frac{\alpha}{4h}\left[(w_{i,j,k+1/2} + w_{i,j,k+3/2})^2 - (w_{i,j,k-1/2} - w_{i,j,k+1/2})^2\right]$$

$$+ \frac{1-\alpha}{64h}\left[(w_{i,j,k+1/2} + w_{i,j,k+3/2} + w_{i+1,j,k+1/2} + w_{i+1,j,k+3/2})^2\right.$$

$$- (w_{i,j,k-1/2} + w_{i,j,k+1/2} + w_{i+1,j,k-1/2} + w_{i+1,j,k+1/2})^2$$

$$+ (w_{i-1,j,k+1/2} + w_{i-1,j,k+3/2} + w_{i,j,k+1/2} + w_{i,j,k+3/2})^2$$

$$- (w_{i-1,j,k-1/2} + w_{i-1,j,k+1/2} + w_{i,j,k-1/2} + w_{i,j,k+1/2})^2$$

$$+ (w_{i,j,k+1/2} + w_{i,j,k+3/2} + w_{i,j+1,k+1/2} + w_{i,j+1,k+3/2})^2$$

$$- (w_{i,j,k-1/2} + w_{i,j,k+1/2} + w_{i,j+1,k-1/2} + w_{i,j+1,k+1/2})^2$$

$$+ (w_{i,j-1,k+1/2} + w_{i,j-1,k+3/2} + w_{i,j,k+1/2} + w_{i,j,k+3/2})^2$$

$$\left. - (w_{i,j-1,k-1/2} + w_{i,j-1,k+1/2} + w_{i,j,k-1/2} + w_{i,j,k+1/2})^2\right] \tag{D-9}$$

```
      PROGRAM  TFC  (INPUT,OUTPUT,TAPE5=INPUT,TAPE6=OUTPUT,TAPE8,TAPE9)
C     ******************************************************************
C     * LANGUAGE:FORTRAN  COMPUTER:CDC7600  COMPILER:RUN76, LBL BERKELEY*
C     * NOMENCLATURE:                                                  *
C     * H       MESH SIZE                                              *
C     * DT      TIME STEP                                              *
C     * U0      MAXIMUN MEAN VELOCITY IN SHEAR FLOW                    *
C     * OMEGA   ROTATION                                               *
C     * C       TURBULENT MODEL CONSTANT                               *
C     * FDC     FINITE DIFFERENCE CONSTANT                             *
C     * L       NUMBER OF TIME STEPS                                   *
C     ******************************************************************
      LARGE PR1(16,16,16),PI1(16,16,16),WAVE(16,16,16)
      LARGE U1(16,16,19),V1(16,16,19),W1(16,16,19)
      LARGE RX1(16,16,16),RY1(16,16,16),RZ1(16,16,16)
      DIMENSION U(22,22,7),V(22,22,7),W(22,22,7)
      DIMENSION EV(20,20,5),PR(20,20,5)
      EQUIVALENCE (EV(1,1,1),PR(1,1,1))
      DIMENSION SX(18,18,3),SY(18,18,3),SZ(18,18,3)
      DIMENSION QR(16,16),QI(16,16)
      DIMENSION N(3),M1(6),M2(6),TRR(16,3),TRI(16,3),E(16)
      COMMON/SCH/QR,QI,N,M1,M2,TRR,TRI,E,ISIGN,PAI
      REAL LAMBDA
      PAI=3.141592653589793
      PAI2=PAI*PAI
      H=1./16.
      H2=H*H
      DT=0.025
      C=0.24
      U0=0.0
      OMEGA=0.0
      FDC=1./3.
      C1=FDC/H
      C2=(1.-FDC)/4./H
      C3=C*C*H
      C4=C1/4.
      C5=C2/16.
      C6=C2/4.
      C7=1./(H2*4.)
      C8=1./(2.*H)
      C9=1./H
      C11=C1/2.
      C12=C2/4.
      CALL TRRTRI
C-----INITIAL DATA:
C-----SUBROUTINE INICON GENERATES THE INITIAL VELOCITY FIELD
C-----ACCORDING TO APPENDIX B
      CALL INICON
      DO 11 K=1,16
      DO 11 J=1,16
      DO 11 I=1,16
      RX1(I,J,K)=0.0
      RY1(I,J,K)=0.0
      RZ1(I,J,K)=0.0
 11   CONTINUE
C-----FIRST STEP IS ADVANCED BY EULER METHOD (ALPHA=1.0),
```

ORIGINAL PAGE IS
OF POOR QUALITY

```
C-----ADAMS-BASHFORTH METHOD IS USED THEREAFTER (ALPHA=1.5)
      ALPHA=1.0
      L=0
      USQR=0.0
      DUDX2=0.0
      DUDX3=0.0
      ENRG=0.0
      DIV=0.0
 6    M=1
      DO 2 K=1,3
      KK=K+16
      DO 2 J=1,16
      DO 2 I=1,16
      U1(I,J,KK)=U1(I,J,K)
      V1(I,J,KK)=V1(I,J,K)
      W1(I,J,KK)=W1(I,J,K)
 2    CONTINUE
      WRITE(6,102) L
 102  FORMAT(1H1,10X,22HNUMBER OF TIME STEP L=,I3)
      WRITE(6,107)
 107  FORMAT(1H ,10X,* U COMPONENT OF VEL FIELD *)
      SMALLIN(QR(1,1),U1(1,1, 9), 256)
      DO 44 I=1,16,8
      WRITE(6,106) I
      WRITE(6,105) (QR(I,J),J=1,16)
 44   CONTINUE
      WRITE(6,108)
 108  FORMAT(1H ,10X,* V COMPONENT OF VEL FIELD *)
      SMALLIN(QR(1,1),V1(1,1, 9), 256)
      DO 45 I=1,16,8
      WRITE(6,106) I
      WRITE(6,105) (QR(I,J),J=1,16)
 45   CONTINUE
      WRITE(6,109)
 109  FORMAT(1H ,10X,* W COMPONENT OF VEL FIELD *)
      SMALLIN(QR(1,1),W1(1,1, 9), 256)
      DO 46 I=1,16,8
      WRITE(6,106) I
      WRITE(6,105) (QR(I,J),J=1,16)
 46   CONTINUE
 1    IF(M.EQ.1) GO TO 8
      K=7
      GO TO 16
 8    DO 20 K5=1,7
      K=K5
      K2=K5+13
      IF(K2.GT.16) K2=K2-16
 16   SMALLIN(QR(1,1),U1(1,1,K2), 256)
      DO 29 J=1,16
      DO 29 I=1,16
      JJ=J+3
      II=I+3
      U(II,JJ,K)=QR(I,J)
 29   CONTINUE
      SMALLIN(QR(1,1),V1(1,1,K2), 256)
```


ORIGINAL PAGE IS
OF POOR QUALITY

```
      DO 89 I=1,16
      DO 89 J=1,16
      JJ=J+3
      II=I+3
      V(II,JJ,K)=QR(I,J)
 89   CONTINUE
      SMALLIN(QR(1,1),W1(1,1,K2), 256)
      DO 99 J=1,16
      DO 99 I=1,16
      JJ=J+3
      II=I+3
      W(II,JJ,K)=QR(I,J)
 99   CONTINUE
C-----EXTEND VELOCITY FIELD PERIODICALLY IN X,Y DIRECTIONS.
      DO 24 J=4,19
      U(1,J,K)=U(17,J,K)
      V(1,J,K)=V(17,J,K)
      W(1,J,K)=W(17,J,K)
      U(2,J,K)=U(18,J,K)
      V(2,J,K)=V(18,J,K)
      W(2,J,K)=W(18,J,K)
      U(3,J,K)=U(19,J,K)
      V(3,J,K)=V(19,J,K)
      W(3,J,K)=W(19,J,K)
      U(20,J,K)=U(4,J,K)
      V(20,J,K)=V(4,J,K)
      W(20,J,K)=W(4,J,K)
      U(21,J,K)=U(5,J,K)
      V(21,J,K)=V(5,J,K)
      W(21,J,K)=W(5,J,K)
      U(22,J,K)=U(6,J,K)
      V(22,J,K)=V(6,J,K)
      W(22,J,K)=W(6,J,K)
 24   CONTINUE
      DO 22 I=1,22
      U(I,1,K)=U(I,17,K)
      V(I,1,K)=V(I,17,K)
      W(I,1,K)=W(I,17,K)
      U(I,2,K)=U(I,18,K)
      V(I,2,K)=V(I,18,K)
      W(I,2,K)=W(I,18,K)
      U(I,3,K)=U(I,19,K)
      V(I,3,K)=V(I,19,K)
      W(I,3,K)=W(I,19,K)
      U(I,20,K)=U(I,4,K)
      V(I,20,K)=V(I,4,K)
      W(I,20,K)=W(I,4,K)
      U(I,21,K)=U(I,5,K)
      V(I,21,K)=V(I,5,K)
      W(I,21,K)=W(I,5,K)
      U(I,22,K)=U(I,6,K)
      V(I,22,K)=V(I,6,K)
      W(I,22,K)=W(I,6,K)
 22   CONTINUE
 20   CONTINUE
```

ORIGINAL PAGE IS
OF POOR QUALITY

```
C-----COMPUTE THE EDDY VISCOSITY COEFFICIENT
      DO 25 K=2,6
      DO 25 J=2,21
      DO 25 I=2,21
      KK=K-1
      JJ=J-1
      II=I-1
      EV(II,JJ,KK)=C3*SQRT(2.*(U(I,J,K)-U(I-1,J,K))**2
     * +2.*(V(I,J,K)-V(I,J-1,K))**2+2.*(W(I,J,K)-W(I,J,K-1))**2
     * +.25*((U(I,J+1,K)-U(I,J,K)+V(I+1,J,K)-V(I,J,K))**2
     * +(U(I-1,J+1,K)-U(I-1,J,K)+V(I,J,K)-V(I-1,J,K))**2
     * +(U(I-1,J,K)-U(I-1,J-1,K)+V(I,J-1,K)-V(I-1,J-1,K))**2
     * +(U(I,J,K)-U(I,J-1,K)+V(I+1,J-1,K)-V(I,J-1,K))**2
     * +(V(I,J,K+1)-V(I,J,K)+W(I,J+1,K)-W(I,J,K))**2
     * +(V(I,J,K)-V(I,J,K-1)+W(I,J+1,K-1)-W(I,J,K-1))**2
     * +(V(I,J-1,K)-V(I,J-1,K-1)+W(I,J,K-1)-W(I,J-1,K-1))**2
     * +(V(I,J-1,K+1)-V(I,J-1,K)+W(I,J,K)-W(I,J-1,K))**2
     * +(W(I+1,J,K)-W(I,J,K)+U(I,J,K+1)-U(I,J,K))**2
     * +(W(I+1,J,K-1)-W(I,J,K-1)+U(I,J,K)-U(I,J,K-1))**2
     * +(W(I,J,K-1)-W(I-1,J,K-1)+U(I-1,J,K)-U(I-1,J,K-1))**2
     * +(W(I,J,K)-W(I-1,J,K)+U(I-1,J,K+1)-U(I-1,J,K))**2))
 25   CONTINUE
C-----COMPUTE R.H.S. OF MOMENTUM EQUATION (PRESSURE GRADIENT
C-----NOT INCLUDED)
      IF(M.EQ.1) GO TO 26
      K=4
      GO TO 27
 26   DO 35 K=2,4
 27   DO 35 J=2,19
      DO 35 I=2,19
      KK=K-1
      JJ=J-1
      II=I-1
      J1=1
      J2=1
      IF(JJ.NE.1) GO TO 58
      J1=-1
      J2=-1
 58   SSX=
     * -C4*((U(I+2,J+1,K+1)+U(I+1,J+1,K+1))**2
     * -(U(I+1,J+1,K+1)+U(I,J+1,K+1))**2)-C5*
     * ((U(I+2,J+1,K+1)+U(I+2,J+2,K+1)+U(I+1,J+2,K+1)+U(I+1,J+1,K+1))**2
     * -(U(I+1,J+1,K+1)+U(I+1,J+2,K+1)+U(I,J+2,K+1)+U(I,J+1,K+1))**2
     * +(U(I+2,J,K+1)+U(I+2,J+1,K+1)+U(I+1,J+1,K+1)+U(I+1,J,K+1))**2
     * -(U(I+1,J,K+1)+U(I+1,J+1,K+1)+U(I,J+1,K+1)+U(I,J,K+1))**2
     * +(U(I+2,J+1,K+2)+U(I+2,J+1,K+1)+U(I+1,J+1,K+1)+U(I+1,J+1,K+2))**2
     * -(U(I+1,J+1,K+2)+U(I+1,J+1,K+1)+U(I,J+1,K+1)+U(I,J+1,K+2))**2
     * +(U(I+2,J+1,K+1)+U(I+2,J+1,K)+U(I+1,J+1,K)+U(I+1,J+1,K+1))**2
     * -(U(I+1,J+1,K+1)+U(I+1,J+1,K)+U(I,J+1,K)+U(I,J+1,K+1))**2)
      SSX=SSX-C4*
     *  ((U(I+1,J+1,K+1)+U(I+1,J+2,K+1))*(V(I+2,J+1,K+1)+V(I+1,J+1,K+1))
     * -(U(I+1,J,K+1)+U(I+1,J+1,K+1))*(V(I+2,J,K+1)+V(I+1,J,K+1)))-C6
     * *((U(I+2,J+1,K+1)+U(I+2,J+2,K+1)+U(I+1,J+2,K+1)+U(I+1,J+1,K+1))*
     * V(I+2,J+1,K+1)
     * -(U(I+2,J,K+1)+U(I+2,J+1,K+1)+U(I+1,J+1,K+1)+U(I+1,J,K+1))*
```


ORIGINAL PAGE IS
OF POOR QUALITY

```
* V(I+2,J,K+1)
* +(U(I+1,J+1,K+1)+U(I+1,J+2,K+1)+U(I,J+2,K+1)+U(I,J+1,K+1))*
* V(I+1,J+1,K+1)
* -(U(I+1,J,K+1)+U(I+1,J+1,K+1)+U(I,J+1,K+1)+U(I,J,K+1))*
* V(I+1,J,K+1))-C5*
*  ((U(I+1,J+1,K+1)+U(I+1,J+2,K+1)+U(I+1,J+1,K+2)+U(I+1,J+2,K+2))*
* (V(I+2,J+1,K+1)+V(I+1,J+1,K+1)+V(I+2,J+1,K+2)+V(I+1,J+1,K+2))
* -(U(I+1,J,K+1)+U(I+1,J+1,K+1)+U(I+1,J,K+2)+U(I+1,J+1,K+2))*
* (V(I+2,J,K+1)+V(I+1,J,K+1)+V(I+2,J,K+2)+V(I+1,J,K+2))
* +(U(I+1,J+1,K)+U(I+1,J+2,K)+U(I+1,J+1,K+1)+U(I+1,J+2,K+1))*
* (V(I+2,J+1,K)+V(I+1,J+1,K)+V(I+2,J+1,K+1)+V(I+1,J+1,K+1))
* -(U(I+1,J,K)+U(I+1,J+1,K)+U(I+1,J,K+1)+U(I+1,J+1,K+1))*
* (V(I+2,J,K)+V(I+1,J,K)+V(I+2,J,K+1)+V(I+1,J,K+1)))
 SSX=SSX-C4
* *((U(I+1,J+1,K+1)+U(I+1,J+1,K+2))*(W(I+2,J+1,K+1)+W(I+1,J+1,K+1))
* -(U(I+1,J+1,K)+U(I+1,J+1,K+1))*(W(I+2,J+1,K)+W(I+1,J+1,K)))-C6
* *((U(I+2,J+1,K+2)+U(I+2,J+1,K+1)+U(I+1,J+1,K+1)+U(I+1,J+1,K+2))*
* W(I+2,J+1,K+1)
* -(U(I+2,J+1,K+1)+U(I+2,J+1,K)+U(I+1,J+1,K)+U(I+1,J+1,K+1))*
* W(I+2,J+1,K)
* +(U(I+1,J+1,K+2)+U(I+1,J+1,K+1)+U(I,J+1,K+1)+U(I,J+1,K+2))*
* W(I+1,J+1,K+1)
* -(U(I+1,J+1,K+1)+U(I+1,J+1,K)+U(I,J+1,K)+U(I,J+1,K+1))*
* W(I+1,J+1,K))-C5*
*  ((U(I+1,J+1,K+1)+U(I+1,J+1,K+2)+U(I+1,J+2,K+1)+U(I+1,J+2,K+2))*
* (W(I+2,J+1,K+1)+W(I+1,J+1,K+1)+W(I+2,J+2,K+1)+W(I+1,J+2,K+1))
* -(U(I+1,J+1,K)+U(I+1,J+1,K+1)+U(I+1,J+2,K)+U(I+1,J+2,K+1))*
* (W(I+2,J+1,K)+W(I+1,J+1,K)+W(I+2,J*2,K)+U(I+1,J+2,K))
* +(U(I+1,J,K+1)+U(I+1,J,K+2)+U(I+1,J+1,K+1)+U(I+1,J+1,K+2))*
* (W(I+2,J,K+1)+W(I+1,J,K+1)+W(I+2,J+1,K+1)+W(I+1,J+1,K+1))
* -(U(I+1,J,K)+U(I+1,J,K+1)+U(I+1,J+1,K)+U(I+1,J+1,K+1))*
* (W(I+2,J,K)+W(I+1,J,K)+W(I+2,J+1,K)+W(I+1,J+1,K)))
 SX(II,JJ,KK)=SSX
* +(8.*(EV(I+1,J,K)*(U(I+2,J+1,K+1)-U(I+1,J+1,K+1))
* -EV(I,J,K)*(U(I+1,J+1,K+1)-U(I,J+1,K+1)))
* + (EV(I,J,K)+EV(I+1,J,K)+EV(I+1,J+1,K)+EV(I,J+1,K))*
* (U(I+1,J+2,K+1)-U(I+1,J+1,K+1)+V(I+2,J+1,K+1)-V(I+1,J+1,K+1))
* -(EV(I,J,K)+EV(I+1,J,K)+EV(I+1,J-1,K)+EV(I,J-1,K))*
* (U(I+1,J+1,K+1)-U(I+1,J,K+1)+V(I+2,J,K+1)-V(I+1,J,K+1))
* +(EV(I,J,K)+EV(I+1,J,K)+EV(I,J,K+1)+EV(I+1,J,K+1))*
* (U(I+1,J+1,K+2)-U(I+1,J+1,K+1)+W(I+2,J+1,K+1)-W(I+1,J+1,K+1))
* -(EV(I,J,K)+EV(I+1,J,K)+EV(I,J,K-1)+EV(I+1,J,K-1))*
* (U(I+1,J+1,K+1)-U(I+1,J+1,K)+W(I+2,J+1,K)-W(I+1,J+1,K)))*C7
 SX(II,JJ,KK)=SX(II,JJ,KK)
* -2.*U0*((FLOAT(JJ-1)*H-(.5+H))*((U(I+2,J+1,K+1)-U(I,J+1,K+1))*C11
* +(U(I+2,J+1,K+2)+2.*U(I+2,J+1,K+1)-2.*U(I,J+1,K+1)-U(I,J+1,K+2)
* +U(I+2,J+1,K)-U(I,J+1,K))*C12)
* +(FLOAT(JJ-1)*H+0.5*H-(.5+H))*
* (U(I+2,J+1,K+1)+U(I+2,J+2,K+1)-U(I,J+2,K+1)-U(I,J+1,K+1))*C12
* +(FLOAT(JJ-1)*H-0.5*H-(.5+H))*
* (U(I+2,J,K+1)+U(I+2,J+1,K+1)-U(I,J+1,K+1)-U(I,J,K+1))*C12)
 SX(II,JJ,KK)=SX(II,JJ,KK)
* -U0*(((FLOAT(JJ-1)*H+.5*H-(.5+H))*(V(I+2,J+1,K+1)+V(I+1,J+1,K+1))
* -(FLOAT(JJ-1)*H-.5*H-(.5+H))*(V(I+2,J,K+1)+V(I+1,J,K+1)))*C11
* +((FLOAT(JJ-1)*H+.5*H-(.5+H))*4.*V(I+2,J+1,K+1)
```

ORIGINAL PAGE IS
OF POOR QUALITY

```
* -(FLOAT(JJ-1)*H-.5*H-(.5+H))*4.*V(I+2,J,K+1)
* +(FLOAT(JJ-1)*H+.5*H-(.5+H))*4.*V(I+1,J+1,K+1)
* -(FLOAT(JJ-1)*H-.5*H-(.5+H))*4.*V(I+1,J,K+1)
* +(FLOAT(JJ-1)*H+.5*H-(.5+H))*
* (V(I+2,J+1,K+1)+V(I+1,J+1,K+1)+V(I+2,J+1,K+2)+V(I+1,J+1,K+2))
* -(FLOAT(JJ-1)*H-.5*H-(.5+H))*
* (V(I+2,J,K+1)+V(I+1,J,K+1)+V(I+2,J,K+2)+V(I+1,J,K+2))
* +(FLOAT(JJ-1)*H+.5*H-(.5+H))*
* (V(I+2,J+1,K)+V(I+1,J+1,K)+V(I+2,J+1,K+1)+V(I+1,J+1,K+1))
* -(FLOAT(JJ-1)*H-.5*H-(.5+H))*
* (V(I+2,J,K)+V(I+1,J,K)+V(I+2,J,K+1)+V(I+1,J,K+1)))*C12)
 SX(II,JJ,KK)=SX(II,JJ,KK)
* -U0*((FLOAT(JJ-1)*H-(.5+H))*
* (W(I+2,J+1,K+1)+W(I+1,J+1,K+1)-W(I+2,J+1,K)-W(I+1,J+1,K))*
* (C11+C2)
* +((FLOAT(JJ-1)*H+.5*H-(.5+H))*
* (W(I+2,J+1,K+1)+W(I+1,J+1,K+1)+W(I+2,J+2,K+1)+W(I+1,J+2,K+1)
* -W(I+2,J+1,K)-W(I+1,J+1,K)-W(I+2,J+2,K)-W(I+1,J+2,K))
* +(FLOAT(JJ-1)*H-.5*H-(.5+H))*
* (W(I+2,J,K+1)+W(I+1,J,K+1)+W(I+2,J+1,K+1)+W(I+1,J+1,K+1)
* -W(I+2,J,K)-W(I+1,J,K)-W(I+2,J+1,K)-W(I+1,J+1,K)))*C12)
* +2.*OMEGA*.25*
* (V(I+2,J,K+1)+V(I+2,J+1,K+1)+V(I+1,J+1,K+1)+V(I+1,J,K+1))
 SSY=-C4*
*  ((V(I+2,J+1,K+1)+V(I+1,J+1,K+1))*(U(I+1,J+1,K+1)+U(I+1,J+2,K+1))
* -(V(I+1,J+1,K+1)+V(I,J+1,K+1))*(U(I,J+1,K+1)+U(I,J+2,K+1)))-C6
* *((V(I+2,J+1,K+1)+V(I+2,J+2,K+1)+V(I+1,J+2,K+1)+V(I+1,J+1,K+1))*
* U(I+1,J+2,K+1)
* -(V(I+1,J+1,K+1)+V(I+1,J+2,K+1)+V(I,J+2,K+1)+V(I,J+1,K+1))*
* U(I,J+2,K+1)
* +(V(I+2,J,K+1)+V(I+2,J+1,K+1)+V(I+1,J+1,K+1)+V(I+1,J,K+1))*
* U(I+1,J+1,K+1)
* -(V(I+1,J,K+1)+V(I+1,J+1,K+1)+V(I,J+1,K+1)+V(I,J,K+1))*
* U(I,J+1,K+1))-C5*
*  ((V(I+2,J+1,K+1)+V(I+1,J+1,K+1)+V(I+2,J+1,K+2)+V(I+1,J+1,K+2))*
* (U(I+1,J+1,K+1)+U(I+1,J+2,K+1)+U(I+1,J+1,K+2)+U(I+1,J+2,K+2))
* -(V(I+1,J+1,K+1)+V(I,J+1,K+1)+V(I+1,J+1,K+2)+V(I,J+1,K+2))*
* (U(I,J+1,K+1)+U(I,J+2,K+1)+U(I,J+1,K+2)+U(I,J+2,K+2))
* +(V(I+2,J+1,K)+V(I+1,J+1,K)+V(I+2,J+1,K+1)+V(I+1,J+1,K+1))*
* (U(I+1,J+1,K)+U(I+1,J+2,K)+U(I+1,J+1,K+1)+U(I+1,J+2,K+1))
* -(V(I+1,J+1,K)+V(I,J+1,K)+V(I+1,J+1,K+1)+V(I,J+1,K+1))*
* (U(I,J+1,K)+U(I,J+2,K)+U(I,J+1,K+1)+U(I,J+2,K+1)))
 SSY=SSY-C4*
*  ((V(I+1,J+2,K+1)+V(I+1,J+1,K+1))**2
* -(V(I+1,J+1,K+1)+V(I+1,J,K+1))**2)-C5*
* ((V(I+2,J+1,K+1)+V(I+2,J+2,K+1)+V(I+1,J+2,K+1)+V(I+1,J+1,K+1))**2
* -(V(I+2,J,K+1)+V(I+2,J+1,K+1)+V(I+1,J+1,K+1)+V(I+1,J,K+1))**2
* +(V(I+1,J+1,K+1)+V(I+1,J+2,K+1)+V(I,J+2,K+1)+V(I,J+1,K+1))**2
* -(V(I+1,J,K+1)+V(I+1,J+1,K+1)+V(I,J+1,K+1)+V(I,J,K+1))**2
* +(V(I+1,J+1,K+1)+V(I+1,J+2,K+1)+V(I+1,J+2,K+2)+V(I+1,J+1,K+2))**2
* -(V(I+1,J,K+1)+V(I+1,J+1,K+1)+V(I+1,J+1,K+2)+V(I+1,J,K+2))**2
* +(V(I+1,J+1,K)+V(I+1,J+2,K)+V(I+1,J+2,K+1)+V(I+1,J+1,K+1))**2
* -(V(I+1,J,K)+V(I+1,J+1,K)+V(I+1,J+1,K+1)+V(I+1,J,K+1))**2)
 SSY=SSY-C4*
*  ((V(I+1,J+1,K+1)+V(I+1,J+1,K+2))*(W(I+1,J+1,K+1)+W(I+1,J+2,K+1))
```

ORIGINAL PAGE IS
OF POOR QUALITY

```
* -(V(I+1,J+1,K)+V(I+1,J+1,K+1))*(W(I+1,J+1,K)+W(I+1,J+2,K)))-C5
* *((V(I+1,J+1,K+1)+V(I+1,J+1,K+2)+V(I+2,J+1,K+1)+V(I+2,J+1,K+2))*
* (W(I+1,J+1,K+1)+W(I+1,J+2,K+1)+W(I+2,J+1,K+1)+W(I+2,J+2,K+1))
* -(V(I+1,J+1,K)+V(I+1,J+1,K+1)+V(I+2,J+1,K)+V(I+2,J+1,K+1))*
* (W(I+1,J+1,K)+W(I+1,J+2,K)+W(I+2,J+1,K)+W(I+2,J+2,K))
* +(V(I,J+1,K+1)+V(I,J+1,K+2)+V(I+1,J+1,K+1)+V(I+1,J+1,K+2))*
* (W(I,J+1,K+1)+W(I,J+2,K+1)+W(I+1,J+1,K+1)+W(I+1,J+2,K+1))
* -(V(I,J+1,K)+V(I,J+1,K+1)+V(I+1,J+1,K)+V(I+1,J+1,K+1))*
* (W(I,J+1,K)+W(I,J+2,K)+W(I+1,J+1,K)+W(I+1,J+2,K)))-C6*
*  ((V(I+1,J+1,K+1)+V(I+1,J+2,K+1)+V(I+1,J+2,K+2)+V(I+1,J+1,K+2))*
* W(I+1,J+2,K+1)
* -(V(I+1,J+1,K)+V(I+1,J+2,K)+V(I+1,J+2,K+1)+V(I+1,J+1,K+1))*
* W(I+1,J+2,K)
* +(V(I+1,J,K+1)+V(I+1,J+1,K+1)+V(I+1,J+1,K+2)+V(I+1,J,K+2))*
* W(I+1,J+1,K+1)
* -(V(I+1,J,K)+V(I+1,J+1,K)+V(I+1,J+1,K+1)+V(I+1,J,K+1))*
* W(I+1,J+1,K))
 SY(II,JJ,KK)=SSY
* +((EV(I,J,K)+EV(I,J+1,K)+EV(I,J+1,K+1)+EV(I,J,K+1))*
* (V(I+1,J+1,K+2)-V(I+1,J+1,K+1)+W(I+1,J+2,K+1)-W(I+1,J+1,K+1))
* -(EV(I,J,K)+EV(I,J,K-1)+EV(I,J+1,K-1)+EV(I,J+1,K))*
* (V(I+1,J+1,K+1)-V(I+1,J+1,K)+W(I+1,J+2,K)-W(I+1,J+1,K))
* +3.*(EV(I,J+1,K)*(V(I+1,J+2,K+1)-V(I+1,J+1,K+1))
* -EV(I,J,K)*(V(I+1,J+1,K+1)-V(I+1,J,K+1)))
* +(EV(I,J,K)+EV(I+1,J,K)+EV(I+1,J+1,K)+EV(I,J+1,K))*
* (V(I+2,J+1,K+1)-V(I+1,J+1,K+1)+U(I+1,J+2,K+1)-U(I+1,J+1,K+1))
* -(EV(I,J,K)+EV(I,J+1,K)+EV(I-1,J+1,K)+EV(I-1,J,K))*
* (V(I+1,J+1,K+1)-V(I,J+1,K+1)+U(I,J+2,K+1)-U(I,J+1,K+1)))*C7
 SY(II,JJ,KK)=SY(II,JJ,KK)
* -U0*((FLOAT(JJ-1)*H-J1*.5*(1.+J2*H))*
* ((V(I+2,J+1,K+1)-V(I,J+1,K+1))*C11
* +(2.*V(I+2,J+1,K+1)+V(I+2,J+1,K+2)-2.*V(I,J+1,K+1)-V(I,J+1,K+2)
* +V(I+2,J+1,K)-V(I,J+1,K))*C12)
* +(FLOAT(JJ-1)*H+.5*H-J1*.5*(1.+J2*H))*
* (V(I+2,J+1,K+1)+V(I+2,J+2,K+1)-V(I,J+2,K+1)-V(I,J+1,K+1))*C12
* +(FLOAT(JJ-1)*H-.5*H-J1*.5*(1.+J2*H))*
* (V(I+2,J,K+1)+V(I+2,J+1,K+1)-V(I,J+1,K+1)-V(I,J,K+1))*C12)
* -2.*OMEGA*0.25*
* (U(I+1,J+1,K+1)+U(I+1,J+2,K+1)+U(I,J+2,K+1)+U(I,J+1,K+1))
 SSZ=-C4*
*  ((W(I+2,J+1,K+1)+W(I+1,J+1,K+1))*(U(I+1,J+1,K+2)+U(I+1,J+1,K+1))
* -(W(I+1,J+1,K+1)+W(I,J+1,K+1))*(U(I,J+1,K+2)+U(I,J+1,K+1)))-C5
* *((W(I+2,J+1,K+1)+W(I+1,J+1,K+1)+W(I+2,J+2,K+1)+W(I+1,J+2,K+1))*
* (U(I+1,J+1,K+2)+U(I+1,J+1,K+1)+U(I+1,J+2,K+2)+U(I+1,J+2,K+1))
* -(W(I+1,J+1,K+1)+W(I,J+1,K+1)+W(I+1,J+2,K+1)+W(I,J+2,K+1))*
* (U(I,J+1,K+2)+U(I,J+1,K+1)+U(I,J+2,K+2)+U(I,J+2,K+1))
* +(W(I+2,J,K+1)+W(I+1,J,K+1)+W(I+2,J+1,K+1)+W(I+1,J+1,K+1))*
* (U(I+1,J,K+2)+U(I+1,J,K+1)+U(I+1,J+1,K+2)+U(I+1,J+1,K+1))
* -(W(I+1,J,K+1)+W(I,J,K+1)+W(I+1,J+1,K+1)+W(I,J+1,K+1))*
* (U(I;J,K+2)+U(I,J,K+1)+U(I,J+1,K+2)+U(I,J+1,K+1)))-C6*
*  ((W(I+2,J+1,K+2)+W(I+2,J+1,K+1)+W(I+1,J+1,K+1)+W(I+1,J+1,K+2))*
* U(I+1,J+1,K+2)
* -(W(I+1,J+1,K+2)+W(I+1,J+1,K+1)+W(I,J+1,K+1)+W(I,J+1,K+2))*
* U(I,J+1,K+2)
* +(W(I+2,J+1,K+1)+W(I+2,J+1,K)+W(I+1,J+1,K)+W(I+1,J+1,K+1))*
```

ORIGINAL PAGE IS
OF POOR QUALITY

```
     * U(I+1,J+1,K+1)
     * -(W(I+1,J+1,K+1)+W(I+1,J+1,K)+W(I,J+1,K)+W(I,J+1,K+1))*
     * U(I,J+1,K+1))
      SSZ=SSZ-C4*
     *  ((W(I+1,J+1,K+1)+W(I+1,J+2,K+1))*(V(I+1,J+1,K+1)+V(I+1,J+1,K+2))
     * -(W(I+1,J,K+1)+W(I+1,J+1,K+1))*(V(I+1,J,K+1)+V(I+1,J,K+2)))-C5
     * *((W(I+1,J+1,K+1)+W(I+1,J+2,K+1)+W(I+2,J+1,K+1)+W(I+2,J+2,K+1))*
     * (V(I+1,J+1,K+1)+V(I+1,J+1,K+2)+V(I+2,J+1,K+1)+V(I+2,J+1,K+2))
     * -(W(I+1,J,K+1)+W(I+1,J+1,K+1)+W(I+2,J,K+1)+W(I+2,J+1,K+1))*
     * (V(I+1,J,K+1)+V(I+1,J,K+2)+V(I+2,J,K+1)+V(I+2,J,K+2))
     * +(W(I,J+1,K+1)+W(I,J+2,K+1)+W(I+1,J+1,K+1)+W(I+1,J+2,K+1))*
     * (V(I,J+1,K+1)+V(I,J+1,K+2)+V(I+1,J+1,K+1)+V(I+1,J+1,K+2))
     * -(W(I,J,K+1)+W(I,J+1,K+1)+W(I+1,J,K+1)+W(I+1,J+1,K+1))*
     * (V(I,J,K+1)+V(I,J,K+2)+V(I+1,J,K+1)+V(I+1,J,K+2)))-C6*
     *  ((W(I+1,J+1,K+1)+W(I+1,J+2,K+1)+W(I+1,J+2,K+2)+W(I+1,J+1,K+2))*
     * V(I+1,J+1,K+2)
     * -(W(I+1,J,K+1)+W(I+1,J+1,K+1)+W(I+1,J+1,K+2)+W(I+1,J,K+2))*
     * V(I+1,J,K+2)
     * +(W(I+1,J+1,K)+W(I+1,J+2,K)+W(I+1,J+2,K+1)+W(I+1,J+1,K+1))*
     * V(I+1,J+1,K+1)
     * -(W(I+1,J,K)+W(I+1,J+1,K)+W(I+1,J+1,K+1)+W(I+1,J,K+1))*
     * V(I+1,J,K+1))
      SSZ=SSZ-C4*
     *  ((W(I+1,J+1,K+1)+W(I+1,J+1,K+2))**2-
     * (W(I+1,J+1,K)+W(I+1,J+1,K+1))**2)-C5*
     * ((W(I+1,J+1,K+1)+W(I+1,J+1,K+2)+W(I+2,J+1,K+1)+W(I+2,J+1,K+2))**2
     * -(W(I+1,J+1,K)+W(I+1,J+1,K+1)+W(I+2,J+1,K)+W(I+2,J+1,K+1))**2
     * +(W(I,J+1,K+1)+W(I,J+1,K+2)+W(I+1,J+1,K+1)+W(I+1,J+1,K+2))**2
     * -(W(I,J+1,K)+W(I,J+1,K+1)+W(I+1,J+1,K)+W(I+1,J+1,K+1))**2
     * +(W(I+1,J+1,K+1)+W(I+1,J+1,K+2)+W(I+1,J+2,K+1)+W(I+1,J+2,K+2))**2
     * -(W(I+1,J+1,K)+W(I+1,J+1,K+1)+W(I+1,J+2,K)+W(I+1,J+2,K+1))**2
     * +(W(I+1,J,K+1)+W(I+1,J,K+2)+W(I+1,J+1,K+1)+W(I+1,J+1,K+2))**2
     * -(W(I+1,J,K)+W(I+1,J,K+1)+W(I+1,J+1,K)+W(I+1,J+1,K+1))**2)
      SZ(II,JJ,KK)=SSZ
     * +((EV(I,J,K+1)+EV(I+1,J,K+1)+EV(I+1,J,K)+EV(I,J,K))*
     * (W(I+2,J+1,K+1)-W(I+1,J+1,K+1)+U(I+1,J+1,K+2)-U(I+1,J+1,K+1))
     * -(EV(I-1,J,K+1)+EV(I,J,K+1)+EV(I,J,K)+EV(I-1,J,K))*
     * (W(I+1,J+1,K+1)-W(I,J+1,K+1)+U(I,J+1,K+2)-U(I,J+1,K+1))
     * +(EV(I,J,K+1)+EV(I,J,K)+EV(I,J+1,K)+EV(I,J+1,K+1))*
     * (W(I+1,J+2,K+1)-W(I+1,J+1,K+1)+V(I+1,J+1,K+2)-V(I+1,J+1,K+1))
     * -(EV(I,J-1,K+1)+EV(I,J-1,K)+EV(I,J,K)+EV(I,J,K+1))*
     * (W(I+1,J+1,K+1)-W(I+1,J,K+1)+V(I+1,J,K+2)-V(I+1,J,K+1))
     * +8.*(EV(I,J,K+1)*(W(I+1,J+1,K+2)-W(I+1,J+1,K+1))
     * -EV(I,J,K)*(W(I+1,J+1,K+1)-W(I+1,J+1,K))))*C7
      SZ(II,JJ,KK)=SZ(II,JJ,KK)
     * -U0*((FLOAT(JJ-1)*H-(.5+H))*((W(I+2,J+1,K+1)-W(I,J+1,K+1))*C11
     * +(W(I+2,J+1,K+2)+2.*W(I+2,J+1,K+1)-2.*W(I,J+1,K+1)-W(I,J+1,K+2)
     * +W(I+2,J+1,K)-W(I,J+1,K))*C12)
     * +(FLOAT(JJ-1)*H+0.5*H-(.5+H))*
     * (W(I+2,J+1,K+1)+W(I+2,J+2,K+1)-W(I,J+1,K+1)-W(I,J+2,K+1))*C12
     * +(FLOAT(JJ-1)*H-0.5*H-(.5+H))*
     * (W(I+2,J,K+1)+W(I+2,J+1,K+1)-W(I,J,K+1)-W(I,J+1,K+1))*C12)
 35   CONTINUE
C-----ADVANCE SX,SY,SZ IN TIME
      K=2
```


ORIGINAL PAGE IS
OF POOR QUALITY

```
      SMALLIN(QI(1,1),U1(1,1,M), 256)
      SMALLIN(QR(1,1),RX1(1,1,M), 256)
      DO 60 J=1,16
      DO 60 I=1,16
      QI(I,J)=QI(I,J)+(ALPHA*SX(I+1,J+1,K)-.5*QR(I,J))*DT
 60   CONTINUE
      SMALLOUT(QI(1,1),U1(1,1,M), 256)
      DO 12 J=1,16
      DO 12 I=1,16
      QI(I,J)=SX(I+1,J+1,2)
 12   CONTINUE
      SMALLOUT(QI(1,1)  ,RX1(1,1,M), 256)
      SMALLIN(QI(1,1),V1(1,1,M), 256)
      SMALLIN(QR(1,1),RY1(1,1,M), 256)
      DO 61 J=1,16
      DO 61 I=1,16
      QI(I,J)=QI(I,J)+(ALPHA*SY(I+1,J+1,K)-.5*QR(I,J))*DT
 61   CONTINUE
      SMALLOUT(QI(1,1),V1(1,1,M), 256)
      DO 14 J=1,16
      DO 14 I=1,16
      QI(I,J)=SY(I+1,J+1,2)
 14   CONTINUE
      SMALLOUT(QI(1,1)  ,RY1(1,1,M), 256)
      SMALLIN(QI(1,1),W1(1,1,M), 256)
      SMALLIN(QR(1,1),RZ1(1,1,M), 256)
      DO 62 J=1,16
      DO 62 I=1,16
      QI(I,J)=QI(I,J)+(ALPHA*SZ(I+1,J+1,K)-.5*QR(I,J))*DT
 62   CONTINUE
      SMALLOUT(QI(1,1),W1(1,1,M), 256)
      DO 15 J=1,16
      DO 15 I=1,16
      QI(I,J)=SZ(I+1,J+1,2)
 15   CONTINUE
      SMALLOUT(QI(1,1)  ,RZ1(1,1,M), 256)
C-----FORM THE R.H.S. OF POISSON EQUATION
      C10=1./(DT*ALPHA)
      K=4
      DO 30 J=4,19
      DO 30 I=4,19
      JJ=J-3
      II=I-3
      QI(II,JJ)=(U(I,J,K)-U(I-1,J,K)+V(I,J,K)-V(I,J-1,K)+W(I,J,K)
     * -W(I,J,K-1))*C9
      QR(II,JJ)=QI(II,JJ)*C10+
     * (SX(I-2,J-2,K-2)-SX(I-3,J-2,K-2)+SY(I-2,J-2,K-2)-SY(I-2,J-3,K-2)+
     * SZ(I-2,J-2,K-2)-SZ(I-2,J-2,K-3))*C9
C-----COMPUTE DIVERGENCE, TURBULENT ENERGY
      DIV=DIV+QI(II,JJ)
      USQR=U(I,J,K)**2+USQR
      DUDX=(U(I,J,K)-U(I-1,J,K))/H
      DUDX2=DUDX**2+DUDX2
      DUDX3=DUDX**3+DUDX3
      ENRG=ENRG+U(I,J,K)**2+V(I,J,K)**2+W(I,J,K)**2
```

ORIGINAL PAGE IS
OF POOR QUALITY

```
 30    CONTINUE
       IF (M.EQ. 9) GO TO 9
       GO TO 7
 9     WRITE(6,103)
 103   FORMAT(1H ,10X,*DIVERGENCE V *)
       WRITE (6,104) M
 104   FORMAT(1H ,10X,2HM=,I2)
       DO 19 I=1,16,8
       WRITE (6,106) I
 106   FORMAT(1H ,10X,2HI=,I2)
       WRITE(6,105) (QI(I,J),J=1,16)
 105   FORMAT(2X,8(E16.7))
 19    CONTINUE
 7     SMALLOUT(QR(1,1),PR1(1,1,M), 256)
C-----SHIFT U,V,W,SX,SY,SZ ONE PLANE IN Z DIRECTION
       DO 32 K=1,6
       DO 32 J=1,22
       DO 32 I=1,22
       U(I,J,K)=U(I,J,K+1)
       V(I,J,K)=V(I,J,K+1)
       W(I,J,K)=W(I,J,K+1)
 32    CONTINUE
       DO 34 K=1,2
       DO 34 J=1,18
       DO 34 I=1,18
       SX(I,J,K)=SX(I,J,K+1)
       SY(I,J,K)=SY(I,J,K+1)
       SZ(I,J,K)=SZ(I,J,K+1)
 34    CONTINUE
       IF(M.EQ.16) GO TO 38
       M=M+1
       K2=K2+1
       GO TO 1
 38    DO 55 K=1,16
       DO 55 J=1,16
       DO 55 I=1,16
       PI1(I,J,K)=0.0
 55    CONTINUE
C-----INVERT THE POISSON EQUATION BY SUBROUTINE PSNEQN
       CALL PSNEQN
       WRITE(6,110)
 110   FORMAT(1H ,10X,* PRESSURE FIELD *)
       SMALLIN(QR(1,1),PR1(1,1, 9), 256)
       DO 47 I=1,16,8
       WRITE(6,106) I
       WRITE(6,105) (QR(I,J),J=1,16)
 47    CONTINUE
C-----ADVANCE PRESSURE GRADIENT IN TIME
       M=1
       K4=15
 50    DO 41 K=1,3
       K3=K4+K
       IF(K3.GT.16) K3=K3-16
       IF(K3.GT.16) K3=K3-16
       SMALLIN(QR(1,1),PR1(1,1,K3), 256)
```


ORIGINAL PAGE IS
OF POOR QUALITY

```
      DO 42 J=1,16
      DO 42 I=1,16
      JJ=J+1
      II=I+1
      PR(II,JJ,K)=QR(I,J)
 42   CONTINUE
C-----EXTEND PRESSURE FIELD PERIODICALLY IN X,Y DIRECTIONS
      DO 39 J=2,17
      PR(1,J,K)=PR(17,J,K)
      PR(18,J,K)=PR(2,J,K)
 39   CONTINUE
      DO 43 I=1,18
      PR(I,1,K)=PR(I,17,K)
      PR(I,18,K)=PR(I,2,K)
 43   CONTINUE
 41   CONTINUE
      K=2
      DO 54 J=1,16
      DO 54 I=1,16
      QR(I,J)=-(PR(I+2,J+1,K)-PR(I+1,J+1,K))*C9
 54   CONTINUE
      SMALLIN(QI(1,1),U1(1,1,M ), 256)
      DO 52 J=1,16
      DO 52 I=1,16
      QI(I,J)=QI(I,J)+QR(I,J)*ALPHA*DT
 52   CONTINUE
      SMALLOUT(QI(1,1),U1(1,1,M ), 256)
      SMALLIN(QI(1,1),RX1(1,1,M ), 256)
      DO 53 J=1,16
      DO 53 I=1,16
      QI(I,J)=QI(I,J)+QR(I,J)
 53   CONTINUE
      SMALLOUT(QI(1,1),RX1(1,1,M ), 256)
      DO 64 J=1,16
      DO 64 I=1,16
      QR(I,J)=-(PR(I+1,J+2,K)-PR(I+1,J+1,K))*C9
 64   CONTINUE
      SMALLIN(QI(1,1),V1(1,1,M ), 256)
      DO 65 I=1,16
      DO 65 J=1,16
      QI(I,J)=QI(I,J)+QR(I,J)*ALPHA*DT
 65   CONTINUE
      SMALLOUT(QI(1,1),V1(1,1,M ), 256)
      SMALLIN(QI(1,1),RY1(1,1,M ), 256)
      DO 63 J=1,16
      DO 63 I=1,16
      QI(I,J)=QI(I,J)+QR(I,J)
 63   CONTINUE
      SMALLOUT(QI(1,1),RY1(1,1,M ), 256)
      DO 74 J=1,16
      DO 74 I=1,16
      QR(I,J)=-(PR(I+1,J+1,K+1)-PR(I+1,J+1,K))*C9
 74   CONTINUE
      SMALLIN(QI(1,1),W1(1,1,M ), 256)
      DO 75 I=1,16
```


ORIGINAL PAGE IS
OF POOR QUALITY

```
      DO 75 J=1,16
      QI(I,J)=QI(I,J)+QR(I,J)*ALPHA*DT
 75   CONTINUE
      SMALLOUT(QI(1,1),W1(1,1,M ), 256)
      SMALLIN(QI(1,1),RZ1(1,1,M ), 256)
      DO 73 J=1,16
      DO 73 I=1,16
      QI(I,J)=QI(I,J)+QR(I,J)
 73   CONTINUE
      SMALLOUT(QI(1,1),RZ1(1,1,M ), 256)
      IF(M.EQ.16) GO TO 40
      M=M+1
      K4=K4+1
      GO TO 50
 40   L=L+1
C-----COMPUTE TAYLOR MICROSCALE, SKEWNESS
      LAMBDA=SQRT(USQR/DUDX2)
      DUDX2=DUDX2/ 4096.
      DUDX3=DUDX3/ 4096.
      SKEW=DUDX3/DUDX2**1.5
      ENRG=ENRG/ 4096.
      WRITE(6,111) SKEW,ENRG,DIV,LAMBDA
 111  FORMAT(// ,10X,10HSKEWNESSX=,E16.7,5X,7HENERGY=,E16.7,
     * 5X,11HDIVERGENCE=,E16.7,5X,8HLAMBDAX=,E16.7)
      DIV=0.0
      ENRG=0.0
      USQR=0.0
      DUDX2=0.0
      DUDX3=0.0
      IF(L.GT.0) ALPHA=1.5
      IF(L.GT.  0) GO TO 78
      GO TO 6
 78   CONTINUE
      STOP
      END
```


ORIGINAL PAGE IS
OF POOR QUALITY

```
      SUBROUTINE PSNEQN
C     ******************************************************************
C     * POISSON SOLVER FOR 16 CUBE POINTS WITH PERIODIC B.C. BY FFT    *
C     * ALGORITHM                                                      *
C     * WAVE(I,J,K) IS THE WAVE NUMBER K' DEFINED IN CHAPTER III       *
C     * ISIGN=1, ISIGN=-1 ARE FOR FORWARD AND BACKWARD TRANSFORMS,     *
C     * RESPECTIVELY                                                   *
C     ******************************************************************
      LARGE PR1(16,16,16),PI1(16,16,16),WAVE(16,16,16)
      DIMENSION N(3),M1(6),M2(6),TRR(16,3),TRI(16,3),E(16)
      DIMENSION QR(16,16),QI(16,16)
      COMMON/SCM/QR,QI,N,M1,M2,TRR,TRI,E,ISIGN,PAI
      H=1./16.
      H2=H*H
      H3=H2*H
      NN=16
      NN3=NN*NN*NN
      C1=1./NN3
      C2=PAI/NN
      C3=1./H2
      ISIGN=1
      CALL FFTX
      CALL FFTY
      CALL FFTZ.
      DO 26 K=1,16
      DO 26 J=1,16
      DO 26 I=1,16
      PR1(I,J,K)=PR1(I,J,K)*C1/WAVE(I,J,K)
      PI1(I,J,K)=PI1(I,J,K)*C1/WAVE(I,J,K)
 26   CONTINUE
      PR1(1,1,1)=0.0
      PI1(1,1,1)=0.0
      ISIGN=-1
      CALL FFTZ
      CALL FFTY
      CALL FFTX
      RETURN
      END
```

ORIGINAL PAGE IS
OF POOR QUALITY

```
      SUBROUTINE FFTX
C     ******************************************************************
C     * FAST FOURIER TRANSFORM IN X DIRECTION                          *
C     * ISIGN=1, ISIGN=-1 ARE FOR FORWARD AND BACKWARD TRANSFORMS,     *
C     * RESPECTIVELY.  THE FORWARD TRANSFORM RETURNS 16 TIMES          *
C     * THE REQUIRED RESULT. FOR DEFINITION OF FFT SEE APPENDIX C      *
C     ******************************************************************
      LARGE PR1(16,16,16),PI1(16,16,16),WAVE(16,16,16)
      DIMENSION N(3),M1(6),M2(6),TRR(16,3),TRI(16,3),E(16)
      DIMENSION QR(16,16),QI(16,16)
      COMMON/SCH/QR,QI,N,M1,M2,TRR,TRI,E,ISIGN,PAI
      DO 200 K=1,16
      DO 200 J=1,16
      DO 100 M=1,3
      JJ=N(M)
      KK=0
 5    II=KK+JJ+1
      KK=II+JJ-1
      DO 10 I=II,KK
      L=I-JJ
      Z=-PR1(L,J,K)
      T=-PI1(L,J,K)
      PR1(L,J,K)=PR1(I,J,K)+PR1(L,J,K)
      PI1(L,J,K)=PI1(I,J,K)+PI1(L,J,K)
      Z=PR1(I,J,K)+Z
      T=PI1(I,J,K)+T
      PR1(I,J,K)=Z*TRR(I,M)-T*TRI(I,M)*ISIGN
 10   PI1(I,J,K)=Z*TRI(I,M)*ISIGN+T*TRR(I,M)
      IF(KK.NE.16) GO TO 5
 100  CONTINUE
      DO 110 I=2,16,2
      PR1(I,J,K)=-PR1(I,J,K)+PR1(I-1,J,K)
 110  PI1(I,J,K)=-PI1(I,J,K)+PI1(I-1,J,K)
      DO 120 I=1,15,2
      PR1(I,J,K)=2.*PR1(I,J,K)-PR1(I+1,J,K)
 120  PI1(I,J,K)=2.*PI1(I,J,K)-PI1(I+1,J,K)
      DO 20 L=1,6
      I1=M1(L)
      I2=M2(L)
      DUM1=PR1(I2,J,K)
      PR1(I2,J,K)=PR1(I1,J,K)
      PR1(I1,J,K)=DUM1
      DUM1=PI1(I2,J,K)
      PI1(I2,J,K)=PI1(I1,J,K)
      PI1(I1,J,K)=DUM1
 20   CONTINUE
 200  CONTINUE
      RETURN
      END
```


ORIGINAL PAGE IS
OF POOR QUALITY

```
      SUBROUTINE FFTY
C     ******************************************************************
C     * FAST FOURIER TRANSFORM IN Y DIRECTION                          *
C     ******************************************************************
      LARGE PR1(16,16,16),PI1(16,16,16),WAVE(16,16,16)
      DIMENSION N(3),M1(6),M2(6),TRR(16,3),TRI(16,3),E(16)
      DIMENSION QR(16,16),QI(16,16)
      COMMON/SCM/QR,QI,N,M1,M2,TRR,TRI,E,ISIGN,PAI
      DO 200 K=1,16
      DO 200 I=1,16
      DO 100 M=1,3
      JJ=N(M)
      KK=0
 5    II=KK+JJ+1
      KK=II+JJ-1
      D   0 J=II,KK
      L=J-JJ
      Z=-PR1(I,L,K)
      T=-PI1(I,L,K)
      PR1(I,L,K)=PR1(I,J,K)+PR1(I,L,K)
      PI1(I,L,K)=PI1(I,J,K)+PI1(I,L,K)
      Z=PR1(I,J,K)+Z
      T=PI1(I,J,K)+T
      PR1(I,J,K)=Z*TRR(J,M)-T*TRI(J,M)*ISIGN
 10   PI1(I,J,K)=Z*TRI(J,M)*ISIGN+T*TRR(J,M)
      IF(KK.NE.16) GO TO 5
 100  CONTINUE
      DO 110 J=2,16,2
      PR1(I,J,K)=-PR1(I,J,K)+PR1(I,J-1,K)
 110  PI1(I,J,K)=-PI1(I,J,K)+PI1(I,J-1,K)
      DO 120 J=1,15,2
      PR1(I,J,K)=2.*PR1(I,J,K)-PR1(I,J+1,K)
 120  PI1(I,J,K)=2.*PI1(I,J,K)-PI1(I,J+1,K)
      DO 20 L=1,6
      I1=M1(L)
      I2=M2(L)
      DUM1=PR1(I,I2,K)
      PR1(I,I2,K)=PR1(I,I1,K)
      PR1(I,I1,K)=DUM1
      DUM1=PI1(I,I2,K)
      PI1(I,I2,K)=PI1(I,I1,K)
      PI1(I,I1,K)=DUM1
 20   CONTINUE
 200  CONTINUE
      RETURN
      END
```

```
      SUBROUTINE FFTZ
C     ******************************************************************
C     * FAST FOURIER TRANSFORM IN Z DIRECTION                          *
C     ******************************************************************
      LARGE PR1(16,16,16),PI1(16,16,16),WAVE(16,16,16)
      DIMENSION N(3),M1(6),M2(6),TRR(16,3),TRI(16,3),E(16)
      DIMENSION QR(16,16),QI(16,16)
      COMMON/SCM/QR,QI,N,M1,M2,TRR,TRI,E,ISIGN,PAI
      DO 200 J=1,16
      DO 200 I=1,16
      DO 100 M=1,3
      JJ=N(M)
      KK=0
 5    II=KK+JJ+1
      KK=II+JJ-1
      DO 10 K=II,KK
      L=K-JJ
      Z=-PR1(I,J,L)
      T=-PI1(I,J,L)
      PR1(I,J,L)=PR1(I,J,K)+PR1(I,J,L)
      PI1(I,J,L)=PI1(I,J,K)+PI1(I,J,L)
      Z=PR1(I,J,K)+Z
      T=PI1(I,J,K)+T
      PR1(I,J,K)=Z*TRR(K,M)-T*TRI(K,M)*ISIGN
 10   PI1(I,J,K)=Z*TRI(K,M)*ISIGN+T*TRR(K,M)
      IF(KK.NE.16) GO TO 5
 100  CONTINUE
      DO 110 K=2,16,2
      PR1(I,J,K)=-PR1(I,J,K)+PR1(I,J,K-1)
 110  PI1(I,J,K)=-PI1(I,J,K)+PI1(I,J,K-1)
      DO 120 K=1,15,2
      PR1(I,J,K)=2.*PR1(I,J,K)-PR1(I,J,K+1)
 120  PI1(I,J,K)=2.*PI1(I,J,K)-PI1(I,J,K+1)
      DO 20 L=1,6
      I1=M1(L)
      I2=M2(L)
      DUM1=PR1(I,J,I2)
      PR1(I,J,I2)=PR1(I,J,I1)
      PR1(I,J,I1)=DUM1
      DUM1=PI1(I,J,I2)
      PI1(I,J,I2)=PI1(I,J,I1)
      PI1(I,J,I1)=DUM1
 20   CONTINUE
 200  CONTINUE
      RETURN
      END
```


ORIGINAL PAGE IS
OF POOR QUALITY

```
      SUBROUTINE TRRTRI
C     ******************************************************************
C     * INITIATION OF THE TRIGONOMETRIC FUNCTIONS TRR,TRI REQUIRED FOR  *
C     * THE FFT SUBROUTINES, AND WAVE (THE WAVE NUMBER K') FOR PSNEQN   *
C     ******************************************************************
      LARGE PR1(16,16,16),PI1(16,16,16),WAVE(16,16,16)
      DIMENSION N(3),M1(6),M2(6),TRR(16,3),TRI(16,3),E(16)
      DIMENSION QR(16,16),QI(16,16)
      COMMON/SCM/QR,QI,N,M1,M2,TRR,TRI,E,ISIGN,PAI
      DATA M1/2,3,4,6,8,12/
      DATA M2/9,5,13,11,15,14/
      DATA E/0.,1.,2.,3.,4.,5.,6.,7.,-8.,-7.,-6.,-5.,-4.,-3.,-2.,-1./
      H=1./16.
      H2=H*H
      NN=16
      C2=PAI/NN
      C3=1./H2
      N(1)=8
      N(2)=4
      N(3)=2
      DO 24 K=1,16
      DO 24 J=1,16
      DO 24 I=1,16
      WAVE(I,J,K)=-4.*(SIN(C2*E(I))**2+SIN(C2*E(J))**2
     * +SIN(C2*E(K))**2)*C3
 24   CONTINUE
      WAVE(1,1,1)=1.0
      DO 10 M=1,3
      L=N(M)
      J=1
 30   K=J+2*N(M)-1
      DO 20 I=J,K
      IF(I.GT.L)    GO TO 22
      TRR(I,M)=1.
      TRI(I,M)=0.
      GO TO 20
 22   TRR(I,M)=COS(PAI*(I-1)/N(M))
      TRI(I,M)=-SIN(PAI*(I-1)/N(M))
 20   CONTINUE
      IF(K.EQ.16) GO TO 10
      L=K+N(M)
      J=K+1
      GO TO 30
 10   CONTINUE
      RETURN
      END
```

ORIGINAL PAGE IS
OF POOR QUALITY

```
      SUBROUTINE INICON
C     ******************************************************************
C     * INITIATION OF A RANDOM FIELD WHICH SATISFY CONDITIONS SET IN   *
C     * APPENDIX B. THE TWO REQUIRED FIELDS TO START WITH ARE          *
C     * GENERATED IN SUBROUTINE RANDM                                  *
C     * SUBROUTINE SPECT3 EVALUATES THE THREE-DIMENSIONAL ENERGY       *
C     * SPECTRUM OF THE GENERATED FIELD                                *
C     ******************************************************************
      LARGE PR1(16,16,16),PI1(16,16,16),WAVE(16,16,16)
      LARGE U1(16,16,19),V1(16,16,19),W1(16,16,19)
      LARGE U2(16,16,18),V2(16,16,18),W2(16,16,18)
      DIMENSION QR(16,16),QI(16,16)
      DIMENSION SR(16,16,6),SI(16,16,6)
      DIMENSION N(3),M1(6),M2(6),TRR(16,3),TRI(16,3),E(16)
      COMMON/SCM/QR,QI,N,M1,M2,TRR,TRI,E,ISIGN,PAI
      H=1./16.
      HN=16.
      HN3=HN*HN*HN
      CALL RANDM
      ARG=2.*PAI/HN
      DO 70 K=1,9
      LL=K+9
      SMALLIN(SR(1,1,1),U1(1,1,K), 256)
      SMALLIN(SI(1,1,1),U1(1,1,LL  ), 256)
      SMALLIN(SR(1,1,2),V1(1,1,K), 256)
      SMALLIN(SI(1,1,2),V1(1,1,LL  ), 256)
      SMALLIN(SR(1,1,3),W1(1,1,K), 256)
      SMALLIN(SI(1,1,3),W1(1,1,LL  ), 256)
      SMALLIN(SR(1,1,4),U2(1,1,K), 256)
      SMALLIN(SI(1,1,4),U2(1,1,LL  ), 256)
      SMALLIN(SR(1,1,5),V2(1,1,K), 256)
      SMALLIN(SI(1,1,5),V2(1,1,LL  ), 256)
      SMALLIN(SR(1,1,6),W2(1,1,K), 256)
      SMALLIN(SI(1,1,6),W2(1,1,LL  ), 256)
      KK=K-9
      DO 72 J=1,16
      DO 72 I=1,16
      JJ=J-1
      II=I-1
      IF(J.GT. 8) JJ=J-17
      IF(I.GT. 8) II=I-17
      ARG1=ARG*II
      TRC1=1.-COS(ARG1)
      TRS1=SIN(ARG1)
      ARG1=ARG*JJ
      TRC2=1.-COS(ARG1)
      TRS2=SIN(ARG1)
      ARG1=ARG*KK
      TRC3=1.-COS(ARG1)
      TRS3=SIN(ARG1)
      A=TRC1*SR(I,J,4)+TRC2*SR(I,J,5)+TRC3*SR(I,J,6)
      B=TRS1*SI(I,J,1)+TRS2*SI(I,J,2)+TRS3*SI(I,J,3)
      C=TRC1*SI(I,J,4)+TRC2*SI(I,J,5)+TRC3*SI(I,J,6)
      D=TRS1*SR(I,J,1)+TRS2*SR(I,J,2)+TRS3*SR(I,J,3)
      E1=SR(I,J,1)**2+SR(I,J,2)**2+SR(I,J,3)**2
      E2=SR(I,J,4)**2+SR(I,J,5)**2+SR(I,J,6)**2
```

ORIGINAL PAGE IS
OF POOR QUALITY

```
      E3=SI(I,J,1)**2+SI(I,J,2)**2+SI(I,J,3)**2
      E4=SI(I,J,4)**2+SI(I,J,5)**2+SI(I,J,6)**2
      E5=SR(I,J,1)*SR(I,J,4)+SR(I,J,2)*SR(I,J,5)+SR(I,J,3)*SR(I,J,6)
      E6=SI(I,J,1)*SI(I,J,4)+SI(I,J,2)*SI(I,J,5)+SI(I,J,3)*SI(I,J,6)
      EEE=(E1+E2+E3+E4)/2.
      DDD=A*B*C*D
      IF(DDD.NE.0.0) GO TO 71
      BBB=A*C
      IF(B.EQ.0.0.AND.BBB.NE.0.0) GO TO 75
      CCC=B*D
      IF(C.EQ.0.0.AND.CCC.NE.0.0) GO TO 77
      IF(C.EQ.0.0.AND.D.EQ.0.0.AND.B.NE.0.0) GO TO 79
      IF(A.EQ.0.0.AND.B.EQ.0.0.AND.C.NE.0.0) GO TO 200
      IF(A.NE.0.0.AND.B.EQ.0.0.AND.C.EQ.0.0.AND.D.EQ.0.0) GO TO 210
      IF(A.EQ.0.0.AND.B.EQ.0.0.AND.C.EQ.0.0.AND.D.NE.0.0) GO TO 220
      IF(A.NE.0.0.AND.B.EQ.0.0.AND.C.EQ.0.0.AND.D.NE.0.0) GO TO 230
      IF(A.EQ.0.0.AND.B.EQ.0.0.AND.C.EQ.0.0.AND.D.EQ.0.0) GO TO 81
 71   BETA=RGEN(X1)
      IF(BETA.EQ.0.0) GO TO 71
 771  GAMA=A/B*BETA
      F1=E1+D**2/C**2*E4
      F2=2.*BETA*E5-2.*GAMA*D/C*E6
      F3=BETA**2*E2+GAMA**2*E3-EEE
      F4=F2*F2-4.*F1*F3
      IF(F4.GT.0.0) GO TO 772
      BETA=BETA/2.
      GO TO 771
 772  ALPHA=(-F2-SQRT(F4))/2./F1
      DELTA=-D/C*ALPHA
      GO TO 73
 75   GAMA=RGEN(X2)
      IF(GAMA.EQ.0.0) GO TO 75
      BETA=B/A*GAMA
      F1=E1+D**2/C**2*E4
      F2=2.*BETA*E5-2.*GAMA*D/C*E6
      F3=BETA**2*E2+GAMA**2*E3-EEE
      F4=F2*F2-4.*F1*F3
      IF(F4.LT.0.0) GO TO 75
      ALPHA=(-F2-SQRT(F4))/2./F1
      DELTA=-D/C*ALPHA
      GO TO 73
 77   DELTA=RGEN(X3)
      IF(DELTA.EQ.0.0) GO TO 77
      ALPHA=-C/D*DELTA
      F1=E2+A**2/B**2*E3
      F2=2.*ALPHA*E5
      F3=ALPHA**2*E1+DELTA**2*E4+2.*ALPHA*DELTA*E6-EEE
      F4=F2*F2-4.*F1*F3
      IF(F4.LT.0.0) GO TO 77
      BETA=(-F2-SQRT(F4))/2./F1
      GAMA=BETA*A/B
      GO TO 73
 79   ALPHA=RGEN(X4)
      DELTA=RGEN(X5)
      IF(ALPHA.EQ.0.0.OR.DELTA.EQ.0.0) GO TO 79
 779  F1=E2+A**2/B**2*E3
```


ORIGINAL PAGE IS
OF POOR QUALITY

```
      F2=2.*ALPHA*E5
      F3=ALPHA**2*E1+DELTA**2*E4+2.*ALPHA*DELTA*E6-EEE
      F4=F2*F2-4.*F1*F3
      IF(F4.GT.0.0) GO TO 780
      ALPHA=ALPHA/2.
      DELTA=DELTA/2.
      GO TO 779
780   BETA=(-F2-SQRT(F4))/2./F1
      GAMA=BETA*A/B
      GO TO 73
200   BETA=RGEN(X6)
      GAMA=RGEN(X7)
      IF(BETA.EQ.0.0.OR.GAMA.EQ.0.0) GO TO 200
201   F1=E1+D**2/C**2*E4
      F2=2.*(BETA*E5-GAMA*D/C*E6)
      F3=BETA**2*E2+GAMA**2*E3-EEE
      F4=F2*F2-4.*F1*F3
      IF(F4.GT.0.0) GO TO 202
      BETA=BETA/2.
      GAMA=GAMA/2.
      GO TO 201
202   ALPHA=(-F2-SQRT(F4))/2./F1
      DELTA=-D/C*ALPHA
      GO TO 73
210   GAMA=RGEN(X8)
      DELTA=RGEN(X9)
      BETA=0.0
      IF(GAMA.EQ.0.0.OR.DELTA.EQ.0.0)GO TO 210
211   F4=(EEE-GAMA**2*E3-DELTA**2*E4-2.*GAMA*DELTA*E6)/E1
      IF(F4.GT.0.0) GO TO 212
      GAMA=GAMA/2.
      DELTA=DELTA/2.
      GO TO 211
212   ALPHA=-SQRT(F4)
      GO TO 73
220   GAMA=RGEN(X12)
      DELTA=RGEN(X13)
      ALPHA=0.0
      IF(GAMA.EQ.0.0.OR.DELTA.EQ.0.0) GO TO 220
221   F4=(EEE-GAMA**2*E3-DELTA**2*E4-2.*GAMA*DELTA*E6)/E2
      IF(F4.GT.0.0) GO TO 222
      GAMA=GAMA/2.
      DELTA=DELTA/2.
      GO TO 221
222   BETA=-SQRT(F4)
      GO TO 73
230   BETA=0.0
      ALPHA=0.0
      GAMA=RGEN(X14)
      IF(GAMA.EQ.0.0) GO TO 230
232   F1=E4
      F2=2.*GAMA*E6
      F3=GAMA**2*E3-EEE
      F4=F2*F2-4.*F1*F3
      IF(F4.GT.0.0) GO TO 231
      GAMA=GAMA/2.
```


ORIGINAL PAGE IS
OF POOR QUALITY

```
      GO TO 232
231   DELTA=(-F2-SQRT(F4))/2./F1
      GO TO 73
81    CONTINUE
      DELTA=0.0
      BETA=0.0
      ALPHA=0.0
      GAMA=0.0
73    SR(I,J,1)=ALPHA*SR(I,J,1)+BETA*SR(I,J,4)
      SI(I,J,1)=GAMA*SI(I,J,1)+DELTA*SI(I,J,4)
      SR(I,J,2)=ALPHA*SR(I,J,2)+BETA*SR(I,J,5)
      SI(I,J,2)=GAMA*SI(I,J,2)+DELTA*SI(I,J,5)
      SR(I,J,3)=ALPHA*SR(I,J,3)+BETA*SR(I,J,6)
      SI(I,J,3)=GAMA*SI(I,J,3)+DELTA*SI(I,J,6)
72    CONTINUE
      SMALLOUT(SR(1,1,1),U1(1,1,K), 256)
      SMALLOUT(SI(1,1,1),U2(1,1,K), 256)
      SMALLOUT(SR(1,1,2),V1(1,1,K), 256)
      SMALLOUT(SI(1,1,2),V2(1,1,K), 256)
      SMALLOUT(SR(1,1,3),W1(1,1,K), 256)
      SMALLOUT(SI(1,1,3),W2(1,1,K), 256)
70    CONTINUE
      ISIGN=-1
      DO 74 K=1,9
      M=K
      SMALLIN(QR(1,1),U1(1,1,K), 256)
      SMALLIN(QI(1,1),U2(1,1,K), 256)
      IF(M.EQ. 9) M=M-16
      MM=M+8
      SMALLOUT(QR(1,1),PR1(1,1,MM  ), 256)
      SMALLOUT(QI(1,1),PI1(1,1,MM  ), 256)
74    CONTINUE
      DO 76 K=10,16
      LL=18-K
      DO 76 J=1,16
      DO 76 I=1,16
      IF(I.EQ. 9.OR.J.EQ. 9) GO TO 1
      JJ=18-J
      II=18-I
      IF(JJ.EQ.17) JJ=1
      IF(II.EQ.17) II=1
      PR1(II,JJ,LL)=PR1(I,J,K)
      PI1(II,JJ,LL)=-PI1(I,J,K)
      GO TO 76
1     PR1(I,J,LL)=0.0
      PI1(I,J,LL)=0.0
76    CONTINUE
      CALL FFTZ
      CALL FFTY
      CALL FFTX
      DO 78 K=1,16
      DO 78 J=1,16
      DO 78 I=1,16
      U1(I,J,K)=PR1(I,J,K)
78    CONTINUE
      DO 84 K=1,9
```


ORIGINAL PAGE IS
OF POOR QUALITY

```
      M=K
      SMALLIN(QR(1,1),V1(1,1,K), 256)
      SMALLIN(QI(1,1),V2(1,1,K), 256)
      IF(M.EQ. 9) M=M-16
      MM=M+8
      SMALLOUT(QR(1,1),PR1(1,1,MM  ), 256)
      SMALLOUT(QI(1,1),PI1(1,1,MM  ), 256)
84    CONTINUE
      DO 86 K=10,16
      LL=18-K
      DO 86 J=1,16
      DO 86 I=1,16
      IF(I.EQ. 9.OR.J.EQ. 9) GO TO 2
      JJ=18-J
      II=18-I
      IF(JJ.EQ.17) JJ=1
      IF(II.EQ.17) II=1
      PR1(II,JJ,LL)=PR1(I,J,K)
      PI1(II,JJ,LL)=-PI1(I,J,K)
      GO TO 86
2     PR1(I,J,LL)=0.0
      PI1(I,J,LL)=0.0
86    CONTINUE
      CALL FFTZ
      CALL FFTY
      CALL FFTX
      DO 88 K=1,16
      DO 88 J=1,16
      DO 88 I=1,16
      V1(I,J,K)=PR1(I,J,K)
88    CONTINUE
      DO 94 K=1,9
      M=K
      SMALLIN(QR(1,1),W1(1,1,K), 256)
      SMALLIN(QI(1,1),W2(1,1,K), 256)
      IF(M.EQ. 9) M=M-16
      MM=M+8
      SMALLOUT(QR(1,1),PR1(1,1,MM  ), 256)
      SMALLOUT(QI(1,1),PI1(1,1,MM  ), 256)
94    CONTINUE
      DO 96 K=10,16
      LL=18-K
      DO 96 J=1,16
      DO 96 I=1,16
      IF(I.EQ. 9.OR.J.EQ. 9) GO TO 3
      JJ=18-J
      II=18-I
      IF(JJ.EQ.17) JJ=1
      IF(II.EQ.17) II=1
      PR1(II,JJ,LL)=PR1(I,J,K)
      PI1(II,JJ,LL)=-PI1(I,J,K)
      GO TO 96
3     PR1(I,J,LL)=0.0
      PI1(I,J,LL)=0.0
96    CONTINUE
      CALL FFTZ
```

ORIGINAL PAGE IS
OF POOR QUALITY

```
      CALL FFTY
      CALL FFTX
      DO 98 K=1,16
      DO 98 J=1,16
      DO 98 I=1,16
      W1(I,J,K)=PR1(I,J,K)
 98   CONTINUE
      CALL SPECT3
      RETURN
      END



      SUBROUTINE RANDM
C     ******************************************************************
C     * INITIATION OF TWO RANDOM FIELDS REQUIRED FOR INICON            *
C     ******************************************************************
      LARGE PR1(16,16,16),PI1(16,16,16),WAVE(16,16,16)
      LARGE U1(16,16,19),V1(16,16,19),W1(16,16,19)
      LARGE U2(16,16,18),V2(16,16,18),W2(16,16,18)
      DIMENSION QR(16,16),QI(16,16)
      DIMENSION SR(16,16,6),SI(16,16,6)
      DIMENSION N(3),M1(6),M2(6),TRR(16,3),TRI(16,3),E(16)
      COMMON/SCM/QR,QI,N,M1,M2,TRR,TRI,E,ISIGN,PAI
      DIMENSION EN(14)
C-----EN IS E(K), THE THREE-DIMENSIONAL ENERGY SPECTRUM, AND IS GIVEN
C-----AS A FUNCTION OF K AT 2*PAI, 4*PAI, 6*PAI, ETC.
      DATA EN/.52,1.5,1.3,.96,.66,.46,.33,.23,.16,.105,.072,.05,.032,.0/
      HN=16.
      ARG=2.*PAI/HN
      DO 20 K=1,9
      KK=K-9
      DO 10 J=1,16
      DO 10 I=1,16
      JJ=J-1
      IF(J.GT.8) JJ=J-17
      II=I-1
      IF(I.GT.8)II=I-17
      IF(II.EQ.0.AND.JJ.EQ.0.AND.KK.EQ.0) GO TO 10
      Y=RGEN(X)
      ZETA=2.*PAI*Y
      A1=1.-COS(ARG*II)
      A2=1.-COS(ARG*JJ)
      A3=1.-COS(ARG*KK)
      R=SQRT(A1**2+A2**2+A3**2)
      PHI=ACOS(A3/R)
      IF(A1.NE.0.) GO TO 5
      IF(A2.GT.0.0) THETA=PAI/2.
      IF(A2.LT.0.0) THETA=-PAI/2.
```

ORIGINAL PAGE IS
OF POOR QUALITY

```
      IF(A2.EQ.0.0) THETA=2.*PAI*Y
      GO TO 2
5     CONTINUE
      THETA=ATAN2(A2,A1)
2     CONTINUE
      AMAG=SQRT(FLOAT(II*II+JJ*JJ+KK*KK))*2.*PAI
      WN=AMAG/(2.*PAI)
      IWN=WN
      IWNP1=IWN+1
      ABSVEL=(EN(IWN)+(EN(IWNP1)-EN(IWN))*(WN-IWN))/(2.*PAI*AMAG**2)
      Y1=RGEN(X1)
      VELR=SQRT(Y1*ABSVEL)
      VELI=SQRT((1.-Y1)*ABSVEL)
      U1(I,J,K) =-(COS(ZETA)*COS(PHI)*COS(THETA)+SIN(ZETA)*SIN(THETA))
     * *VELR
      V1(I,J,K) =(-COS(ZETA)*COS(PHI)*SIN(THETA)+SIN(ZETA)*COS(THETA))
     * *VELR
      W1(I,J,K) =COS(ZETA)*SIN(PHI)*VELR
      U1(I,J,K+9) =-(COS(ZETA)*COS(PHI)*COS(THETA)+SIN(ZETA)*SIN(THETA))
     * *VELI
      V1(I,J,K+9) =(-COS(ZETA)*COS(PHI)*SIN(THETA)+SIN(ZETA)*COS(THETA))
     * *VELI
      W1(I,J,K+9) =COS(ZETA)*SIN(PHI)*VELI
10    CONTINUE
20    CONTINUE
      U1(1,1,9)=0.0
      V1(1,1,9)=0.0
      W1(1,1,9)=0.0
      U1(1,1,18)=0.0
      V1(1,1,18)=0.0
      W1(1,1,18)=0.0
      DO 60 K=1,9
      KK=K-9
      DO 50 J=1,16
      DO 50 I=1,16
      JJ=J-1
      IF(J.GT.8) JJ=J-17
      II=I-1
      IF(I.GT.8)II=I-17
      IF(II.EQ.0.AND.JJ.EQ.0.AND.KK.EQ.0) GO TO 50
      Y=RGEN(X)
      ZETA=2.*PAI*Y
      A1=SIN(ARG*II)
      A2=SIN(ARG*JJ)
      A3=SIN(ARG*KK)
      R=SQRT(A1**2+A2**2+A3**2)
      PHI=ACOS(A3/R)
      IF(A1.NE.0.) GO TO 6
      IF(A2.GT.0.0) THETA=PAI/2.
      IF(A2.LT.0.0) THETA=-PAI/2.
      IF(A2.EQ.0.0) THETA=2.*PAI*Y
      GO TO 4
6     CONTINUE
      THETA=ATAN2(A2,A1)
4     CONTINUE
      AMAG=SQRT(FLOAT(II*II+JJ*JJ+KK*KK))*2.*PAI
```

ORIGINAL PAGE IS
OF POOR QUALITY

```
      WN=AMAG/(2.*PAI)
      IWN=WN
      IWNP1=IWN+1
      ABSVEL=(EN(IWN)+(EN(IWNP1)-EN(IWN))*(WN-IWN))/(2.*PAI*AMAG**2)
      Y2=RGEN(X2)
      VELR=SQRT(Y2*ABSVEL)
      VELI=SQRT((1.-Y2)*ABSVEL)
      U2(I,J,K) =-(COS(ZETA)*COS(PHI)*COS(THETA)+SIN(ZETA)*SIN(THETA))
     * *VELR
      V2(I,J,K) =(-COS(ZETA)*COS(PHI)*SIN(THETA)+SIN(ZETA)*COS(THETA))
     * *VELR
      W2(I,J,K) =COS(ZETA)*SIN(PHI)*VELR
      U2(I,J,K+9) =-(COS(ZETA)*COS(PHI)*COS(THETA)+SIN(ZETA)*SIN(THETA))
     * *VELI
      V2(I,J,K+9) =(-COS(ZETA)*COS(PHI)*SIN(THETA)+SIN(ZETA)*COS(THETA))
     * *VELI
      W2(I,J,K+9) =COS(ZETA)*SIN(PHI)*VELI
50    CONTINUE
60    CONTINUE
      U2(1,1,9)=0.0
      V2(1,1,9)=0.0
      W2(1,1,9)=0.0
      U2(1,1,18)=0.0
      V2(1,1,18)=0.0
      W2(1,1,18)=0.0
      RETURN
      END
```

ORIGINAL PAGE IS
OF POOR QUALITY

```
      SUBROUTINE SPECT3
C     ******************************************************************
C     * EVALUATION OF THREE-DIMENSIONAL ENERGY SPECTRUM                *
C     ******************************************************************
      LARGE PR1(16,16,16),PI1(16,16,16),ENERGY(16,16,16)
      LARGE U1(16,16,19),V1(16,16,19),W1(16,16,19)
      DIMENSION QR(16,16),QI(16,16)
      DIMENSION N(3),M1(6),M2(6),TRR(16,3),TRI(16,3),E(16)
      COMMON/SCM/QR,QI,N,M1,M2,TRR,TRI,E,ISIGN,PAI
      PAI2=PAI*PAI
      H=1./16.
      H2=H*H
      H3=H2*H
      NN=16
      NN3=NN*NN*NN
      C=0.6
C-----TRANSFORMATION OF VELOCITY FIELD TO WAVE NUMBER SPACE, AND
C-----FORMATION OF THE TURBULENT KINETIC ENERGY
      ISIGN=1
      DO 10 J=1,16
      DO 10 I=1,16
      QI(I,J)=0.0
 10   CONTINUE
      DO 12 K=1,16
      SMALLIN(QR(1,1),U1(1,1,K), 256)
      SMALLOUT(QR(1,1),PR1(1,1,K), 256)
      SMALLOUT(QI(1,1),PI1(1,1,K), 256)
 12   CONTINUE
      CALL FFTX
      CALL FFTY
      CALL FFTZ
      DO 14 K=1,16
      DO 14 J=1,16
      DO 14 I=1,16
      PR1(I,J,K)=(PR1(I,J,K)/NN3)**2+(PI1(I,J,K)/NN3)**2
 14   CONTINUE
      DO 16 K=1,16
      SMALLIN(QR(1,1),PR1(1,1,K), 256)
      SMALLOUT(QR(1,1),ENERGY(1,1,K), 256)
 16   CONTINUE
      DO 20 J=1,16
      DO 20 I=1,16
      QI(I,J)=0.0
 20   CONTINUE
      DO 22 K=1,16
      SMALLIN(QR(1,1),V1(1,1,K), 256)
      SMALLOUT(QR(1,1),PR1(1,1,K), 256)
      SMALLOUT(QI(1,1),PI1(1,1,K), 256)
 22   CONTINUE
      CALL FFTX
      CALL FFTY
      CALL FFTZ
      DO 24 K=1,16
      DO 24 J=1,16
      DO 24 I=1,16
      PR1(I,J,K)=(PR1(I,J,K)/NN3)**2+(PI1(I,J,K)/NN3)**2
```


ORIGINAL PAGE IS
OF POOR QUALITY

```
 24    CONTINUE
       DO 26 K=1,16
       SMALLIN(QR(1,1),PR1(1,1,K), 256)
       SMALLIN(QI(1,1),ENERGY(1,1,K), 256)
       DO 28 J=1,16
       DO 28 I=1,16
       QI(I,J)=QI(I,J)+QR(I,J)
 28    CONTINUE
       SMALLOUT(QI(1,1),ENERGY(1,1,K), 256)
 26    CONTINUE
       DO 30 J=1,16
       DO 30 I=1,16
       QI(I,J)=0.0
 30    CONTINUE
       DO 32 K=1,16
       SMALLIN(QR(1,1),W1(1,1,K), 256)
       SMALLOUT(QR(1,1),PR1(1,1,K), 256)
       SMALLOUT(QI(1,1),PI1(1,1,K), 256)
 32    CONTINUE
       CALL FFTX
       CALL FFTY
       CALL FFTZ
       DO 34 K=1,16
       DO 34 J=1,16
       DO 34 I=1,16
       PR1(I,J,K)=(PR1(I,J,K)/NN3)**2+(PI1(I,J,K)/NN3)**2
 34    CONTINUE
       DO 36 K=1,16
       SMALLIN(QR(1,1),PR1(1,1,K), 256)
       SMALLIN(QI(1,1),ENERGY(1,1,K), 256)
       DO 38 J=1,16
       DO 38 I=1,16
       QI(I,J)=(QI(I,J)+QR(I,J))
 38    CONTINUE
       SMALLOUT(QI(1,1),ENERGY(1,1,K), 256)
 36    CONTINUE
C-----EVALUATION OF THE 3-D ENERGY SPECTRUM
       WRITE(6,100)
 100   FORMAT(1H ,10X,*THREE-DIMENSIONAL ENERGY SPECTRUM*)
       M=1
       EE=0.0
       WN=FLOAT(M-1)*2.*PAI
       LL=1
       WRITE(6,101) WN,EE
 101   FORMAT(1H ,10X,2HK=,F6.2,5X,5HE(K)=,E16.7)
       DO 42 M=2,15
       WN=FLOAT(M-1)*2.*PAI
       EE=0.0
       RADP=WN+PAI
       RADM=WN-PAI
       LL=0
       DO 44 K=1,16
       SMALLIN(QR(1,1),ENERGY(1,1,K), 256)
       DO 44 J=1,16
       DO 44 I=1,16
       KK=K-1
```

ORIGINAL PAGE IS
OF POOR QUALITY

```
      IF(K.GT. 8) KK=K-17
      JJ=J-1
      IF(J.GT. 8) JJ=J-17
      II=I-1
      IF(I.GT. 8) II=I-17
      R2=FLOAT(II*II+JJ*JJ+KK*KK)
      RR=SQRT(R2)*2.*PAI
      IF(RR.LT.RADP.AND.RR.GE.RADM) GO TO 46
      GO TO 45
46    LL=LL+1
      EE=EE+QR(I,J)
45    CONTINUE
44    CONTINUE
      EE=EE/(FLOAT(LL))
      EE=4.*PAI*C*EE*WN*WN
      WRITE(6,101) WN,EE
42    CONTINUE
      CALL TRRTRI
      RETURN
      END
```


ORIGINAL PAGE IS
OF POOR QUALITY

SAMPLE OUTPUT

THREE-DIMENSIONAL ENERGY SPECTRUM

K= 0.00	E(K)=	0.
K= 6.28	E(K)=	4.5003845E-03
K= 12.57	E(K)=	1.2903968E-02
K= 18.85	E(K)=	1.2782809E-02
K= 25.13	E(K)=	1.0592158E-02
K= 31.42	E(K)=	7.4289617E-03
K= 37.70	E(K)=	5.0153241E-03
K= 43.98	E(K)=	3.7422405E-03
K= 50.27	E(K)=	2.5924518E-03
K= 56.55	E(K)=	1.6204211E-03
K= 62.83	E(K)=	9.4052200E-04
K= 69.12	E(K)=	4.8530870E-04
K= 75.40	E(K)=	3.7091281E-04
K= 81.68	E(K)=	1.4621541E-04
K= 87.96	E(K)=	2.1298272E-04

ORIGINAL PAGE IS
OF POOR QUALITY

```
NUMBER OF TIME STEP L=  0
 U COMPONENT OF VEL FIELD
I= 1
-2.8576813E-02  -7.0347339E-03   2.1571555E-02   1.9920119E-02   2.3752786E-02  -1.6176594E-02  -1.3308830E-02  -3.0043927E-02
-5.0597277E-02  -2.9896102E-02  -3.0552746E-02  -1.4314896E-02  -1.9253435E-02  -4.3586057E-02  -1.1078643E-02   2.9174775E-02
I= 9
-1.0991899E-02   8.5896393E-03   5.8638267E-02   3.5101630E-02   3.5843505E-02   2.2515855E-02   2.3031691E-02   2.7132673E-02
-2.0880525E-02   1.4550951E-02   1.1678625E-02  -1.8899412E-03  -2.1359736E-02  -4.0302598E-03  -3.8008995E-02  -3.0704101E-02
 V COMPONENT OF VEL FIELD
I= 1
-7.9940066E-03  -1.3929724E-02  -2.0152500E-02  -3.7924601E-02  -5.9696914E-02  -3.0293187E-02   1.1577200E-02   2.5772654E-02
 2.3418684E-02   2.1652726E-03   3.9071224E-02   7.1785902E-02   5.2960241E-02   5.7079720E-03  -2.1197679E-02  -1.8112820E-02
I= 9
 2.7120163E-02   2.7218727E-02   2.9390284E-02   6.1024009E-02   9.0802699E-02   6.6724224E-02   2.3937263E-02   1.8283696E-03
 1.9781816E-03  -3.8082663E-03  -7.3570722E-03  -4.8629504E-02  -5.5532829E-02  -2.3423091E-02  -1.6318443E-03   3.1033649E-02
 W COMPONENT OF VEL FIELD
I= 1
-1.8569185E-03   2.6818964E-02   1.0110091E-02   9.3246550E-04   8.0017245E-03  -1.2303907E-02  -1.0388645E-02  -3.8046011E-03
 1.9990735E-02   3.9269755E-02  -5.3660981E-03  -5.2313049E-02  -1.5564772E-02   1.5904302E-02   1.2053977E-02  -1.6875839E-02
I= 9
 3.6010713E-02  -2.3558359E-02  -5.9681541E-02  -7.8400893E-02  -8.2280713E-02  -1.5579057E-02   2.3902135E-02   4.1620433E-03
 1.5655371E-02   3.2278213E-02   2.7333025E-02   6.8181348E-02   9.9110871E-02   5.4172905E-02   3.0124981E-02   5.1730710E-02
 DIVERGENCE V
K= 9
I= 1
-3.1970423E-14  -3.0198066E-14  -8.6185278E-14  -3.7303498E-14  -3.9079850E-14   1.7763568E-14   1.4210855E-14   6.7501560E-14
 1.6431301E-14   1.4210855E-14   0.             -1.7763568E-14  -2.1316282E-14  -5.3290705E-14  -1.4210855E-14   7.1054274E-15
I= 9
 7.1054274E-15   1.9539925E-14   0.              3.5527137E-15   0.             -5.6843419E-14   1.9984014E-14   5.7731597E-14
 4.9293902E-14   3.0198066E-14  -1.4210855E-14  -3.5527137E-15   0.             -7.1054274E-15   7.1054274E-15   4.9737992E-14
 PRESSURE FIELD
I= 1
 4.1662166E-04   6.8036833E-04   3.9025449E-04   1.5836837E-04   1.8901220E-04   2.7277449E-04   4.0115030E-04  -5.4855660E-06
-1.7928844E-04   1.7348522E-04   6.8033261E-05  -1.0817013E-04  -2.2832621E-04   2.3267268E-04  -2.7256878E-04  -2.6213916E-04
I= 9
 1.6507560E-04   6.1744136E-04   1.4270762E-04  -4.5486424E-04  -8.6182050E-04  -9.5105668E-04  -5.1136588E-04   4.5265839E-05
 3.9824503E-04   4.1945018E-04  -1.8474638E-04  -7.8366576E-04  -8.6023654E-04   1.0634926E-04   8.6873833E-04   2.1268526E-04

SKEWNESSX=  -4.0392408E-03     ENERGY=  2.7576261E-03     DIVERGENCE=  -1.0507119E-14     LAMBDAX=  9.4250444E-02
```


ORIGINAL PAGE IS
OF POOR QUALITY

REFERENCES

Arakawa, A., 1966, "Computational design of long-term numerical integration of the equations of fluid motions: I. Two-dimensional incompressible flow," J. Comp. Phys., Vol. 1, 1, p. 119.

Batchelor, G. K., 1953, The Theory of Homogeneous Turbulence, Cambridge University Press.

Batchelor, G. K., 1967, An Introduction to Fluid Dynamics, Cambridge University Press.

Champagne, F. H., V. G. Harris, and S. Corrsin, 1970, "Experiments on nearly homogeneous turbulent shear flow," J. Fluid Mech., Vol. 41, part 1, p. 81.

Clark, R., 1975, Ph.D. Thesis, Thermosciences Division, Dept. of Mech. Engrg., Stanford University, to be published.

Cochran, W. T., et al.,1967, "What is the Fast Fourier Transform?," Proc. IEEE, Vol. 55, 10, p. 1664

Comte-Bellot, G. and S. Corrsin, 1971, "Simple Eulerian time correlation of full and narrow-band velocity signals in grid-generated 'isotropic' turbulence," J. Fluid Mech., Vol. 48, part 2, p. 273.

Corrsin, S., 1963, "Encyclopedia of physics," Vol. VIII/2, (Ed. Flügge, S. and C. Truesdell), Springer-Verlag, Berlin.

Deardorff, J. W., 1970, "A numerical study of three-dimensional turbulent channel flow at large Reynolds numbers," J. Fluid Mech., Vol. 41, part 2, p. 453.

Deardorff, J. W., 1971, "On the magnitude of the subgrid scale eddy coefficient," J. Com. Phys., Vol. 7, p. 120.

Deardorff, J. W., 1972, "Numerical investigation of neutral and unstable planetary boundary layers," J. Atmos. Sci., Vol. 29, p. 91.

Fox, D. G. and S. A. Orszag, 1973, "Pseudo spectral approximation to two-dimensional turbulence," J. Comp. Phys., Vol. 11, p. 612.

Fromm, J. E., 1963, "A method for computing nonsteady incompressible viscous fluid flows," Los Alamos Sci. Lab. Rep. LA-2910.

Gear, W. C., 1971, Numerical Initial Value Problems in Ordinary Differential Equations, Prentice-Hall, New Jersey.

Halleen,R. M. and J.P. Johnston, 1967, "The influence of rotation on flow in a long rectangular channel--an experimental study," Report MD-18, Thermoscience Division, Dept. of Mech. Engrg., Stanford University.

Harlow, F. H. and J. E. Welch, 1965, "Numerical calculation of time-dependent viscous incompressible flow of fluid with free surface," Phys. Fluids, Vol. 8, p. 2182.

Harris, V. G., 1974, "Experimental studies in a field of nearly homogeneous sheared turbulent flow," Ph.D. Thesis, Johns Hopkins University.

Hinze, J. O., 1959, Turbulence, McGraw-Hill, New York.

Johnston, J. P., 1974, "The effects of rotation on boundary layers in turbomachine rotors," NASA SP 304, p. 207.

Kwak, D., W. C. Reynolds, and J. H. Ferziger, 1975, "Three-dimensional time dependent computation of turbulent flow," Report No. TF-5, Dept. of Mech. Engrg., Stanford University.

Leith, C. E., 1965, "Numerical simulation of the earth atmosphere," Methods in Computational Physics, Vol. 4, p. 1.

Leonard, A., 1974, "On the energy cascade in large-eddy simulations of turbulent fluid flows," Adv. in Geophysics, Vol. 18A, p. 237.

Lilly, D. K., 1965, "On the computational stability of numerical solutions of time-dependent non-linear geophysical fluid dynamics problems," Mon. Weather Rev., Vol. 93, 1, p. 11.

Lilly, D. K., 1966, "On the application of the eddy viscosity concept in the inertial sub-range of turbulence," NCAR Manuscript No. 123.

Lilly, D. K., 1967, "The representation of small-scale turbulence in numerical simulation experiments," Proc. of the IBM Scientific Computation Symposium on Environmental Sciences, IBM Form No. 320-1951, p. 195.

Orszag, S. A., 1969, "Numerical methods for the simulation of turbulence," Phys. Fluids, Suppl. II, p. 250.

Orszag, S. A., 1971a, "Numerical simulation of incompressible flows within simple boundaries. I. Galerkin (spectral) representation," Studies in Applied Math., Vol. 1, 4, p. 293.

Orszag, S. A., 1971b, "Numerical simulation of incompressible flows within simple boundaries: accuracy," J. Fluid Mech., Vol. 49, p. 75.

Orszag, S. A. and G. S. Patterson, 1972, "Numerical simulation of three-dimensional homogeneous isotropic turbulence," Phys. Rev. Lett., Vol. 28, 2, p. 76.

Reynolds, W. C., 1975, "Computation of turbulent flows," Report No. TF-4, Mechanical Engineering Department, Stanford University.

Richardson, L. F., 1927, "The deferred approached to the limit, part 1, single lattice," Phil. Trans., A226, p. 299.

Rotta, J. C., 1951, Zeitschrift für Physik, Vol. 129, (I), p. 547.

Rotta, J. C., 1962, "Turbulent boundary layers in incompressible flow," Progress in Aeronautical Sciences, Vol. 2, (Ed. Ferri, A., D. Küchemann, and L. H. Sterne), Pergamon, Oxford.

Schumann, U., 1973, "Ein verfahren zur direkten numerischen simulation turbulenter stromungen in platten-und ringspaltkanalen und über sein andwendung zur unterschung von turbulenzmodellen," NASA Tech. Trans. TT F 15, 391.

Smagorinsky, J., 1963, "General circulation experiments with the primitive equations. I. The basic experiment," Mon. Wea. Rev., Vol. 91, p. 99.

Smagorinsky, J., S. Manabe and J. L. Holloway, 1965, Mon. Wea. Rev., Vol. 93, p. 727.

Tennekes, H. and J. L. Lumley, 1972, A First Course in Turbulence, M.I.T. Press.

Williams, G. P., 1969, "Numerical integration of the three-dimensional Navier-Stokes equations for incompressible flow," J. Fluid Mech., Vol. 37, part 4, p. 727

Winant, C. D. and F. K. Browand, 1974, "Vortex pairing: the mechanism of turbulent mixing-layer growth at moderate Reynolds numbers," J. Fluid Mech., Vol. 63, part 2, p. 237.